CAPÍTOL 4

CONCLUSIONS

En aquest capítol, s'exposen les conclusions de tots els estudis teòrics realitzats i que s'han presentat en aquesta tesi doctoral. A continuació, es remarquen, doncs, una sèrie de conclusions per a cada estudi.

La molècula 3-hidroxiflavona (3HF) dóna lloc a una clara fluorescència amb desplaçament cap a la regió roja de l'espectre electrònic i mostra una ràpida transferència protònica inversa vers el tautòmer enòlic a l'estat electrònic fonamental singlet (S_0). Des del punt de vista metodològic, amb l'estudi de la molècula 3HF hem posat de manifest la importància de la possibilitat d'optimització d'estats excitats amb el mètode *Time Dependent* (TD), ja que aquest és una millora substancial respecte el mètode *Configuration Interaction Singles* (CIS).

Pel que fa a la transferència protònica fotoinduïda que té lloc al 2-(2'-hidroxifenil)-4-metiloxazole (HPMO) en fase gas, cal destacar que: (a) la reacció estudiada a l'estat fonamental (S_0) és clarament endoèrgica i amb una barrera força alta. Això explica l'absència de reacció a l'estat fonamental; (b) al primer estat electrònic singlet excitat (S_1) es produeix una inversió de l'estabilitat relativa dels tautòmers. S'estabilitzen més els productes, arribant a una situació exoèrgica; (c) a l'estat S_1 s'hi troba també una reducció molt significativa de la barrera de transferència protònica respecte l'estat S_0. És aquesta reducció, juntament amb la inversió abans esmentada, la que possibilita la transferència protònica.

Respecte a la formació del complex ciclodextrínic (CD) HPMO/β-CD, podem concloure que: (a) el complex d'inclusió es troba afavorit termodinàmicament. S'observa que el *guest* té tendència a interaccionar llurs anells aromàtics amb els hidroxils primaris de la ciclodextrina i, si això no és possible, amb els secundaris; també

els grups funcionals que presenta el *guest* s'inclouen –en la mesura del possible- dins la ciclodextrina, mantenint alhora les interaccions dels anells aromàtics; (b) l'anàlisi conformacional del complex d'inclusió mostra dos modes d'inclusió, un dels quals presenta major estabilitat. No obstant això, existeix la possibilitat d'un equilibri conformacional entre les diferents inclusions; (c) en algunes estructures s'han obtingut unes distàncies H···H intermoleculars sorprenentment curtes, que resulten dubtoses car no tenen sentit físic. Aleshores, l'anàlisi exhaustiu de diferents mètodes de càlcul ens porta a dubtar de la validesa d'alguns mètodes semiempírics per a tractar sistemes supramoleculars. És necessari, doncs, emprar mètodes electrònics fiables per a l'estudi de sistemes supramoleculars, però això implica un gran esforç computacional. Molts dels mètodes semiempírics tradicionals no s'han dissenyat explícitament per descriure interaccions intermoleculars i, com a conseqüència d'això, donen uns resultats que no tenen sentit físic quan s'apliquen tant en el tractament de tot un sistema supramolecular com restringint-lo a una regió d'aquest en un càlcul híbrid ONIOM. El que sembla ser una excepció d'això és el mètode PM5, el qual és un mètode força prometedor ja que dóna uns resultats prou raonables per aquest sistema; (d) els mètodes *ab initio*, amb unes bases suficientment acurades donen uns resultats raonables, però són computacionalment massa cars per tractar la majoria de sistemes supramoleculars.

El nostre estudi sobre la transferència protònica fotoinduïda (PIPT) en el complex HPMO/β-CD mostra que: (a) analitzant teòricament la PIPT en el HPMO en fase gas i al complex d'inclusió, no s'observa una diferència significativa entre els dos casos. És a dir, l'efecte de l'entorn no dóna lloc a una variació significativa de la velocitat de la reacció, ans el contrari, són força semblants; (b) la CD té efectes sobre la transferència protònica a nivell molecular. La CD produeix una sobreestabilització del tautòmer cetònic respecte a l'enòlic a l'estat excitat que fa estabilitzar més l'estat de transició i, per tant disminuir així més la barrera energètica. Però aquest efecte es veu contrarestat per la diferent situació energètica en què es troba la molècula després de la transició vertical; (c) no hi ha cap variació geomètrica important dels mínims corresponents als tautòmers enòlics a S_0 i S_1 entre la situació en fase gas i dins la CD. Per tant, l'efecte de les transicions verticals que es produeixen tenen purament caràcter energètic, descartant així alteracions geomètriques significatives en comparar els dos casos.

De la formació dels rotàmers enòlics i cetònics de l'HPMO dins la CD podem dir que mentre per al procés de rotació de l'enol i de la forma cetònica a S_0 la termodinàmica no presenta diferències significatives respecte en fase gas, en la formació del rotàmer cetònic a S_1, esdevé de major importància l'efecte de la CD en l'estabilització d'aquest, comparant-ho amb la situació en fase gas.

En el sistema tropolona, el nostre estudi sobre la geometria del seu mínim a l'estat excitat $\tilde{A}^1B_2$ mostra que aquesta molècula és totalment plana (simetria C_s) en aquest estat electrònic i que la transferència protònica esdevé totalment simètrica.

Respecte a la formació de complexos d'inclusió tropolona-CD, cal dir que: (a) la formació del complex tropolona/α-CD no és termodinàmicament favorable i no es trenca la simetria energètica del doble pou corresponent a la transferència protònica intramolecular; (b) la formació del complex tropolona/β-CD és força favorable termodinàmicament i trenca la simetria energètica; (c) la inserció del dímer de la tropolona en la β-CD esdevé també favorable termodinàmicament, essent favorable, a més, la formació del dímer de la tropolona en fase gas. La inserció del dímer de la tropolona en la β-CD produeix una gran deformació en aquesta.

Pel que fa al sistema del 7-Azaindole complexat amb *n* molècules d'aigua (essent *n*=1-4), hem arribat a les següents conclusions: (a) hi ha una inversió de l'estabilitat relativa dels tautòmers en passar de l'estat fonamental (S_0) a l'excitat S_1. A més, la reacció és endergònica a S_0 i exergònica a S_1; (b) es produeix una substancial disminució de les barreres energètiques a S_1 respecte S_0 que afavoreix la consecució de la transferència protònica; (c) la reacció de transferència protònica més lenta a S_1 es dóna en el *cluster* 7-AzaI$(H_2O)_3$ i la més ràpida en el 7-AzaI$(H_2O)_4$; no obstant això, en tots els casos esdevé concertada, però no sincrònica; (d) la disposició adequada de les molècules d'aigua juga un paper primordial en la possibilitat de donar-se la transferència protònica. D'aquesta manera, la reacció pot tenir lloc més fàcilment en un agregat molecular d'aigües que no en solució aquosa.

Els càlculs electrònics de la tautomerització de la 1,4-dimetilantrona (1,4-MAT) i el seu isotopòmer 1,4-DMAT als estats S_0 i primer triplet excitat (T_1) revelen que la tautomerització és molt improbable a S_0 però es veu energèticament afavorida a T_1.

Els càlculs de les constants cinètiques k(E) de la transferència protònica a T_1 per a la 1,4-MAT i la 1,4-DMAT, mitjançant la teoria microcanònica RRKM tenint en compte, a més, l'efecte túnel, mostren que k(E) decreix ràpidament quan l'energia es troba per sota la barrera de potencial. Aleshores, els valors experimentals de les constants cinètiques i el gran KIE obtingut només poden ser explicats si la transferència protònica té lloc via efecte túnel a una energia lleugerament per sota de la barrera de potencial adiabàtica. Així, els nostres càlculs proporcionen una explicació de l'absència de fosforescència que s'observa experimentalment per la 1,4-MAT i el gran efecte cinètic d'isòtop (KIE) en la transferència protònica intramolecular mesurat respecte l'espècie 1,4-DMAT.

Respecte al sistema 6,9-dimetilbenzosuberona (6,9-MBS), cal destacar que: (a) a S_0 la reacció de transferència protònica no pot tenir lloc a causa de la gran endoergicitat i d'una barrera energètica massa alta. En canvi, a T_1 tant aquesta endoergicitat com la barrera energètica es redueixen substancialment, la qual cosa fa que la transferència protònica sigui més probable; (b) en els tautòmers cetònics de la família de les ortometilarilcetones, de la que la 6,9-MBS forma part, un major caràcter $n\rightarrow\pi^*$ porta a una reactivitat més gran en processos de transferència protònica; (c) la transferència protònica té lloc via efecte túnel a energies lleugerament per sota de la barrera de potencial adiabàtica i el KIE no presenta cap tendència anòmala; (d) a temperatures baixes, el domini de la fosforescència esdevé molt rellevant sobre la transferència protònica en la 6,9-MBS; (e) entre els isòmers 6,9-MBS, 6,8-MBS i 2,3-MBS, el primer presenta una interacció spin-òrbita força superior als altres. Això indica que la constant de desactivació fosforescent (k_P) depèn significativament de la posició dels substituents metílics en aquestes molècules.

CAPÍTOL 5

PUBLICACIONS

En aquest capítol es presenten els articles que s'inclouen a la tesi com a compendi de publicacions. Aquests són:

- ARTICLE 1: R. Casadesús, M. Moreno, J.M. Lluch, "The photoinduced intramolecular proton transfer in 2-(2'-hydroxyphenyl)-4-methyloxazole embedded in β-cyclodextrin", *Chemical Physics Letters*, **356**, (2002), 423-430. [pàgina 102]

- ARTICLE 2: R. Casadesús, M. Moreno, J.M. Lluch, "A theoretical study of ground and first excited singlet state proton transfer reaction in isolated 7-azaindole-water complexes", *Chemical Physics*, **290**, (2003), 319-336. [pàgina 110]

- ARTICLE 3: R. Casadesús, M. Moreno, J.M. Lluch, "Kinetic isotope effect on the photoenolization of *o*-methylanthrone. A microcanonical transition state theory calculation", *Journal of Physical Chemistry A*, **108**, (2004), 4536-4541. [pàgina 128]

22 April 2002

ELSEVIER

Chemical Physics Letters 356 (2002) 423–430

CHEMICAL PHYSICS LETTERS

www.elsevier.com/locate/cplett

The photoinduced intramolecular proton transfer in 2-(2′-hydroxyphenyl)-4-methyloxazole embedded in β-cyclodextrin

Ricard Casadesús, Miquel Moreno *, José M. Lluch

Departament de Química, Universitat Autònoma de Barcelona, 08193 Bellaterra, Barcelona, Spain

Received 30 August 2001; in final form 19 February 2002

Abstract

Some photocromic compounds involve photoinduced intramolecular proton transfer (PIPT) as a consequence of a fast electronic redistribution due to electronic excitation. In this study, we have examined the PIPT that occurs in 2-(2′-hydroxyphenyl)-4-methyloxazole (HPMO) in gas phase and encapsulated in β-cyclodextrin (β-CD). An hybrid method has been employed for electronic calculations of the confined geometry. Even though our results indicate that there is no significant difference between the PIPT process of HPMO in gas phase and encapsulated in β-CD, we also show that the effect of the confinement on the intramolecular proton transfer is not negligible. © 2002 Published by Elsevier Science B.V.

1. Introduction

Presently one of the most active research fields in physical chemistry is the study of reactions in nanocavities [1–19]. Such structures are unique and can be formed through covalent and weak, non-covalent bonding. Cyclodextrins (CDs) are one of the most thoroughly studied cavities of such structures [2–4]. They are cyclic oligosaccharides usually consisting of different number of glucose units. The most used CDs have 6, 7 and 8 glucose units and they are called α- β- or γ-CD, respectively. These compounds form a hydrofobic cavity and are able to encapsulate molecules of appropriate size [3,5,6].

This molecular recognition process of CD has attracted much attention due to its wide potential applications [7–9]. Photochemistry and photophysics of a CD-encapsulated guest molecule can be altered significantly by inclusion complex formation due to the influence of the hydrophobic cavity interior and to the limitation of molecular mobility inside the cavity [10–16]. In this way, increasing attention has been given to the study of the excited-state dynamics of aromatic molecules in CD cavities [11,14,17]. Among them the works that make use of femtochemistry techniques are remarkable in that they provide the more unambiguous insight on the mechanism of these processes as they are able to obtain real-time data of the molecular motions [11,18,19].

2-(2′-hydroxyphenyl)-4-methyloxazole (HPMO) is a heterocyclic molecule with two moieties, capable of establishing an intramolecular hydrogen

* Corresponding author. Fax: +34-935812920.
E-mail address: mmf@klingon.uab.es (M. Moreno).

0009-2614/02/$ - see front matter © 2002 Published by Elsevier Science B.V.
PII: S0009-2614(02)00401-3

bond. Upon electronic excitation the molecule undergoes a photoinduced intramolecular proton transfer (PIPT) reaction. Evidence for the occurrence of proton transfer in the excited state comes from the observation of a large Stokes shift in the emission spectra of HPMO [14,18,20]. Femtosecond studies in aprotic solvents have shown that after the first excitation femtosecond pulse, a second pulse delayed less than 300 fs is already able to produce the fluorescence emission of the keto form in the excited state. That means that proton transfer in the first electronically singlet excited state is an ultrafast process that takes place in much less than 300 fs [11,18,19]. Recently the effect of encapsulation of HPMO in β-CD on the dynamics of the proton motion and the influence of the interaromatic ring rotation has been studied at the femtosecond level [11,18,19]. The published results suggest that due to the caging effect of CD the rotational process is clearly slowed down to the subpicosecond scale [11].

From a theoretical point of view, the study of encapsulation of guest molecules by CDs has been severely limited by the large molecular size of the whole system. So, works usually make use of some empirical force field to deal with the interactions or, at its best, they use semiempirical quantum chemistry methods such as AM1 or PM3. Obviously the force field is unable to cope with actual reactions that imply the cleavage and formation of chemical bonds such as the proton transfer in HPMO. Semiempirical methods can deal with these problems but even so, and as far as we know, there is no published work dealing with actual chemical reactions inside nanocavities.

Recently the quantum chemistry world has turned its interest to the development of the so-called hybrid techniques that make use of different methods to deal with different parts of the system [21]. The idea behind these methods is that chemical reactions in large systems directly imply only a few number of atoms so that these are treated by a high (and accurate) method. The rest of the system can be satisfactorily dealt with by a less accurate (and computationally cheaper) method. Among these hybrid methods, the ONIOM method developed by the group of Morokuma is specially appealing as it can combine virtually any quantum chemistry or molecular mechanics method with each other [22]. As ONIOM has been launched quite recently, it has not been extensively used so that for many kinds of reactions (including proton transfers) it is not known how good can be the ONIOM scheme in dealing with them.

Then the goal of this Letter is twofold: First of all, as we are dealing with the proton-transfer reaction in HPMO in the first electronically singlet excited state in gas phase or in non-interacting solvents and encapsulated in β-CD, we will analyse the factors that govern the interaction between host and guest and how these factors are able to modify the rate of the intramolecular proton-transfer reaction. As we will use the ONIOM method to deal with the supramolecular system (a full high-level quantum chemistry calculation for the whole HPMO: β-CD system is clearly out of bounds for the present state-of-the-art methods in quantum chemistry), our second aim will be to test whether the ONIOM method is able to deal with such a complicated problem that includes a photoreaction in a supramolecular setting.

2. Calculational details

For the isolated HPMO molecule an ab initio method has been used. In particular the ground electronic state is studied by the restricted Hartree–Fock (HF) method with the split-valence 6-31G(d) basis set that includes a set of d polarisation functions on atoms other than hydrogens [23]. To deal with the first electronically singlet excited state, we used an all-single configuration interaction scheme (CIS) with a spin-restricted HF reference ground state [24]. Stationary points were located through the minimisation procedure of Schlegel [25] by using redundant internal coordinates. Introduction of correlation energy with the Møller-Plesset perturbative theory up to second order has not been considered as geometry optimisation is not possible within this method. Besides, this method has proved very unreliable giving too low energy barriers for proton-transfer reactions [26].

As explained in the preceding section, the study of the same reaction with the HPMO encapsulated

in a β-CD molecule has been done by making use of the ONIOM method [22]. In this method one can define up to three layers of atoms that are to be dealt at different levels. We have restricted the layers to only two (high and low levels). The obvious choice has been to put the HPMO molecule in the high level layer and the whole CD in the low level layer. In order to obtain results that can be compared with the gas phase calculations, the high level was the same used to deal with the reaction in the absence of CD. That is; HF for the ground state and CIS for the first electronically singlet excited state with the 6-31G(d) basis set. For the lower level we have used the semiempirical PM3 method of Stewart [27]. Direct location of the transition states was carried out only for the gas phase system. This procedure is not computationally available in the ONIOM calculation so that for the encapsulated system a reaction coordinate procedure has been used to approximately locate the transition states. In particular the structure of the transition state corresponding to the isolated HPMO molecule was taken and a grid of points was devised upon small displacements of the three distances (O–H, N–H and O–N) mainly involved in the proton-transfer process. At each point of the grid the rest of the geometrical parameters were optimised. The approximate position of the transition state was located in the reduced potential energy surface computed that way.

All the calculations have been performed with the GAUSSIAN 98 series of programs [28].

3. Results and discussion

Let us first briefly summarise the results of HPMO in gas phase. Fig. 1 presents the geometries of the stationary points corresponding to the proton transfer in both the ground and the first electronically singlet excited states (S_0 and S_1, respectively). The S_1 state comes from the HOMO–LUMO ($\pi \rightarrow \pi^*$) transition. Both orbitals are delocalised between the whole π system of the two rings.

Fig. 2 depicts the energy profile for the proton-transfer process. As it might be expected, results are very similar to those previously obtained by using the same electronic level for hydroxyphenyloxazole (HPO), where the 4-methyl group has been withdrawn [20]. Fig. 2 also indicates the position of the structure obtained upon a vertical electronic transition from the minimum of the ground state. From this point, the energy barrier to overcome is only of 1.69 kcal/mol so that the proton transfer may take place quite easily through quantum tunnelling. A similar conclusion was obtained for HPO [20]. Therefore the methyl group does not play any significant effect in the whole photochemistry of the HPMO molecule. Of course CIS results are not enough accurate to give quantitative results for a so small energy barrier. In any case our results indicate that upon photoexcitation the proton-transfer process may occur in a short time scale.

The structure of β-CD has been optimised at the semiempirical PM3 level. The structural parameters known from the X-ray study [29] were used as a starting point. The final parameters are not very different from the initial (experimental) ones so that the PM3 method seems good enough to deal with β-CD.

Next step was to introduce the HPMO (guest) molecule inside β-CD (host). Previously, an extensive conformational search was performed for the HPMO in its more stable form (E). This is the structure that enters the β-CD cavity prior to the irradiation that leads to the proton transfer and subsequent conformational changes of the product.

In this search, different conformational minima were found. The two more relevant structures are shown in Fig. 3. They are labelled **E1** and **E2** and both have less energy than the separated host and guest. In both cases the oxazole ring is sequestered by the CD cavity whereas the phenol moiety is mostly out of the CD cavity. This results agrees with the experimental evidence based on analysis of the ^{1}H-NMR spectra [14]. By considering the CD as a truncated cone, the two structures differ in the orientation of the host. **E1** has the phenol ring near the cavity of smaller diameter whereas in **E2** it is found near the cavity of larger diameter. **E2** is somewhat more stable than **E1** by 4.43 kcal/mol, so that an equilibrium between both structures may exist as experimentally observed in other CD encapsulated systems [30].

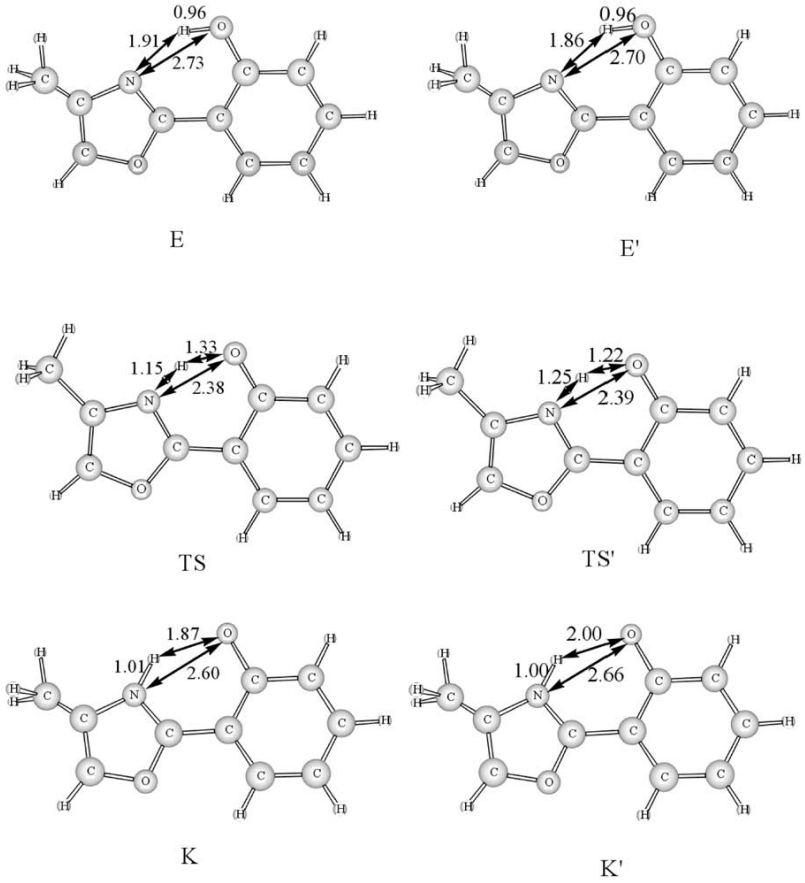

Fig. 1. Geometries of the stationary points for the proton transfer. E, TS and K refer to the enol (reactant), transition state and keto (product) structures in the ground electronic state. E′, TS′ and K′ are for the first electronically singlet excited state. The distances between the atoms implied in the proton-transfer reaction are given in Å.

As we are dealing with quite large structures, it is not easy to analyse the nature of the intermolecular forces that keep the guest inside the host. The geometry of HPMO is not greatly affected by CD. In particular the intramolecular O–H···N hydrogen bond is not perturbed as the interatomic distances between the three implied atoms are not appreciably modified upon encapsulation. Besides that, HPMO retains its planarity in **E1** whereas in **E2** it shows a small deviation of 2.7° between the planes of the two aromatic rings. Analysis of the host–guest interatomic distances discloses for **E1** the existence of one H(host)–O(guest) distance of 1.90 Å and three H(host)–H(guest) distances lower than 2.0 Å. For **E2** there are four H(host)–H(guest) distances lower than 2.0 Å. Another clue to the stabilisation of these two structures can be seen by looking at the dipole moments of the host and guest. For **E1** the dipole moment of the host and guest are 1.78 and 2.47 D, respectively. However in **E2** they amount to 1.89 and 2.50 D, respectively. The angle between the two dipole moments is 119° in **E1** and 141° in **E2**. A value closer to 180° indicates a more favourable dipole–dipole interaction [31,32].

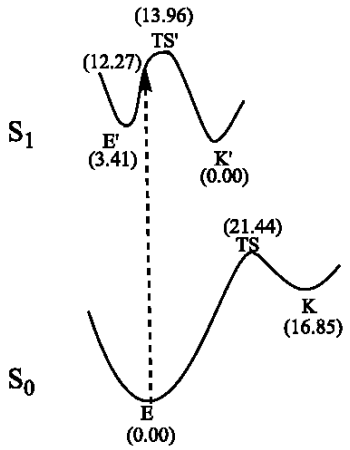

Fig. 2. Schematic energy profile for the proton-transfer process showing the relative energies of each stationary point in kcal/mol. Structures are labelled as in Fig. 1. The dashed line indicates the vertical transition (see text).

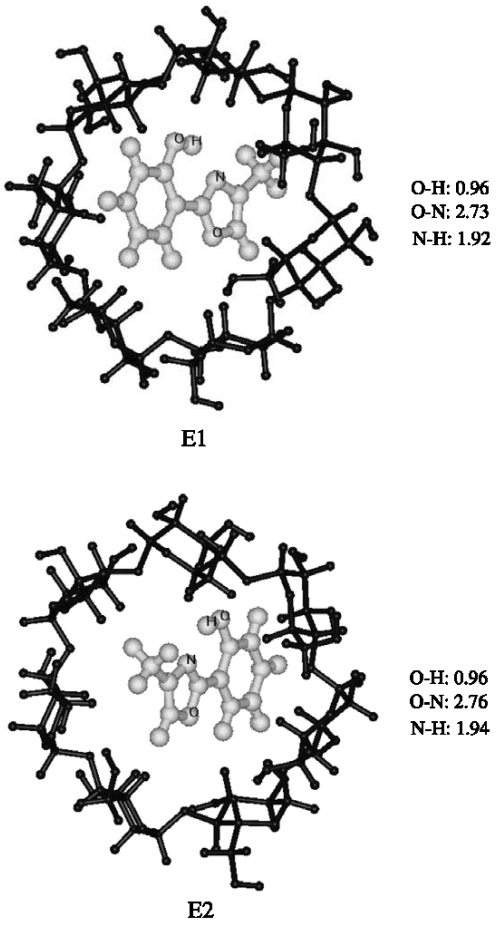

Fig. 3. Structures of the two more stable minima corresponding to the enol form of HPMO inside the β-CD. Distances between the atoms implied in the intramolecular hydrogen bond are given in Å.

An extensive search of internal conformations of the enol structure inside the CD has also been undertaken. In fact, the experimental work envisaged several configurations of the host:guest complex having different angles between the oxazole and the phenol rings that may lead to the slowing of the tautomerisation process. Our study has not revealed any additional minima except the one corresponding to the 180° rotation of the two rings. This structure is also present in the isolated HPMO and its relative energy is not greatly modified upon encapsulation.

Let us now consider the intramolecular proton transfer in **E1** and **E2** complexes. Fig. 4 shows the schematic energy profile for both ground and excited electronic states. When comparing with the gas phase results (Fig. 2), it is clear that there are no dramatic changes. In S_0 the keto structure is more stable and the barrier is lowered upon encapsulation. The endothermicity and the energy barrier is still high enough to prevent the proton-transfer reaction in this state. As for S_1, encapsulation also produces a remarkable stabilisation of the photoproduct, the exothermicity increasing by more than 3 kcal/mol. The energy barriers do not suffer such a great change though they are clearly lower in both complexes. This lowering of the barriers for the proton transfer does not necessarily mean that PIPT reaction in the cage is faster as the energy barrier must be considered not from the minimum of the excited state, but from the structure resulting from the vertical transition. From this structure the barriers are much lower and comparison with the gas phase results reveals that the barrier is slightly higher for complex **E1** whereas it is lower for complex **E2**. As in gas phase, these results indicate that proton transfer may take place quite easily through a quantum tunnelling mechanism.

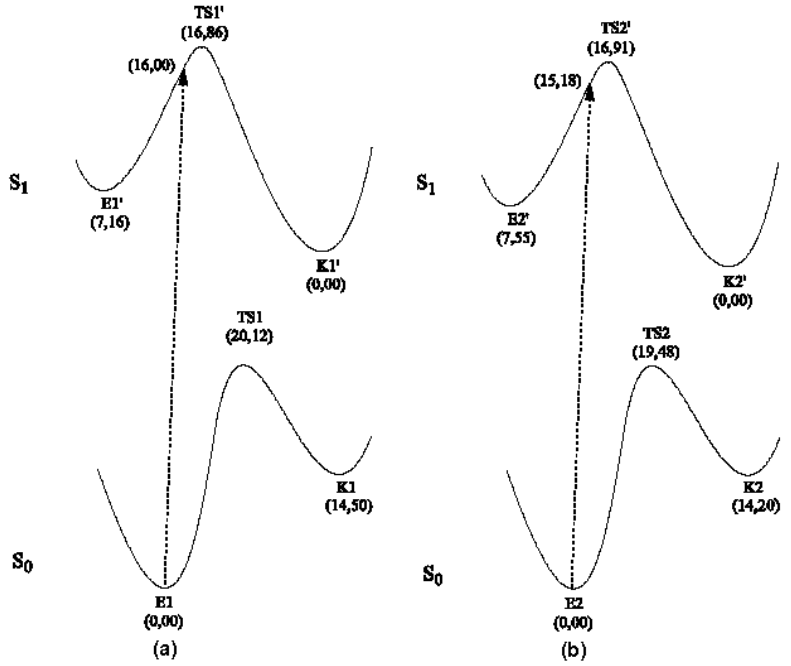

Fig. 4. Schematic energy profile for the proton-transfer process showing the relative energies of each stationary point in kcal/mol. Structures are labelled as in Figs. 3 and 5. The dashed line indicates the vertical transition (see text). (a) and (b) correspond, respectively, to the process taking place from **E1** and **E2** structures (see Fig. 3).

Fig. 5 depicts the structures of the transition states and the keto tautomers in S_1 for both complexes. The distances of the (O–H–N) bonds involved in the PIPT reaction are also posted in Fig. 5. We notice no major differences from the isolated HPMO results (see Fig. 1).

At this point it can be reminded that an equilibrium between **E1** and **E2** is probably present so that it is to be expected that changes in the rate of the PIPT reaction will not be detected upon encapsulation in β-CD. This does not mean that encapsulation does not alter the proton-transfer reaction but that antagonist effects act in opposite directions so that no appreciable difference between the reaction rates in aprotic media (or gas phase) and inside the CD cavity can be observed. These results are in accordance with recent experimental data on HPMO encapsulated in heptakis-(2,6-di-*O*-methyl)-β-CD and in other cavities [19]. No changes in the proton-transfer rates were observed for the host–guest complexes of CD as compared with the HPMO system in apolar solvent.

Finally we have also calculated the Stokes shift between the vertical transition of the enol form and the emission of the keto tautomer when it fluoresces to the ground state. The calculated values are 10276 cm^{-1} for **E1** and 10667 cm^{-1} for **E2**, in good agreement with the value of ca. 10000 cm^{-1} experimentally reported [11]. These data seems to support the use of the ONIOM scheme and the CIS methodology to deal with these complex systems.

In conclusion, our theoretical results have shown that no other minima than the original enol form and the 180° rotamer exist for the HPMO molecule encapsulated in β-CD. These two minima are also present in the isolated HPMO system. For the intramolecular proton transfer in the first electronically singlet excited state, our results also point to important modifications of the exothermicities upon encapsulation, but only small changes in the energy barriers. As an equilibrium between different host–guest complexes is expected and the energy barriers are

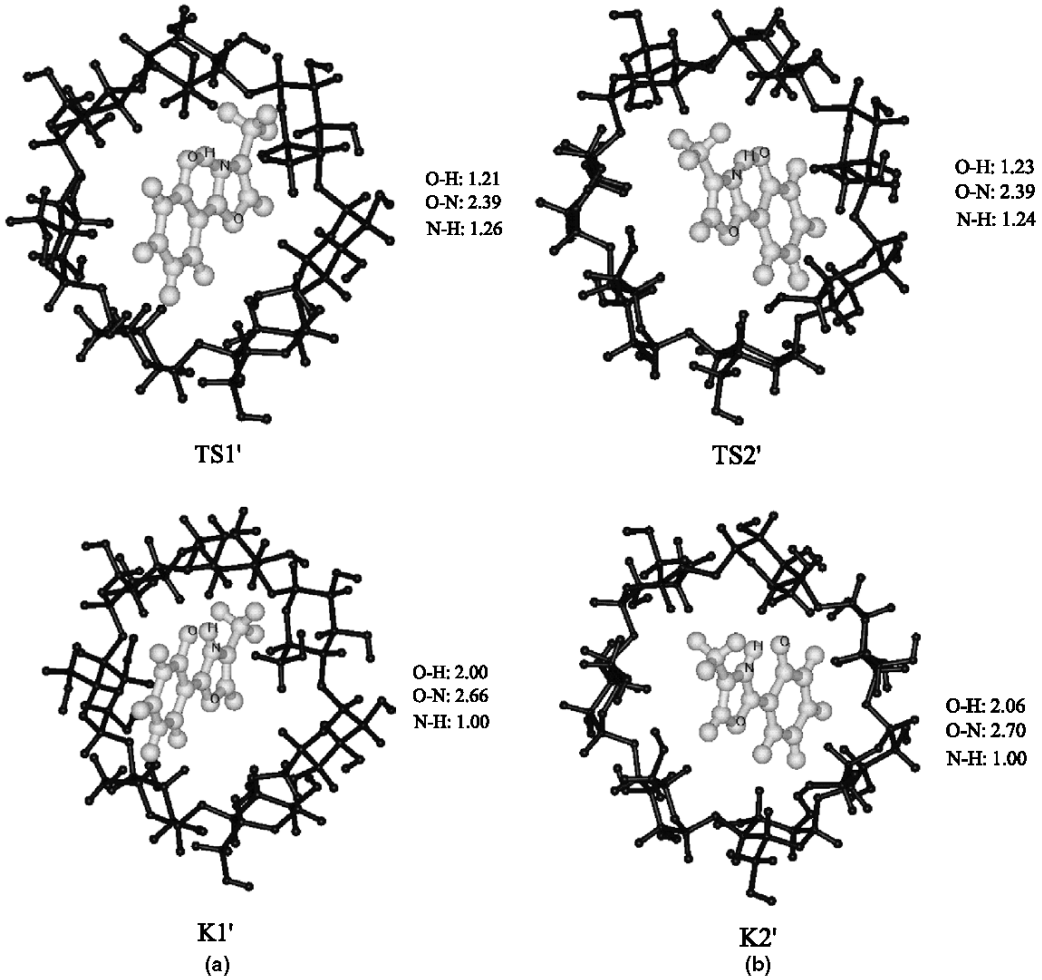

Fig. 5. Structures of the transition states and keto products for the proton-transfer reaction in the excited state. (a) and (b) correspond, respectively, to the process taking place from **E1** and **E2** structures (see Figs. 3 and 4). Distances between the atoms implied in the proton-transfer reaction are given in Å.

different, it may be that there are no appreciable differences between proton-transfer rates for free and caged HPMO.

Acknowledgements

Financial support from the Dirección General de Enseñanza Superior (DGES) through project PB98-0915 is gratefully acknowledged. The use of the computational facilities of the CESCA and CEPBA coordinated by the C^4 are also gratefully acknowledged. Finally we are also indebted to Abderrazzak Douhal for helpful discussions and a very careful reading of the manuscript.

References

[1] K.E. Drexler, Nanosystems: Molecular Machinery, Manufacturing and Computation, Wiley, New York, 1992.
[2] J. Szejtli, Cyclodextrins and Their Inclusion Complexes, Académiai Kiadó, Budapest, 1982.

[3] Special issue (5) on Cyclodextrins, Chem. Rev. 98 (1998).
[4] Z-P. Yi, H.-L. Chen, Z.-Z. Huang, Q. Huang, J.-S. Yu, J. Chem. Soc. Perkin Trans. 2 (2000) 121.
[5] W. Schlenk, Fortschr. Chem. Forsch. 2 (1951) 92.
[6] W. Schlenk, V.M. Sand, J. Am. Chem. Soc. 83 (1961) 2312.
[7] J. Szejtli, Cyclodextrin Technology, Kluwer Academic Publishers, Dordrecht, 1988.
[8] G. Wenz, Angew. Chem. Int. Ed. Engl. 33 (1994) 803.
[9] P. Bortolus, S. Monti, in: D.C. Neckers, et al. (Eds.), Advances in Photochemistry, Wiley, New York, 1996.
[10] A. Douhal, F. Amat-Guerri, A.U. Acuña, Angew. Chem. Int. Ed. Engl. 36 (1997) 1514.
[11] A. Douhal, T. Fiebig, M. Chachisvilis, A.H. Zewail, J. Phys. Chem. A 102 (1998) 1657.
[12] M. Milewski, W. Augustyniak, A. Maciejewski, J. Phys. Chem. A 102 (1998) 7427.
[13] A. Douhal, Ber. Bunsenges. Phys. Chem. 102 (1998) 448.
[14] I. García-Ochoa, M.-A. Díez López, M.H. Viñas, L. Santos, E. Martínez Ataz, F. Amat-Guerri, A. Douhal, Chem. Eur. J. 5 (1999) 897.
[15] W.M. Nau, X. Zhang, J. Am. Chem. Soc. 121 (1999) 8022.
[16] G. Grabner, K. Rechthaler, B. Mayer, G. Köhler, K. Rotkiewicz, J. Phys. Chem. A 104 (2000) 1365.
[17] S. Bajad, R. Jiménez, S.J. Rosenthal, V. Fidler, G.R. Fleming, E.W. Castner Jr., J. Chem. Soc. Faraday Trans. 91 (1995) 867.
[18] A. Douhal, Femtochemistry in Nanocavities, to be published.
[19] A.H. Zewail, A. Douhal, D. Zhong, Proc. Natl. Acad. Sci. USA 97 (2000) 14056.
[20] V. Guallar, J.M. Lluch, M. Moreno, F. Amat-Guerri, A. Douhal, J. Phys. Chem. 100 (1996) 19789.
[21] F. Maseras, in: T.R. Cundari (Ed.), Computational Organometallic Chemistry, Marcel Dekker, New York, 2001, p. 159.
[22] S. Dapprich, I. Komáromi, K.S. Byun, K. Morokuma, M.J. Frisch, J. Mol. Struct. (THEOCHEM) 461-462 (1999) 1.
[23] P.C. Hariharan, J.A. Pople, Mol. Phys. 27 (1974) 209.
[24] J.B. Foresman, M. Head-Gordon, J.A. Pople, M.J. Frisch, J. Phys. Chem. 96 (1992) 135.
[25] H.B. Schlegel, J. Comput. Chem. 17 (1996) 49.
[26] K. Luth, S. Scheiner, J. Phys. Chem. 98 (1994) 3582.
[27] J.J.P. Stewart, J. Comput. Chem. 10 (1989) 209.
[28] M.J. Frisch et al., GAUSSIAN 98, Gaussian Inc, Pittsburg, 1998.
[29] C. Betzel, W. Saenger, B.E. Hingerty, G.M. Brown, J. Am. Chem. Soc. 106 (1984) 7545.
[30] L. Liu, Q.-X. Guo, J. Phys. Chem. B 103 (1999) 3461.
[31] M. Kitagawa, M. Sakurai, H. Hoshi, Chem. Lett. (1988) 895.
[32] D.M. Davies, J.R. Savage, J. Chem. Res. (S) (1993) 94.

Available online at www.sciencedirect.com
SCIENCE DIRECT®
Chemical Physics 290 (2003) 319–336
Chemical Physics
www.elsevier.com/locate/chemphys

A theoretical study of the ground and first excited singlet state proton transfer reaction in isolated 7-azaindole–water complexes

Ricard Casadesús, Miquel Moreno*, José M. Lluch

Departament de Química, Universitat Autònoma de Barcelona, Campus de Bellaterra, 08193 Bellaterra, Barcelona, Spain

Received 2 January 2003

Abstract

A systematic study of the proton transfer in the 7-azaindole water clusters (7-AI$(H_2O)_n$; $n = 1$ 4) in both the ground and first excited singlet electronic states is undertaken. DFT(B3LYP) calculations for the ground electronic state shows that the more stable geometry of the initial normal tautomer presents a cyclic set of hydrogen bonds that links the two nitrogen atoms of the base across the waters. For the $n = 4$ cluster the water molecules adopt a double ring structure so that two cycles of hydrogen bonds are found there. From this structure full tautomerization implies only one transition state so that a concerted but non-synchronous process is predicted by our theoretical calculations. This behavior is found both in the ground and the excited states where CIS geometry optimizations and TD(B3LYP) energy calculations are performed. The difference between both states is the height of the energy barrier that is much lower in the excited state. Another clear difference between both electronic states is that full tautomerization is an endergonic process in the ground state whereas it is clearly exergonic (then favorable) in the excited state. This is so because electronic excitation implies a charge transfer from the five-member cycle to the six-member one of 7-azaindole so that the proton transfer from the pyrrolic side to the pyridinic one is favored. These results clearly indicate that full tautomerization will not likely occur in the ground state but it will be quite easy (and fast) in the excited state. Reaction is already feasible in the S_1 1:1 complex but it is faster in the 1:2 complex. However the reaction slows again for the 1:3 complex and, finally, reaches a new maximum for the largest cluster studied here, the $n = 4$ case. These results, which are in agreement with experimental data, are explained in terms of the number of hydrogen bonds that are involved in the transfer. The proton transfer through a ring formed by the substrate and two water molecules is found to be the more efficient one, at least in this system.

1. Introduction

Proton (or hydrogen atom) transfer represents one of the most fundamental processes involved in chemical reactions as well as in living systems [1].

* Corresponding author. Tel.: +34-93-5812174; fax: +34-93-5812920.
E-mail address: mmf@klingon.uab.es (M. Moreno).

0301-0104/03/$ - see front matter © 2003 Elsevier Science B.V. All rights reserved.
doi:10.1016/S0301-0104(03)00173-3

In the later field the so called excited state proton transfer (ESPT) reactions are of paramount importance and so they have received considerable attention [2]. Among many molecules undergoing this type of photoreaction, 7-azaindole (7-AI) deserves special attention as it has been the subject of many experimental [3–25] as well as theoretical [26–46] studies. The reason of that is the resemblance of the molecule with the DNA base units and other molecules involved in biological life cycles. It has also been claimed that the 7-AI can advantageously replace tryptophan, customarily considered as the standard optical probe of protein structure and dynamics [47].

The more stable isomer of 7-AI in the ground state has the hydrogen in the pyrrolic nitrogen (Scheme 1). In the first excited singlet state however, the structure with the hydrogen in the pyridinic nitrogen is more stable. This fact, common to a large number of aromatic systems [48], explains why tautomerization takes place only upon photoactivation. When the hydrogen to be transferred forms an intramolecular hydrogen bond, the interconversion between the two tautomers is usually very fast upon irradiation. In 7-AI, such an intramolecular hydrogen bond linking the donor and acceptor nitrogen atoms is not present so that ESPT, as shown in Scheme 1, is not occurring in the isolated system [49]. However, if 7-AI is in an environment capable of making intermolecular hydrogen bonds with other molecules, then the ESPT may take place quite easily. Special attention has been paid to the case when another 7-AI molecule is used as an intermolecular source of hydrogen bonds. The double H-bonded 7-AI dimer, $(7\text{-AI})_2$, is known to exist in gas phase as well as in many solvent environments. A large number

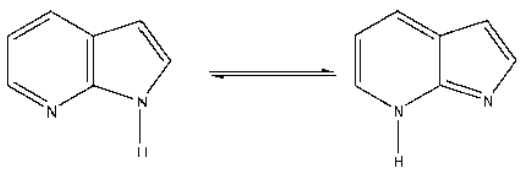

Normal Tautomer Full Tautomer

Scheme 1.

of studies of the photoinduced double proton-transfer reaction in $(7\text{-AI})_2$ have appeared in the last years as $(7\text{-AI})_2$ is considered to be an easy-to-work model of the base pairs naturally occurring in the DNA double helix [3,9–17,19–23,25,26,28, 30,32,35–38,44–46]. In addition to such studies, hydrogen-bonded complexes of 7-AI with different molecules have also been analyzed. In particular, the case of 7-AI clustered with water molecules has also received considerable attention [5–8,24,29,31, 33,34,39–41].

By analyzing the fluorescence spectra of 7-AI in an aprotic solvent upon microaddition of water, Chou et al. [6] come to the conclusion that the ESPT reaction takes place in the 1:1 7-AI–water complex. Besides, the ESPT in such a microsolvation environment is considerably faster than the one observed in bulk water. This difference in time scale is customarily attributed to the time necessary for the rearrangement in the bulk solvation shell in order to attain a favorable proton-transfer geometry with the solvent [31]. It is also assumed that the 1:1 complex is the only one responsible for the tautomerization given that it seems unlikely that the multiple proton transfers needed to accomplish tautomerization in the $7\text{-AI}(H_2O)_n$ complexes with $n \geqslant 2$ will take place simultaneously [4–8,29,50].

The 1:1 complex with water and the possibility that this complex undergoes ESPT has also been the subject of a great deal of theoretical calculations. Earlier studies were restricted to the ground electronic state [29] where the 1:1 complex is seen to be stable. The energy barriers obtained for the proton transfer in the complex, as compared with the values in the isolated 7-AI, point out that upon complexation the barrier dramatically diminishes. For instance, at the Hartree–Fock level of calculation with the energy corrected through the MP2 method the energy barrier obtained for the isolated 7-AI system is 58.7 kcal/mol, but in the 1:1 complex it is of only 19.4 kcal/mol.

Recently, calculations of the first excited singlet state (S_1), the one really involved in the ESPT process, have become feasible. Almost at the same time Chaban and Gordon [33] and Fernández-Ramos et al. [34] have calculated the two tautomers

and the transition state for the proton-transfer reaction of the 1:1 complex in the S_1 state. The energy barriers obtained in the two works are very different because different methods are used: the CIS method used by Fernández-Ramos et al. [34] tends to overestimate the energy barriers for the proton transfer and so they come to a value of 25.2 kcal/mol. On the other hand, Chaban and Gordon [33] use a MCSCF procedure together with a perturbative treatment up to second order (MCQDPT2) to include the dynamic correlation. Without geometry reoptimization they obtain an energy barrier of only 9.8 kcal/mol.

Larger 7-AI–water complexes have received considerably less attention. This is so because, as said above, it is thought that such a complexes cannot be directly involved in the tautomerization as more than one proton-transfer reaction is involved in the full process. In the ground electronic state the structure of the 1:*n* complexes with *n* 1–3 has been theoretically studied by Nakajima et al. [51] and Yokoyama et al. [52]. Both studies lead to the conclusion that in all the cases the structure that forms a ring of waters linking the pyrrolic hydrogen to the pyridinic nitrogen is the more stable one. Electronic [51] and IR [52] spectra of the same complexes confirm these assignments.

The kinetics of the proton-transfer process in such a larger clusters has been the topic of a recent work by Folmer at al. [24] 7-AI$(H_2O)_n$ clusters with *n* 2–4 (the monohydrated cluster was not available to study because of experimental restrictions) were obtained and characterized in gas phase. Ultrafast pumb–probe studies revealed that upon electronic excitation the cluster suffers a fast decay. For *n* 2 and 3 the obtained data were best fitted with a biexponential function yielding a fast first time constant of 360 ± 50 fs, and a second time constant of 6.0 ± 0.5 ps for the *n* 2 clusters. For *n* 3 the time constants of the two processes are somewhat larger (420 ± 80 fs and 6.1 ± 1 ps) whereas for *n* 4 the whole process is much faster and the data are fitted by a single exponential function with a time constant of 1.8 ± 0.3 ps. At first sight these data seem to indicate that in the four waters cluster there is only one process, so that the proton is transferred in a single step through the proton wire formed by the four water molecules. However, a stepwise proton-transfer, as it seems to be the case for the *n* 2 and *n* 3 clusters, could still be occurring in the *n* 4 complex. In this case the first step would be too fast to be observed within the time widths employed in the experiments (150 ± 50 fs). To be remarked that the obtained data are the decay of the signal of the original tautomer so that these experiments cannot discern whether a full tautomerization takes place or, rather, a single proton transfer from the 7-AI to the solvating water molecules occurs.

Theoretical studies of the kinetics of the proton transfer in complexes with more than one water clusters has only been undertaken by Fernández-Ramos et al. [41]. By using a CASSCF method they calculate the stationary points (normal form, full tautomer and transition state) for the proton-transfer reaction in the first excited singlet electronic state of 7-AI complexed with one, two and five water molecules. For the two waters complex (the only one that can be directly compared with experimental data) the calculations indicate a concerted though non-synchronous reaction path with a considerably high energy barrier: 16.94 kcal/mol. However, it is to be expected that this barrier will considerably diminish if dynamic correlation is introduced in the calculation. In fact the same authors [40] had previously calculated the barrier for the *n* 2 complex in the ground electronic state obtaining a lower energy barrier (13.66 kcal/mol) by using a more correlated method (MP2).

The purpose of this work is to perform a systematic study of the proton transfer in the 7-AI$(H_2O)_n$ clusters for *n* 1–4. Our main interest is the first excited singlet electronic state, where the reaction is known to take place, but the ground state will also be studied mainly for comparative purposes. It is also necessary to know the more stable geometry of the 1:*n* cluster in the ground state as this is the structure that will be photoexcited. The energies and structures of both tautomers as well as the transition state(s) linking them will be calculated and analyzed in order to shed light on the mechanism of such a complicated, though very interesting, processes.

2. Theoretical methods

All calculations were performed with the double-ζ quality 6-31G(d) basis set which includes a set of d-polarization functions on atoms other than hydrogens [53]. For the ground state, geometries and energies were obtained with the B3LYP hybrid density functional [54]. The CI all-single excitation with a spin-restricted Hartree–Fock reference ground state (CIS) was used to optimize the geometries and calculate the energies of the first excited singlet electronic state [55]. Energies at the located stationary points were recalculated through the use of the time dependent density functional theory with the B3LYP functional (TD-B3LYP) [56,57].

Stationary points were located through the minimization procedure of Schlegel by using redundant internal coordinates [58]. The nature of the located stationary points was ascertained by diagonalizing the energy second-derivatives matrix. To ensure that the transition states were connecting the expected reactants and products, a full optimization of each transition state was done by slightly shifting the geometry of the transition state in either sense following the direction of the transition vector (the eigenvector corresponding to the negative eigenvalue).

Diagonalization of the second derivative matrix also provides the vibrational harmonic frequencies which were used to evaluate the thermodynamic corrections at 1 atm and 298.15 K to the initially obtained electronic energy by using the standard statistical formulas, assuming that the system behaves as an ideal gas and that the rotational and vibrational degrees of freedom are well described through the rigid rotor and harmonic approximations, respectively [59]. As customarily done, for transition states the imaginary frequency is withdrawn from the calculations of the thermodynamic corrections so that the difference in Gibbs free energy between the transition state and the reactants is the only one parameter needed to calculate the rate constant within the framework of the transition state theory [60].

All the calculations presented here were done with the Gaussian 98 series of programs [61].

3. Results and discussion

Let us first consider the energetics of the formation of the 7-AI$(H_2O)_n$ complexes in the ground electronic state. The more stable structures for the normal tautomer are depicted in Figs. 1(a), 2(a), 3(a) and 4(a) for the n 1–4 clusters. For n 1–3 the complex presents a cyclic structure where a ring of water molecules is formed linking the two nitrogen atoms of 7-AI. This result agrees with experimental evidence [51,52] as well as previous calculations for the 1:2 and 1:3 complexes [51,52]. The analysis of the more stable structure for the n 4 cluster is not so easy. We will come later on to this point.

Table 1 gives the potential energy and the Gibbs free energy for the formation of the cluster from its components. That is, the energies in Table 1 correspond to the reaction

$$7\text{-AI} + n\text{H}_2\text{O} \rightarrow 7\text{-AI}(\text{H}_2\text{O})_n \quad (1)$$

By looking at Table 1 it is clear that the formation of all complexes is energetically favorable as the formation of the cluster involves a negative value of both energies. Interestingly, the stabilization of the cluster increases almost linearly with the number of water molecules so that the complex with four waters is almost four times more stabilized with respect to the separate constituents than the complex with only one water. However, in terms of Gibbs free energy the situation is not so favorable for the formation of the larger clusters. Nevertheless, up to the four waters complex considered here, the formation of the clusters is exergonic. Given that the entropic term disfavors highly ordered structures, it is seen that the increase of stabilization with the size of the cluster is more modest in terms of Gibbs free energy G and for n 4 the trend reverses so that G for the formation of the n 4 cluster from the n 3 is positive. At this point it is worth noting that less ordered structures, with one or more water molecules lying outside the ring of hydrogen bonds have also been calculated for the clusters with three and four water molecules. However these structures are energetically above the ones shown in Figs. 3 and 4 (even in terms of Gibbs free energy) so that they have not been considered here.

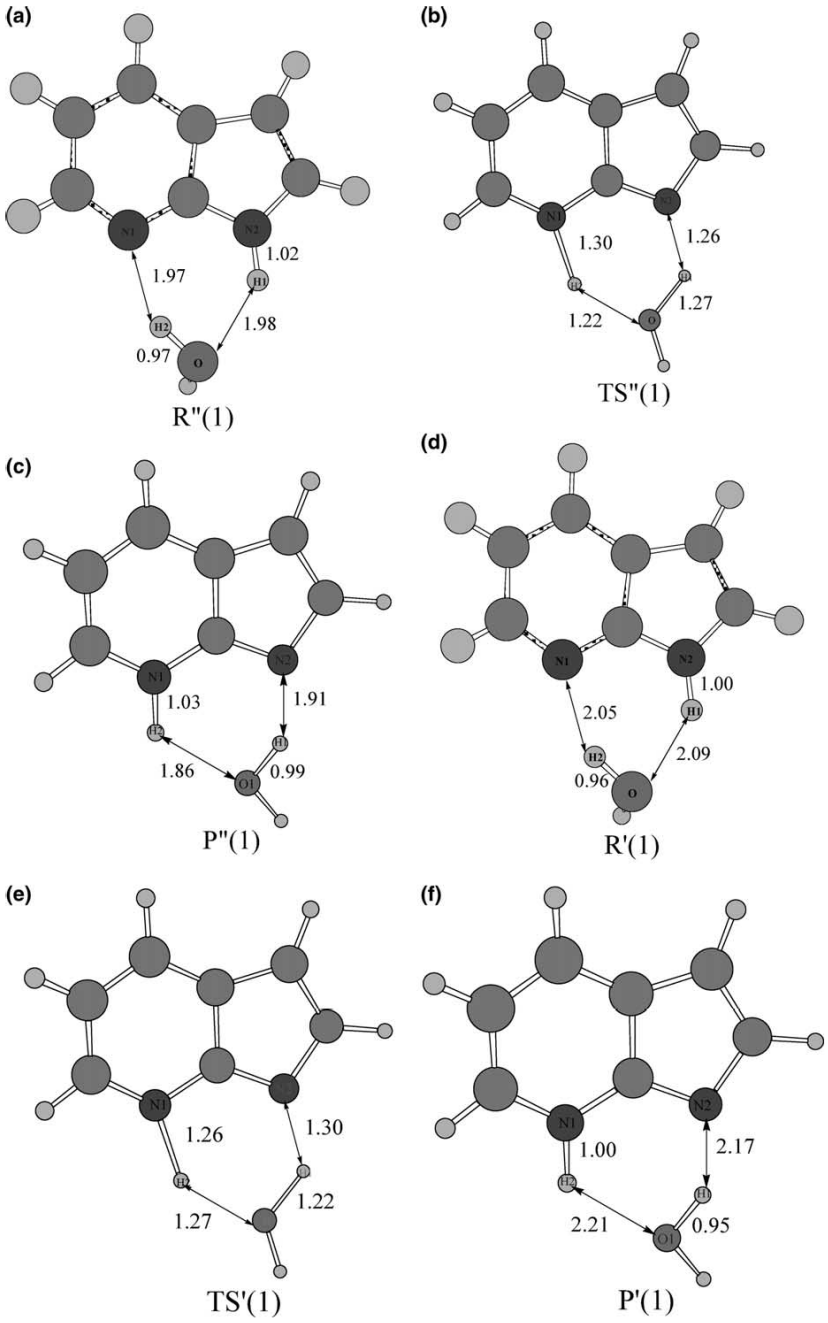

Fig. 1. Geometries of the stationary points located for the 7-AI$(H_2O)_1$ system in the ground and first excited singlet electronic states. Structures labeled R and P are minima whereas TS indicates a transition state. A prime denotes a structure in the excited state and a double prime corresponds to an excited state structure. Distances between selected atoms are given in Å.

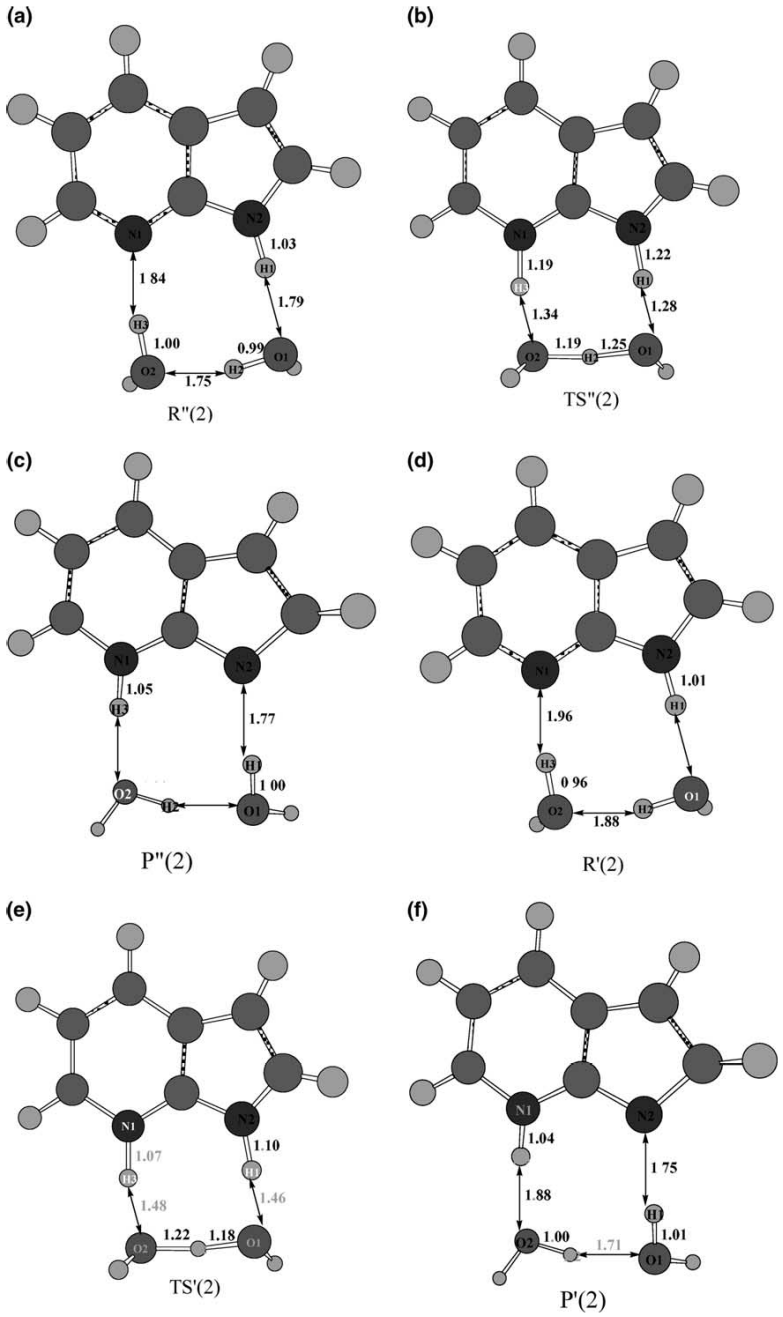

Fig. 2. Geometries of the stationary points located for the 7-AI$(H_2O)_2$ system in the ground and first excited singlet electronic states. Structures labeled R and P are minima whereas TS indicates a transition state. A prime denotes a structure in the excited state and a double prime corresponds to an excited state structure. Distances between selected atoms are given in Å.

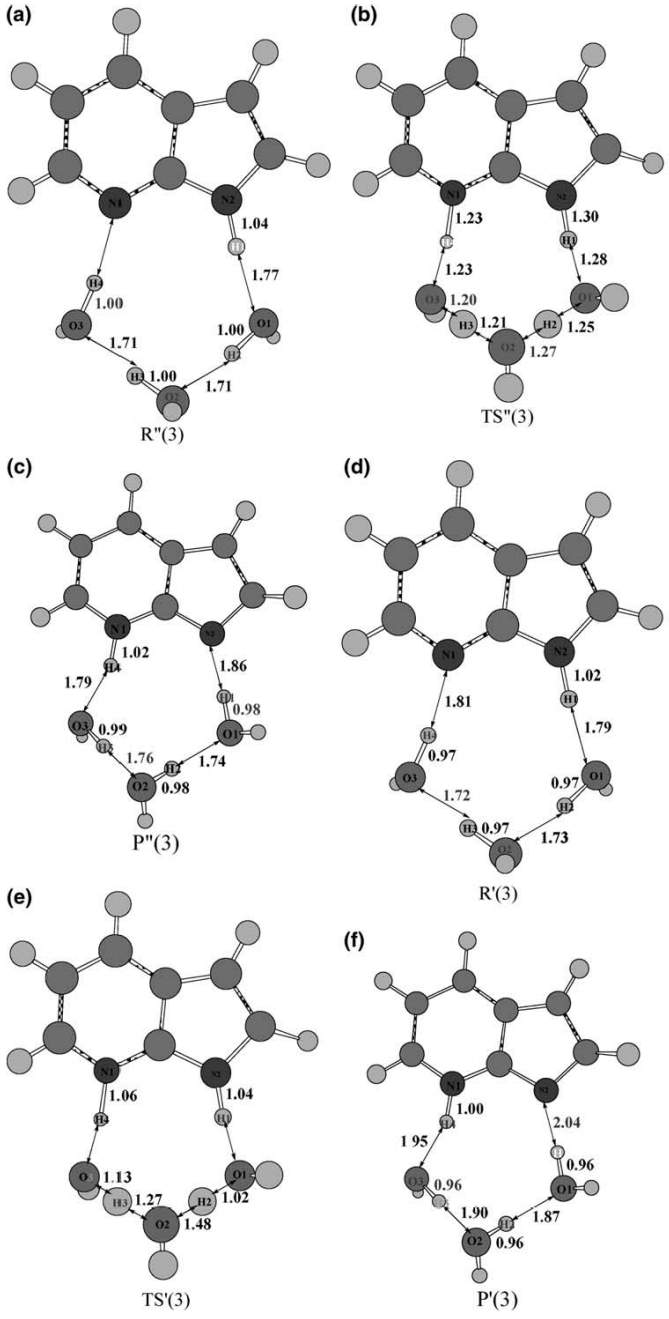

Fig. 3. Geometries of the stationary points located for the 7-AI$(H_2O)_3$ system in the ground and first excited singlet electronic states. Structures labeled R and P are minima whereas TS indicates a transition state. A prime denotes a structure in the excited state and a double prime corresponds to an excited state structure. Distances between selected atoms are given in Å.

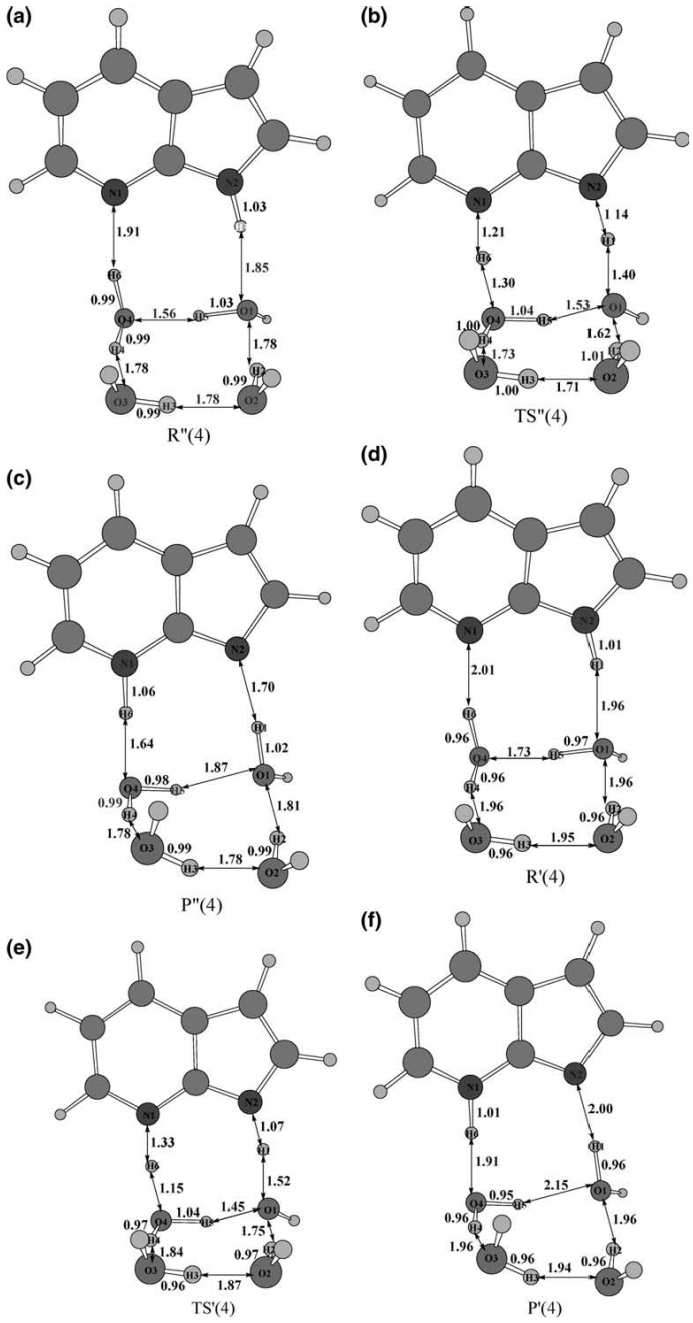

Fig. 4. Geometries of the stationary points located for the 7-AI$(H_2O)_4$ system in the ground and first excited singlet electronic states. Structures labeled R and P are minima whereas TS indicates a transition state. A prime denotes a structure in the excited state and a double prime corresponds to an excited state structure. Distances between selected atoms are given in Å.

Table 1
Energies (in kcal/mol) for the formation of the cluster: 7-AI + nH$_2$O → 7-AI(H$_2$O)$_n$

n	Potential energy (B3LYP)	Gibbs free energy
1	−13.98	−2.41
2	−28.93	−6.13
3	−41.97	−8.58
4	−55.83	−8.51

Some of these structures have also been found for the n 3 complex in previous theoretical works [51,52]. Finally it is worth noting that the basis set superposition error (BSSE) has not been considered. The BSSE correction, which is expected to be small for the hybrid DFT method used here, would slightly decrease the stabilization energies of the progressive larger water clusters posted in Table 1.

Once the cluster of 7-AI with n water molecules has been formed it can suffer a proton transfer reaction that leads to the tautomer. This reaction does not take place easily in the ground electronic state (S_0) as different spectroscopic techniques [51,52] of the complexes with water have lead to the conclusion that only the normal tautomer with the hydrogen in the pyrrolic nitrogen is present in the cluster. However, as explained in the introduction, recent experiments also indicate that upon irradiation, that puts the system in its first excited singlet electronic state (S_1), the normal tautomer suffers a very fast decay leading (probably) to the full tautomer. These ultrafast pump–probe spectroscopic studies do not exclude the possibility of an incomplete tautomerization leading to some zwitterionic structure of the 7-AI(H$_2$O)$_n$ complex [24]. In order to analyze this reaction from a theoretical point of view we have located all the stationary points corresponding to the proton-transfer reaction. Even if our main interest focuses on the excited state we have also considered the ground electronic state in order to be able to compare the reactivity of both states. In the clusters with more than one water more than one geometry has been obtained for the initial complex. However, only the more stable structure has been considered here as this is the structure that will be initially photoexcited.

Tables 2 and 3 present the energies of all the stationary points (minima and transition states) located for the ground and first excited singlet electronic states, respectively. As explained in the theoretical details section, the B3LYP/6-31G(d) method is the only one used in the ground electronic state (Table 2). Direct DFT geometry

Table 2
Relative energies (in kcal/mol) for the stationary points corresponding to the proton-transfer reaction of the 7-AI(H$_2$O)$_n$ complexes in the ground electronic state

Complex	Structure	Potential energy (B3LYP)	Gibbs free energy
7-AI	R$''$(0)	0	0
	TS$''$(0)	65.84	61.25
	P$''$(0)	12.90	13.00
7-AI(H$_2$O)$_1$	R$''$(1)	0	0
	TS$''$(1)	22.54	19.39
	P$''$(1)	10.00	10.17
7-AI(H$_2$O)$_2$	R$''$(2)	0	0
	TS$''$(2)	18.96	14.97
	P$''$(2)	6.84	7.39
7-AI(H$_2$O)$_3$	R$''$(3)	0	0
	TS$''$(3)	22.04	17.79
	P$''$(3)	8.44	8.45
7-AI(H$_2$O)$_4$	R$''$(4)	0	0
	TS$''$(4)	13.21	10.83
	P$''$(4)	8.23	8.15

Table 3
Relative energies (in kcal/mol) for the stationary points corresponding to the proton-transfer reaction of the 7-AI$(H_2O)_n$ complexes in the first excited singlet electronic state

Complex	Structure	Potential energy (CIS)	Potential energy (TD-B3LYP)	Gibbs free energy
7-AI	R′(0)	0	0	0
	TS′(0)	68.40	44.22	45.39
	P′(0)	−21.07	−26.21	−19.71
7-AI$(H_2O)_1$	R′(1)	0	0	0
	TS′(1)	26.94	6.42	5.42
	P′(1)	−18.15	−21.47	−19.82
7-AI$(H_2O)_2$	R′(2)	0	0	0
	TS′(2)	24.35	2.27	1.05
	P′(2)	−15.85	−18.11	−17.48
7-AI$(H_2O)_3$	R′(3)	0	0	0
	TS′(3)	31.63	10.53	9.11
	P′(3)	−14.60	−16.22	−17.36
7-AI$(H_2O)_4$	R′(4)	0	0	0
	TS′(4)	22.29	−0.19	−0.46
	P′(4)	−16.37	−18.23	−18.17

optimizations are not yet available for the excited states so that the CIS method is used to locate the stationary points in the excited state. Given that, accordingly to Brillouin's theorem [62], CIS calculations of the excited state are the equivalent of a Hartree–Fock calculation for the ground state, CIS results will lack dynamical correlation, this fact usually meaning that energy barriers for the proton-transfer reactions will be too high [63]. Introduction of dynamic correlation in the excited state calculations is not a well solved question [64]. In this paper we have opted to use the recent developed time-dependent method within the B3LYP density functional (TD-B3LYP) [56,57]. This level of calculation does not allow for geometry optimization so that the CIS geometries of minima and transition states are recalculated within the TD-B3LYP method. Table 3 reports both CIS and TD-B3LYP energies for the S_1 states. It is clear that in all the cases the quite high energy barriers obtained at the CIS level are lowered to more reasonable values by using the TD-B3LYP methodology. In addition to the potential energy, the Gibbs free energy is also given for each structure in the last column of Tables 2 and 3. For the ground state it corresponds to the B3LYP calculation. In the excited state G is obtained by adding the thermodynamic corrections obtained at the CIS level to the TD-B3LYP potential energies.

Structures in Tables 2 and 3 are systematically named as R (reactant, normal tautomer), TS (transition state) and P (product, full tautomer). As customarily done in spectroscopy, a double prime denotes the ground electronic state (Table 2) whereas a single prime indicates the excited state (Table 3). Finally, a number enclosed in parentheses is used to denote how many water molecules (from 0 to 4) has the complex. From now on we will extensively use this nomenclature to easily refer to each obtained structure. We have performed full optimizations of the transition state structures slightly shifted in each sense indicated by the direction of the transition vector. In this way we have verified that each transition state is actually connecting the expected reactant and product structures as they are given in Tables 2 and 3.

The obtained energies for the ground state reactions, given in Table 2, do not show any unexpected trend. The bare 7-AI molecule (without water) has also been considered though in that case it is clear that tautomerization is not likely to occur. Accordingly, our results for the isolated 7-AI molecule indicate very high energy barriers in

both electronic states. The normal tautomer R″ is always the more stable equilibrium structure in S_0. In fact, the energy difference between both tautomeric forms is not greatly modified with the addition of more water molecules in the cluster. The higher energy difference is found for the isolated 7-AI system whereas the 1:2 water complex has the smallest value within the systems considered in this work. It is also worth noting that inclusion of thermodynamic corrections does not represent any significant change as the relative Gibbs free energy of tautomerization in all the cases differs less than 1 kcal/mol from the purely electronic results. This result contrasts with the ones of Table 1 where entropy played a quite dominant role in the thermodynamics for the formation of the cluster. However, once the complex has been formed, the entropic term is not significantly modified by the proton-transfer reaction. The same applies to the rest of thermodynamic corrections that are quite similar between both tautomers.

Things are different when it comes to analyze the kinetics of the reaction. The transition state energies are far different for the distinct clusters here considered. In the isolated 7-AI molecule the energy barrier is, as expected, quite high. Upon addition of one water molecule, there is a dramatic decrease of the energy barrier (from 65.84 to 22.54 kcal/mol, more than 40 kcal/mol of difference). A further energy decrease, not so spectacular, is observed when going to the n 2 cluster whereas a slight increase is seen for the complex with three water molecules. On the other hand, the four waters case presents a new energy decrease so that this is the complex with the lowest energy barrier among all the studied cases. Now it is not true that Gibbs free energies are similar to the purely electronic ones. The Gibbs free energy of the transition states is always clearly lower than the corresponding difference in potential energies. This can be attributed mainly to the difference in zero point energies. As the transition state has one degree of freedom less (the one that has negative curvature), the zero point energy of the transition state is clearly smaller than the one of the reactant minimum. Entropy plays again no significant role as it changes only slightly along the whole reaction path. Even taking into account these differences, the general trends observed before are maintained in terms of Gibbs free energy. Again for the 7-AI–water clusters there is a clear lowering of the barrier from n 0 to n 1 that continues to n 2 and 4, where the free energy barrier reaches the smallest value. The n 3 complex represents again an exception as, coming from the previous n 2 complex, the free energy barrier slightly increases. In any case, the energy barrier for all the clusters here considered is still quite high so that it can be ensured that this reaction will not take place in the ground electronic state. For the more favorable case, the cluster of 7-AI with four water molecules, the final value of the free energy of activation is not so high (10.83 kcal/mol) so that a thermally activated process could eventually lead to the formation of the tautomer P″(4). However, as the tautomer is not thermodynamically stable, it would quickly revert to the original R″(4) structure.

Things are very different in the excited state. The energy differences presented in Table 3 reveal that now the full tautomer P′ is the more stable structure in all the systems considered including the isolated 7-AI molecule. Even so, the proton-transfer reaction has still to surmount an energy barrier. The energy barrier is in fact still very high in the isolated 7-AI molecule but, again, it abruptly diminishes with the addition of just one water molecule. Addition of more water molecules to the cluster shows the same trend already observed in the ground state: a further lowering in the energy barrier for the 1:2 complex, an increase in the 1:3 one and a new decrease for the 1:4 complex. As explained above, the CIS method was used to obtain and characterize the stationary points in the S_1 potential energy surface but this method is known to overestimate the energy barrier in proton-transfer reactions [63,64]. Our results confirm this hypothesis as energy barriers higher than the ones obtained for the ground state arouse as seen in the third column of Table 3. This result makes no sense and is caused by the different level of calculation used for the two electronic states. To allow a fair comparison we have performed single point electronic calculations using a time dependent formalism to evaluate the B3LYP energy of the excited state. These TD-B3LYP

results are shown in the fourth column of Table 3. At this level of calculation the ordering in energy barriers along the different clusters is not modified but the barrier height is clearly diminished to more reasonable values so that we will use these values for the forthcoming discussions. One drawback of these calculations is that geometries cannot be optimized at this level of calculations. This inconvenient has been shown to lead to energy barriers that are now overcorrected [63]. This explains why for the more favorable case (the 1:4 complex) a negative value of the energy barrier shows up at the TD-B3LYP level. This result just points out that the energy barrier in that case is very small, a result that in fact agrees with experimental evidence that has disclosed that tautomerization of the 7-AI–water complexes in the excited state takes place in the time scale of the femtoseconds.

To understand the role played by the water in the tautomerization and the differences of energies seen for the different clusters it is necessary to turn now the attention to the geometries of the different structures calculated. Figs. 1–4 depict the geometry of each stationary point. The same nomenclature of Tables 2 and 3 is used so that it is easy to match each structure with its energy. The distances in Å of the atoms involved in the proton-transfer reaction are also given in the figures.

It is clear that in absence of water (or any other H-atom donor–acceptor molecule) the 7-AI molecule cannot easily transfer the proton from the pyrrolic to the pyridinic nitrogen as the geometry of the molecule does not allow the formation of an intramolecular hydrogen bond. However, one water molecule is enough to make such a link by establishing a double hydrogen bond with both the H-donor and the H-acceptor nitrogen atoms of 7-AI. This provides the molecule with a proton-wire that, upon a double proton transfer, can proceed to the formation of the tautomer. Fig. 1 shows the geometries of reactant, transition state and product for such a process in the 1:1 complex in both S_0 and S_1 states. If we restrict our attention to the excited state geometries (Fig. 1(d)–(f)), the formation of the double hydrogen bond between water and 7-AI is clearly seen in the initial structure R′(1). In the transition state TS′(1) the two hydrogen atoms involved in hydrogen bonds (one from the basis and the other one from the water molecule) are transferring almost simultaneously as they are both midway between the H-donor and the H-acceptor atoms. At the end this process leads to the full tautomer P′(1) where again two hydrogen bonds between the base and the water are to be found. This mechanism for the excited state is also taking place in the ground state. In fact there are no qualitative differences between the processes in both states as can be ascertained by analyzing now the process that goes from R″(1) to P″(1) passing through TS″(1) (Figs. 1(a)–(c)). The difference between both states lies in the relative energies as commented above. Tautomerization is an endergonic process in S_0 but it is exergonic in S_1. The reason of this difference is found in the nature of the electronic excitation that leads to S_1. It is a $\pi \rightarrow \pi^*$ (HOMO-LUMO) electronic transition that mostly implies a charge transfer from the pyrrol to the pyridine cycle of 7-AI. This charge transfer reverts in a more negative charge of the pyridinic nitrogen in S_1 that makes it more basic, so that in S_1 the pyridine cycle can accommodate with more easiness the transferred proton [28].

As we have just seen the reaction for the 1:1 complex implies a concerted, almost synchronous, double proton transfer. For the 1:2 complex the same process would imply the motion of three hydrogen atoms almost simultaneously. Anyway, this seems to be the case as only one transition state is located. Let us first consider the process in the ground state (Fig. 2(a)–(c)). In that case, as in the previous 1:1 case, the TS″(2) geometry presents all the transferring hydrogens midway between the H-donor and the H-acceptor atoms so that the triple H-atom transfer is almost a synchronous process. Now the excited state is not so similar. Fig. 2(e) shows the transition state for the reaction in S_1. Here only one of the hydrogen atoms (H_2 in Fig. 2(e)) implied in the process is actually "in flight". As for the other two hydrogen atoms involved, H_3 has almost being totally transferred (from O_2 to N_1) whereas H_1 has only begun to move. Even if only one hydrogen is clearly moving in the transition state, the full process is still concerted as we have verified that following the di-

rection of the negative curvature from the transition state we obtain both reactant and product structures with the hydrogens in either side of the reaction, so that no zwitterionic intermediate is envisaged from our theoretical calculations.

The tautomerization in the excited state for the 1:1 and 1:2 complexes we have just analyzed can be compared with the recent results reported by Fernández-Ramos et al. [41] for these complexes. They used the same basis set (6-31G(d)) but a different level of calculation (CASSCF). The results they obtain are not qualitatively different from the ones we have just analyzed. In both cases a concerted reaction path that links the normal form of 7-AI with the full tautomer is found. The two transition states imply a non-synchronous motion of the transferring hydrogen atoms. However, a more careful look at the two sets of geometries reveals some non-negligible differences in the distances between the atoms implied in the full process, this fact being more prominent in the transition states geometries, and, specifically, the one corresponding to the 1:2 complex. As for the energy barriers, given that a method that also lacks dynamical correlation is used, they obtain too high energy barriers, parallel to our (non-correlated) CIS results. Another previous calculation for the tautomerization of the 1:1 complex in S_1 has been reported by Chaban and Gordon [33]. Again the obtained geometries are qualitatively similar to the ones presented here though some differences exist at the quantitative level between their results and ours (and the ones by Fernández-Ramos et al. [41] as well). As for the energy barriers, Chaban and Gordon also found a quite high energy barrier when using a non-dynamically correlated method (MCSCF) that was dramatically lowered upon the introduction (without geometry reoptimization) of the dynamical correlation through a second-order perturbative method. These comparisons are then clearly indicating that our method is good enough, at the present state-of-the-art of the electronic excited state calculations, to analyze the kinetics of the tautomerization in the 7-AI–water clusters.

The next cluster in size is the 1:3 complex, for which there are no previous theoretical calculations. Fig. 3 presents the geometries of all the stationary points located in both S_0 and S_1 electronic states. It is to be noted that the more stable structure for the reactant is again the one with a cyclic structure of waters that involves now four hydrogen bonds that link the water molecules with the base and with themselves. This means that, to accomplish the tautomerization reaction, four hydrogen atoms are to be transferred somehow. It was common sense to expect in that situation a stepwise process. However, again only one transition state that connects the given reactant and product structure is found for both S_0 and S_1 electronic states so that the full process is in fact predicted to be concerted in light of our calculations. As already observed in the previous 1:2 case, the transition state in S_0 shows that all the hydrogens implied in the process are midway from its trip so that the process is almost synchronous. Conversely, in the excited state, where the reaction is known to occur, the transition state points to a more asynchronic path with only one hydrogen (H_3 in Fig. 3(e)) clearly "in flight". As for the other transferring hydrogens, H_1 and H_2 have yet to begin its motion and H_4 has been almost transferred.

One interesting point to discuss here is why for the 1:3 complex the energy barriers are larger than the ones for the previous 1:2 complex thus breaking the tendency towards lower energy barriers for larger water clusters. An analysis of the charge distributions along the different stationary points does not reveal any specific difference when comparing the 1:3 complex with the previous cases. In fact we believe that the difference stems from geometrical considerations as now the process implies a total of four hydrogen atoms to be transferred in a, more or less, concerted path. This means that quite a large number of atoms has to be moved from their more stable position (the one they have in the initial reactant structure) to a somewhat distorted geometry that allows the hydrogen atoms to be transferred. In that sense it is to be noted that the distance between the H-atom donor and the H-atom acceptor clearly diminishes in the transition state, a distortion that reverses in the product. Obviously these short distances are formed in order to facilitate the proton transfer. However, this distortion takes its price in terms of distortion energy. The same reasoning applies

when going from the 1:1 to the 1:2 complex. However, for the 1:1 complex the full ring of H-bonds is made of six atoms. This implies that the two hydrogen bonds are not linear (see Fig. 1), a situation which implies some strain in the ring and adds some difficulty to the transfer of the hydrogen atoms. For the 1:2 case the cyclic H-bonded structure is made of eight atoms. This increment in the number of atoms allows a more relaxed geometry of the H-bonds that now are almost lineal as readily seen in all the structures depicted in Fig. 2. This fact clearly favors the double proton transfer as compared with the strained 1:1 complex. For the 1:3 complex the ring of H-bonds grows up to 10 atoms, but this increase does not represent any additional release of strain in the geometry of the hydrogen bonds so that we can conclude that formation of H-bonded rings with more than eight atoms (the number implied in the 1:2 complex) does not lead to a much more favored, less strained, geometry.

At this point it is interesting to turn our attention to the 1:4 complex. After the considerations we have just made, it could be expected that there will be a further energy barrier increase in that case. However, the structure of the initial cluster R″(4) shown in Fig. 4(a) does not simply consists in a ring of four water molecules linking the two nitrogen atoms of the 7-AI molecule. Instead, there are two cycles of hydrogen bonds that connect both sides of the basis. The larger cycle implies the four water molecules and can be followed in Fig. 4 by the sequence of atoms: N_2–H_1–O_1–H_2–O_2–H_3–O_3–H_4–O_4–H_6–N_1. However, there is a shortcut of hydrogen bonds that also connects N_2 to N_1 that involves only two water molecules. This short ring can be traced down in Fig. 4 by the sequence: N_2–H_1–O_1–H_5–O_4–H_6–N_1. This results in an eight-member ring, just as it was already seen in the 1:2 complex. This particular structure opens the possibility of more than one circuit of concatenated proton transfers. However, only one of such circuits goes from reactant R″(4) to the tautomer P″(4) and this is the one that involves the small eight-member ring. The larger ring does not permit the full transfer as once the H_1 has been transferred to O_1 there is no possibility to further continue towards O_2 but only to O_4 and further on to N_1, in this way closing the short circuit of hydrogen bonds. The only alternative circuit of hydrogen atoms involves the four water molecules without participation of the 7-AI atoms. In fact we have located a transition state (not shown) that links the initial R″(4) structure with another reactant equilibrium geometry that is obtained by the simultaneous transfer of hydrogens labeled 2, 3, 4 and 5 in Fig. 4(a). This alternate equilibrium structure has a slightly higher energy than the former one so that it has not been considered here. As a consequence of all these considerations, the 1:4 complex is in fact a $2+2$ structure with two waters adopting a cyclic structure around the two nitrogen atoms of the base in a fashion similar to the one found for the 1:2 complex. The other two water molecules are forming a secondary ring that will not directly intervene in the series of concatenated proton transfers that will proceed around the short cycle. This explains why the energy barrier in the 1:4 complex is not increasing as it could be expected after the analysis of the 1:3 complex. In fact, the energy barrier should be quite similar to the one of the 1:2 complex and the energies shown in Tables 2 and 3 partially confirm this guess. Nevertheless the two additional waters are not mere spectators of the reaction but they have some role to play. It is not geometric but electronic as their presence enables a charge redistribution along the whole system. This smooths the charge separations that arise in the transition state geometry due to the asynchrony in the motion of the protons. For instance, in the TS′(2) the two waters have total charges of −0.18 a.u. whereas in the TS′(4) structure the two water molecules that are forming the proton wire support an almost null total charge.

Again all the considerations we have just made apply to both S_0 and S_1 states. The complete study of the potential energy surface in S_0 lead to the location of a total of 6 minima and 5 transition structures that connect them. In S_1 we did not perform such a thoroughly study but, as for the other cases, we restricted the calculations to the lowest minimum energy structure and the corresponding product and transition state connecting both minima (as shown in Fig. 4(d)–(f)). In S_1 the energy barrier at the TD-B3LYP level is slightly

negative, a non-physical result that stems, as previously discussed, from the lack of geometry optimization at this level of calculation.

Results for the 1:4 complex may cast some doubt about the validity of the study of the 1:3 complex previously presented as it is conceivable that the higher energy barrier obtained for the concerted motion of four protons could be bypassed by the formation of a structure with a two water ring and an additional water located just outside making a second ring, just the manner we have seen for the 1:4 complex. We have tested this idea and eventually we have obtained such a "bicyclic" structure which is shown in Fig. 5. Even if for this structure a less energetic transition state is to be expected (given that there are less hydrogen bonds involved), the structure shown in Fig. 5 has an energy 5.19 kcal/mol above the more stable minimum R″(3) (Fig. 3(a)). It is then unlikely that such a configuration is to be found for the isolated cluster and so, the reaction will not proceed through this alternate path. The reason of the high energy of this structure is again geometric as the solitary water cannot form perfect (i.e., linear) hydrogen bonds with the other two waters. In the 1:4 complex the two additional waters form a second ring of eight atoms. As previously noted this is just the correct number that permits an almost linear orientation of all the involved hydrogen bonds.

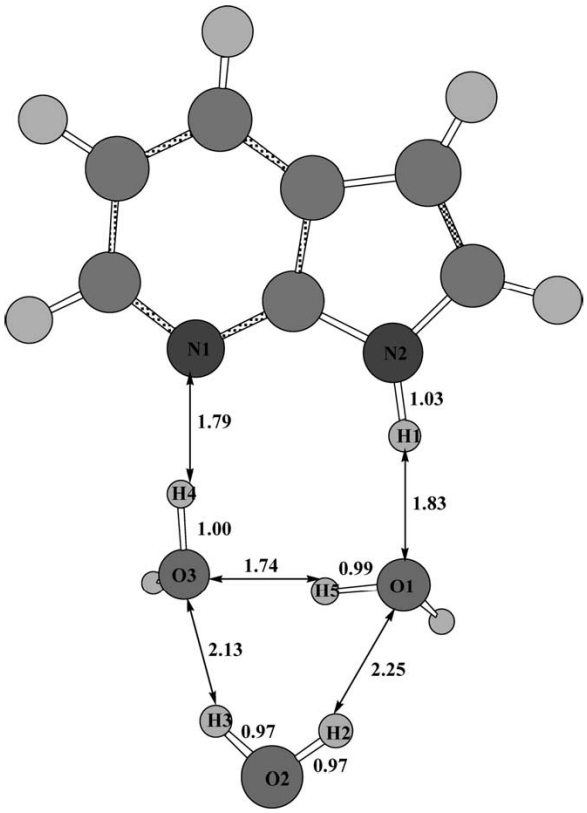

Fig. 5. Geometry of an alternate structure for the 7-AI$(H_2O)_3$ reactant minimum in the ground electronic state. It is to be compared with the (lower energy) R″(3) structure shown in Fig. 3(a). Distances between selected atoms are given in Å.

Finally it is time to analyze from a theoretical point of view the whole process of phototautomerization that takes place in the 1:n 7-AI$(H_2O)_n$ clusters. Before irradiation the clusters will be in their more stable form which are the ones labeled R″(1)–R″(4) accordingly to the number of water molecules involved. Tautomerization is not likely to occur from here as in S_0 there is always a considerable energy barrier to surpass and, besides, the full process is endergonic. Upon photoexcitation to the first excited singlet electronic state S_1, the reaction is no longer impeded as it is now exergonic and the energy barrier is not very high. In fact the relative energy of the transition states shown in Tables 2 and 3 is not a real measure of the energy barrier to surpass as it is measured from the minimum energy structure of the reactant in S_1. Accordingly to the Franck–Condon principle the structure initially obtained upon photoexcitation is the one resulting from a vertical excitation so that the nuclei have no time to reorganize, at least during the time the electronic excitation takes place. From this vertical excitation the energy barriers are obviously lowered. At the CIS level of calculation (the level used to optimize the geometries in the S_1 state) the energies of the vertical excitations with respect to the R′(n) optimized structures are 6.13, 8.32, 10.11 and 9.67 kcal/mol for the n 1–4 7-AI$(H_2O)_n$ complexes respectively. These values more or less follow the trend of increasing the energy with the size of the cluster, an expected result as the larger is the system, the larger will be the stabilization upon full optimization. In any case the energy barriers measured from the vertical transition follow the same trend than the values taken from the corresponding R′(n) minima as are posted in Table 3. The lower energy barriers obtained this way are still more definitely pointing to a very fast process in the excited state, a fact in agreement with the recent experimental work on these clusters [24].

Also in agreement with these experimental data are the predicted rate of the phototautomerization for the different clusters. Both CIS and TD-B3LYP results agree in that the slowest rate is to be found for the 1:3 cluster whereas the fastest one will be the one measured for the 1:4 complex. The 1:2 case will lie somewhere in between. Our results also predict that phototautomerization in the 1:1 complex is not as fast as in 1:2 and 1:4 complexes though it may be slightly faster than the 1:3 case. Unfortunately the 1:1 cluster was not studied because of experimental restrictions. This is an interesting point to elucidate as it has been customarily accepted that the 1:1 complex is the main responsible for the photoreaction taking place in bulk water. However, our results point to the process being much faster in the 1:2 and 1:4 complexes. Giving that our theoretical results also indicate that the formation of the 1:n cluster from the 1:(n 1) one is an exergonic process for n 1–3 we propose the structure of the 1:2 complex as the most likely one to be adopted so as to favor the proton-transfer reaction. The experimental work on these complexes was also not able to discern whether the reaction measured was a full tautomerization or rather a single proton transfer from the 7-AI molecule to the cluster of waters. Our calculation clearly points to the former possibility. In gas phase the charged species are very unstable so that, even if the transition structures only show partial motion of the protons, full tautomerization is always found as the ending point of the reaction. This is so because, as explained above, the transition states directly connect the initial reactant with the full tautomeric product so that the process involves only one step (one transition state). In this sense our results do not clarify the nature of the two time constants experimentally measured for the 1:2 and 1:3 clusters.

Acknowledgements

We are grateful for financial support from the Spanish "Ministerio de Ciencia y Tecnología" and the "Fondo Europeo del Desarrollo Regional" trough Project No. BQU2002-00301, and the use of the computational facilities of the CESCA.

References

[1] (a) A. Douhal, F. Lahmani, A.H. Zewail, Chem. Phys. 207 (1996) 447, and references therein;

(b) H. Limbach, J. Manz (Eds.), Hydrogen Transfer: Experiment and Theory, Ber. Bunsengens. Phys. Chem. 102 (3) (1998);
(c) N. Agmon, M. Gutman (Eds.), Proton Solvation and Proton Mobility, Isr. J. Chem. 39 (3/4) (1999).
[2] A. Müller, H. Ratajack, W. Junge, E. Diemann (Eds.), Electron and Proton Transfer in Chemistry and Biology, Studies in Physical and Theoretical Chemistry, vol. 78, Elsevier, Amsterdam, 1992.
[3] K.C. Ingham, M. Abu-Elgheit, M.A. El-Bayoumi, J. Am. Chem. Soc. 93 (1971) 5023.
[4] R.S. Moog, M. Maroncelli, J. Phys. Chem. 95 (1991) 10359.
[5] C.F. Chapman, M. Maroncelli, J. Phys. Chem. 96 (1992) 8430.
[6] P.-T. Chou, M.L. Martinez, W.C. Cooper, D. McMorrow, S.T. Collins, M. Kasha, J. Phys. Chem. 96 (1992) 5203.
[7] Y. Chen, F. Gai, J.W. Petrich, J. Am. Chem. Soc. 115 (1993) 10158.
[8] Y. Chen, R.L. Rich, F. Gai, J.W. Petrich, J. Phys. Chem. 97 (1993) 1770.
[9] P.-T. Chou, C.-Y. Wei, C.-P. Chang, C.-H. Chiu, J. Am. Chem. Soc. 117 (1995) 7259.
[10] A. Douhal, S.K. Kim, A.H. Zewail, Nature 378 (1995) 260.
[11] R. Lopez-Martens, Pham Long, D. Sogaldi, B. Soep, J. Syage, Ph. Millie, Chem. Phys. Lett. 273 (1997) 219.
[12] T. Suzuki, U. Okuyama, T. Ichimura, J. Phys. Chem. A 101 (1997) 7047.
[13] S. Takeuchi, T. Tahara, Chem. Phys. Lett. 277 (1997) 340.
[14] M. Chachisvilis, T. Fiebig, A. Douhal, A.H. Zewail, J. Phys. Chem. A 102 (1998) 669.
[15] P.-T. Chou, W.-S. Yu, Y.-C. Chen, C.-Y. Wei, S.S. Martinez, J. Am. Chem. Soc. 120 (1998) 12927.
[16] D.E. Folmer, L. Poth, E.S. Wisniewski, A.W. Castleman Jr., Chem. Phys. Lett. 287 (1998) 1.
[17] S. Takeuchi, T. Tahara, J. Phys. Chem. A 102 (1998) 7740.
[18] P.-T. Chou, C.-Y. Wei, G.-R. Wu, W.-S. Chen, J. Am. Chem. Soc. 121 (1999) 12186.
[19] T. Fiebig, M. Chachisvilis, M. Manger, A.H. Zewail, A. Douhal, I. García-Ochoa, A. de la Hoz Ayuso, J. Phys. Chem. A 103 (1999) 7419.
[20] D.E. Folmer, E.S. Wisniewski, S.M. Hurley, A.W. Castleman Jr., Proc. Natl. Acad. Sci. USA 96 (1999) 12980.
[21] J. Catalán, M. Kasha, J. Phys. Chem. A 104 (2000) 10812.
[22] A. Douhal, M. Moreno, J.M. Lluch, Chem. Phys. Lett. 324 (2000) 81.
[23] D.E. Folmer, E.S. Wisniewski, A.W. Castleman Jr., Chem. Phys. Lett. 318 (2000) 637.
[24] D.E. Folmer, E.S. Wisniewski, J.R. Stairs, A.W. Castleman Jr., J. Phys. Chem. A 104 (2000) 10545.
[25] S. Takeuchi, T. Tahara, Chem. Phys. Lett. 347 (2001) 108.
[26] J. Catalán, P. Pérez, J. Theor. Biol. 81 (1979) 213.
[27] J. Catalán, O. Mó, P. Pérez, M. Yáñez, Tetrahedron 39 (1983) 2851.
[28] A. Douhal, V. Guallar, M. Moreno, J.M. Lluch, Chem. Phys. Lett. 256 (1996) 370.
[29] M.S. Gordon, J. Phys. Chem. 100 (1996) 3974.
[30] V. Guallar, M. Moreno, J.M. Lluch, Chem. Phys. 228 (1998) 1.
[31] S. Mente, M. Maroncelli, J. Phys. Chem. A 102 (1998) 3860.
[32] J. Catalán, J.C. Del Valle, M. Kasha, Proc. Natl. Acad. Sci. USA 96 (1999) 8338.
[33] G.M. Chaban, M.S. Gordon, J. Phys. Chem. A 103 (1999) 185.
[34] A. Fernández-Ramos, Z. Smedarchina, W. Siebrand, M.Z. Zgierski, M.A. Ríos, J. Am. Chem. Soc. 121 (1999) 6280.
[35] A.M. Graña, J. Mol. Struct. (THEOCHEM) 466 (1999) 145.
[36] V. Guallar, V.S. Batista, W.H. Miller, J. Chem. Phys. 110 (1999) 9922.
[37] J. Catalán, J.C. del Valle, M. Kasha, Chem. Phys. Lett. 318 (2000) 629.
[38] A. Douhal, M. Moreno, J.M. Lluch, Chem. Phys. Lett. 324 (2000) 75.
[39] A. Kyrychenko, Y. Stepanenko, J. Waluk, J. Phys. Chem. A 104 (2000) 9542.
[40] Z. Smedarchina, W. Siebrand, A. Fernández-Ramos, L. Gorb, J. Leszczynski, J. Chem. Phys. 112 (2000) 566.
[41] A. Fernández-Ramos, Z. Smedarchina, W. Siebrand, M.Z. Zgierski, J. Chem. Phys. 114 (2001) 7518.
[42] M. Moreno, A. Douhal, J.M. Lluch, O. Castaño, L.M. Frutos, J. Phys. Chem. A 105 (2001) 3887.
[43] J.R. Van Hise, Mol. Phys. 99 (2001) 1347.
[44] M. Moreno, J.M. Lluch, A. Douhal, in: A. Douhal, J. Santamaría (Eds.), Femtochemistry and Femtobiology, World Scientific, Singapore, 2002, p. 796.
[45] J. Catalán, P. Pérez, J.C. del Valle, J.L.G. de Paz, M. Kasha, Proc. Natl. Acad. Sci. USA 99 (2002) 5793.
[46] J. Catalán, P. Pérez, J.C. del Valle, J.L.G. de Paz, M. Kasha, Proc. Natl. Acad. Sci. USA 99 (2002) 5799.
[47] A.V. Smirnov, D.S. English, R.L. Rich, J. Lane, L. Teyton, A.W. Schwabacher, S. Luo, R.W. Thornburg, J.W. Petrich, J. Phys. Chem. B 101 (1997) 2758.
[48] A. Douhal, F. Lahmani, A.H. Zewail, Chem. Phys. 207 (1996) 477.
[49] P.-T. Chou, J. Chin. Chem. Soc. 48 (2001) 651.
[50] M. Negrerie, F. Gai, J.-C. Lambry, J.-L. Martin, J.W. Petrich, J. Phys. Chem. 115 (1993) 10158.
[51] A. Nakajima, M. Hirano, R. Asumi, K. Kaya, H. Watanabe, C.C. Carter, J.M. Williamson, T.A. Miller, J. Phys. Chem. A 101 (1997) 392.
[52] H. Yokoyama, H. Watanabe, T. Omi, S. Ishiuchi, M. Fujii, J. Phys. Chem. A 105 (2001) 9366.
[53] M.M. Francl, W.J. Pietro, W.J. Hehre, J.S. Binkley, M.S. Gordon, D.J. DeFrees, J.A. Pople, J. Chem. Phys. 77 (1982) 3654.
[54] (a) C. Lee, W. Yang, R.G. Parr, Phys. Rev. B 37 (1988) 785;
(b) A.D. Becke, J. Chem. Phys. 98 (1993) 5648.
[55] J.B. Foresman, M. Head-Gordon, J.A. Pople, M. Frisch, J. Phys. Chem. 96 (1992) 135.
[56] M.E. Casida, C. Jamorski, K.C. Casida, D.R. Salahub, J. Chem. Phys. 108 (1998) 4439.

[57] R.E. Stratmann, G.E. Scuseria, M.J. Frisch, J. Chem. Phys. 37 (1998) 785.
[58] C. Peng, P.Y. Ayala, H.B. Schlegel, M.J. Frisch, J. Comput. Chem. 17 (1996) 49.
[59] D.A. McQuarrie, Statsitical Thermodynamics, University Science Books, Mill Valley, CA, 1973.
[60] K.J. Laidler, Chemical Kinetics, third ed., Harper Collins, New York, NY, 1987.
[61] M.J. Frisch et al., Gaussian 98, Gaussian Inc., Pittsburgh, PA, 1998.
[62] L. Brillouin, C. R. Acad. Sci. 46 (1934) 618; J. Phys. 7 (1926) 353.
[63] O. Vendrell, M. Moreno, J.M. Lluch, J. Chem. Phys. 117 (2002) 7525.
[64] S. Scheiner, J. Phys. Chem. 104 (2000) 5898.

Kinetic Isotope Effect on the Photoenolization of *o*-Methylanthrone. A Microcanonical Transition State Theory Calculation

Ricard Casadesús, Miquel Moreno,* and José M. Lluch

Departament de Química, Universitat Autònoma de Barcelona, 08193 Bellaterra, Barcelona, Spain

Received: January 13, 2004; In Final Form: March 8, 2004

The photoenolization of 1,4-dimethylanthrone (1,4-MAT) and 1,4-dimethylanthrone-d_8 (1,4-DMAT) in the gas phase and in 2,2,2-trifluoroethanol (TFE) has been studied theoretically in this work. An electronic energy profile with minima and saddle-point structures is determined by density functional theory methods in the ground state (S_0) and in the triplet state (T_1). This study reveals that in the excited state an inversion of stability of the tautomers and a lower energy barrier to overcome makes the proton transfer feasible. Our molecular orbital analysis shows that upon proton transfer, T_1 changes from n,π^* to π,π^* so that a diabatic crossing takes place along the reaction coordinate. This crossing is not influenced by the presence of TFE. Also, upon the photoexcitation to the first excited singlet state (S_1) an intersystem crossing must occur to access T_1. Pure electronic calculations cannot tell us the exact point of the triplet potential energy surface that will be accessed. For this reason we have performed a microcanonical dynamic calculation taking into account the tunneling effect of the hydrogen and deuterium transfer rate constants (k_H and k_D, respectively) on T_1. After the rate-constant calculation we have also calculated the kinetic isotope effect (KIE) to compare with the experimental value. Our results indicate that the predicted large KIE for this reaction can be explained if the proton transfer takes place through tunneling at an energy slightly below the barrier.

Introduction

The study of chemical reactivity in electronically excited states is a challenging task both experimentally and theoretically. After the absorptive act the electronically excited molecule can rearrange or fragment (photochemical reaction) or can lose its excitation energy to return to the ground state (photophysical process). A number of different physical unimolecular de-excitation pathways is possible. Fluorescence and phosphorescence, depending on whether the spin multiplicity is retained or not along the transition, respectively, are radiative processes that involve the emission of electromagnetic radiation. In turn, radiationless processes involve the conversion of one molecular quantum state to another at constant energy without emission of radiation. Internal conversion (IC) and intersystem crossing (ISC), respectively, correspond to an allowed transition between electronic states of the same spin multiplicity or a forbidden transition between electronic states of different spin multiplicities.[1] In addition, bimolecular or termolecular de-excitations through the energy transfer to other molecules by collisions (thermal decay) can also occur. On the other hand, the electronically excited molecules are often born with some vibrational excitation. In this case, a vibrational relaxation can occur either by collisions with other molecules or, if collisions are infrequent (i.e., in a low pressure gas), by emission of infrared radiation. As a matter of fact, the fate of the electronically excited molecules results from a complicated and competitive interplay of all those possibilities.[2]

A classical example in this field is the photoenolization of *o*-methyl aryl ketones, which has been studied from long time ago.[3−8] The reaction mechanism, illustrated in Scheme 1 for 1,4-dimethylanthrone, is nowadays well established. High yields

SCHEME 1

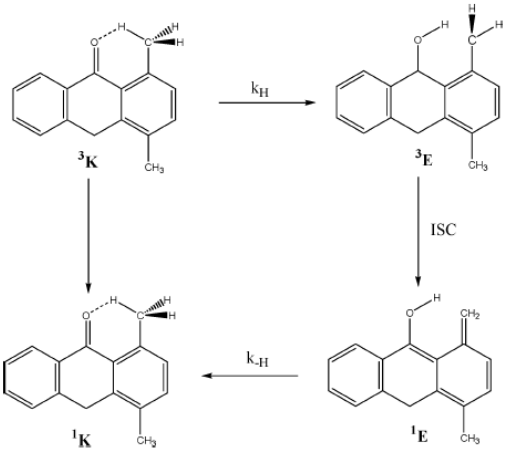

of the triplet ketone ^{3}**K** are formed by a rapid ISC after the initial excitation of the aryl ketone chromophore.[9−12] An adiabatic hydrogen transfer from the *o*-methyl group to the carbonyl oxygen occurs on the triplet surface to give a triplet enol ^{3}**E**, followed by an ISC decay to the ground-state singlet enol ^{1}**E**, which finally reverts to the starting singlet ketone ^{1}**K** through a hydrogen-transfer reaction to complete an overall cyclic process. Several experimental studies with conformationally restricted compounds have concluded that both hydrogen-transfer reactions occur by quantum mechanical tunneling at ultralow reaction temperatures[13−16] (e.g., 4−100 K).

o-Methylanthrones are an especially interesting case. Garcia-Garibay and co-workers have studied experimentally the pho-

* Corresponding author. E-mail: mmf@klingon.uab.es.

10.1021/jp040025a CCC: $27.50
Published on Web 04/21/2004

toenolization of 1,4-dimethylanthrone (1,4-MAT) and 1,4-dimethylanthrone-d_8 (1,4-DMAT) in methylcyclohexane, ethanol, and 2,2,2-trifluoroethanol.[17] They have determined the hydrogen/deuterium-transfer rates of the triplet ketone ^{3}**K** by emission spectroscopy at very low temperatures. These reaction rates were calculated from the total triplet decay rate by subtracting contributions from radiative (phosphorescence) and thermal processes, which were assumed from model compounds lacking the *o*-methyl group (for instance, anthrone or 2,3-dimethylanthrone). They have shown that deuterium transfer of the triplet ketone ^{3}**K** in 1,4-DMAT at very low temperatures (ca. 15−90 K) is slow enough to compete with radiative and thermal decay and so, phosphorescence emission was detected. In the case of 1,4-DMAT in ethanol a curved Arrhenius plot of the total triplet decay rate indicated that deuterium transfer between 18 and 40 K occurs by quantum-mechanical tunneling, with a tunneling rate constant k_D falling between 1.5×10^3 and 7.5×10^3 s^{-1}. This value compares reasonably well with the corresponding rate calculated in methylcyclohexane (2×10^3 s^{-1} between 18 and 30 K). Very interestingly, no phosphorescence emission was observed in the nondeuterated compound 1,4-MAT. Thus Garcia-Garibay and co-workers have suggested that hydrogen transfer of the triplet ketone ^{3}**K** ($k_H \geq 10^7$ s^{-1}) is too fast to allow for phosphorescence to compete with it. Then, the large primary kinetic isotope effect ($k_H/k_D > 10^3$) in the hydrogen/deuterium-transfer rates of the triplet ketone ^{3}**K** would cause an unexpected large isotope effect on phosphorescence emission.

The purpose of this paper is to calculate the hydrogen- and deuterium-transfer unimolecular rate constants of the triplet ketone ^{3}**K** in 1,4-MAT and 1,4-DMAT, respectively, as a function of the energy, to discuss if the kinetic isotope effect (KIE) is large enough to explain the lack of phosphorescence emission in 1,4-MAT. To this aim, we will use electronic structure calculations along with the microcanonical transition state theory. Given the experimental background, quantum mechanical tunneling effects will have to be explicitly calculated.

Theoretical Methods

As we have explained before, we perform electronic and dynamic calculations to describe better the reactivity of *o*-methylanthrones. For this reason we have divided this section into two parts.

Electronic Structure Methods. Density functional theory (DFT) methods have been used in all electronic calculations, and they were performed with the double-ζ quality 6-31G(d) basis set, which includes a set of d-polarization functions on atoms other than hydrogens.[18] For the ground state, geometries and energies were obtained with the B3LYP hybrid density functional.[19] The UB3LYP hybrid density functional was used to optimize the geometries and calculate the energies of the first triplet electronic state. For the first singlet excited state (S_1) calculation we have used the time dependent DFT formalism[20,21] with the B3LYP functional.

Stationary points were located through the minimization procedure of Schlegel by using redundant internal coordinates.[22] The nature of the located stationary points was ascertained by diagonalizing the energy second-derivatives matrix. To ensure that the transition states were connecting the expected reactants and products, a full optimization of each transition state was done by slightly shifting the geometry of the transition state in either sense following the direction of the transition vector (the eigenvector corresponding to the negative eigenvalue). Diagonalization of the second derivative matrix also provides the vibrational harmonic frequencies used later for the dynamic study. This diagonalization was done both for 1,4-MAT and 1,4-DMAT.

The bulk effect of the solvent was introduced through the isodensity surface-polarized continuum model[23] (IPCM). We used an electronic density of 0.0001 au to define the cavity. The value provided for the dielectric constant was that of 2,2,2-trifluoroethanol (26.5), the most polar solvent used in the experimental study.[24] The IPCM calculations were carried out in both the ground and first triplet electronic states without reoptimization of the geometries.

All the calculations presented here were done with the Gaussian 98 series of programs.[25]

Dynamic Method. Electronic excitation from the ground singlet state (S_0) of 1,4-MAT probably leaves the molecule with some vibrational energy excess above the lowest vibrational level of the first singlet excited state (S_1). After some vibrational relaxation, the molecules populate vibrational states, which make possible the geometries in the region where S_1 and the first triplet electronic state (T_1) potential energy surfaces touch or nearly touch. Then, 1,4-MAT has a nonnegligible probability to jump to an isoenergetic vibrational level of T_1. The lost electronic energy (as T_1 is lower than S_1) is imparted to the nuclei in the form of kinetic energy, in such a way that again an excess of vibrational energy is accumulated. It is not possible to know the energy (E) with which 1,4-MAT will emerge on T_1. However, the hydrogen transfer from ^{3}**K** to ^{3}**E** will occur by quantum-mechanical tunneling only if $E < V^{AG}$, where V^{AG} is the corresponding adiabatic vibrational ground-state energy barrier in the triplet electronic state. As a consequence, we have calculated the rate constants within a range of E values around V^{AG}.

To obtain the microcanonical rate constant including tunneling in the triplet state, we have tried initially to use the following equation due to Miller,[26] which is based on the RRKM theory:[27]

$$k_{QM}(E) = \frac{(m-1)!\prod_{i=1}^{m} h\nu_i}{hE^{m-1}} \sum_{\mathbf{n}} P[E - V^{\ddagger} - \epsilon_n^{vib,\ddagger}] \quad (1)$$

with

$$\epsilon_{\mathbf{n}}^{vib,\ddagger} = \sum_{i=1}^{m-1} h\nu_i^{\ddagger}\left(n_i + \frac{1}{2}\right) \quad (2)$$

where m is the number of vibrational degrees of freedom (m = 87 for 1,4-MAT), $\{\nu_i\}$ and $\{\nu_i^{\ddagger}\}$ are respectively the normal-mode frequencies at the reactant molecule and transition state, P is the tunneling probability in the reaction coordinate, $V^{\ddagger}$ is the classical potential energy barrier, and $\mathbf{n} = n_1, n_2, ..., n_{m-1}$ are the vibrational quantum numbers. Indeed, all those magnitudes correspond to the triplet state. Note that

$$V^{AG} = V^{\ddagger} + \sum_{i=1}^{m-1} \frac{1}{2} h\nu_i^{\ddagger} \quad (3)$$

In the original formulation, the tunneling probability was calculated for a one-dimensional Eckart potential.[28] Instead, we have used here the semiclassical WKB approximation[28] substituting $P[E - V^{\ddagger} - \epsilon_{\mathbf{n}}^{vib,\ddagger}]$ in eq 1 by $P(E,\epsilon_{\mathbf{n}}^{vib,\ddagger})$:

$$P(E,\epsilon_{\mathbf{n}}^{\mathrm{vib},\ddagger}) = \begin{cases} 0 & E < E_0 \\ \dfrac{1}{1+e^{2\theta(E)}} & E_0 < E \le V^{\ddagger} + \epsilon_{\mathbf{n}}^{\mathrm{vib},\ddagger} \\ 1 - P[2(V^{\ddagger} + \epsilon_{n}^{\mathrm{vib},\ddagger}) - E] & V^{\ddagger} + \epsilon_{n}^{\mathrm{vib},\ddagger} \le E \le 2(V^{\ddagger} + \epsilon_{\mathbf{n}}^{\mathrm{vib},\ddagger}) - E_0 \\ 1 & 2(V^{\ddagger} + \epsilon_{\mathbf{n}}^{\mathrm{vib},\ddagger}) - E_0, E \end{cases} \quad (4)$$

where E_0 is the energy of the ground vibrational state of 1,4-MAT in the triplet state (the hydrogen transfer is exoergic), and $\theta(E)$ is the classical action integral through the barrier:

$$\theta(E) = \frac{1}{\hbar}\int_{s_1}^{s_2}\sqrt{2[V(s) + \epsilon_{\mathbf{n}}^{\mathrm{vib},\ddagger} - E]}\, ds \quad (5)$$

where s is the arc length along the reaction path in mass-weighted Cartesian coordinates, s_1 and s_2 are the classical turning points at energy E, and $V(s)$ is the classical potential energy (that is, without the zero-point energy correction) along the reaction path in the triplet state. This reaction path was built up by means of a linear interpolation in mass-weighted Cartesian coordinates linking the transition-state structure with the reactant structure (the ^{3}**K** minimum energy structure), and then with the product structure (the ^{3}**E** minimum energy structure). Several single-point energy calculations where necessary to obtain an energy profile of $V(s)$ so that, the integral in eq 5 could be calculated numerically through a Simpson method.

In eq 5 we have always used the transition state frequencies $\{\nu_i^{\ddagger}\}$ to evaluate the vibrational energy contribution. Although we realize that vibrational frequencies corresponding to the normal modes, which are orthogonal to the reaction path, depend on s, we assume that in the threshold region where tunneling is important those frequencies are not very different from the ones corresponding to the transition state.

The problem with eq 1 is that it involves summations of all possible vibrational quantum numbers.[29] In the case of sizable molecules such as 1,4-MAT, this implies 86 summations that become computationally unaffordable. Then, we have used the concept of density of states for vibrational modes, $\rho(E_{\mathrm{vib}})$, to substitute the multiple summations in eq 1 by just one summation over E_{vib}, the energy distributed in transition-state vibrational modes. We have employed the classical density of states for the harmonic oscillator to evaluate $\rho(E_{\mathrm{vib}})$. Although this implies the neglect of quantization of the vibrational energy levels, the huge amount of vibrational modes in 1,4-MAT makes this approximation reasonable in practice. So, the microcanonical rate constant including tunneling is finally calculated by

$$k_{\mathrm{QM}}(E) = \frac{(m-1)\prod_{i=1}^{m}\nu_i}{E^{m-1}\prod_{i=1}^{m-1}\nu_i^{\ddagger}}\sum_{E_{\mathrm{vib}}} P(E,E_{\mathrm{vib}})E_{\mathrm{vib}}^{m-2}\Delta E_{\mathrm{vib}} \quad (6)$$

where ΔE_{vib} is the vibrational energy increment and $P(E,E_{\mathrm{vib}})$ is obtained from eqs 4 and 5 by substituting $\epsilon_n^{\mathrm{vib},\ddagger}$ by E_{vib}. Indeed, the lower limit of the summation in eq 6 is the zero-point energy of the transition state (the summation of the second term in eq 3).

For the sake of comparison we have also calculated the classical microcanonical rate constant (that is, without tunneling) k_{clas}. To this aim, in eq 6 we have substituted the tunneling probability given in eq 4 by the classical expression:

$$P(E,E_{\mathrm{vib}}) = \begin{cases} 0 & E < V^{\ddagger} + E_{\mathrm{vib}} \\ 1 & E \ge V^{\ddagger} + E_{\mathrm{vib}} \end{cases} \quad (7)$$

The dynamic calculations were repeated for 1,4-DMAT, whose normal-mode frequencies and tunneling probabilities are different from the ones corresponding to the 1,4-MAT, so causing the KIE.

In this paper we have not taken into account the effect of the rotational degrees of freedom when calculating the rate constant, in such a way that eq 6 corresponds to a total angular momentum null. This should not affect the KIE in a significant way.

Results and Discussion

As in the preceding section, we present first the electronic structure results of *o*-methylanthrone and later on the dynamic results such as the rate constants of 1,4-MAT and 1,4-DMAT and the corresponding kinetic isotope effect.

Electronic Structure Results. Figure 1 depicts the energy profile for the proton-transfer processes. As can be seen, proton transfer should not occur in the ground state because of the large endothermicity of 39.11 kcal/mol and the huge energy barrier of 43.11 kcal/mol for the process. Conversely, on the triplet surface an inversion of relative tautomeric stability is shown, so that now the enol tautomer is more stable than the keto one by 4.36 kcal/mol. This fact makes the proton-transfer reaction in T_1 more likely. Hence, from the triplet-state minimum energy geometry, the energy barrier to overcome is only 7.68 kcal/mol. We have also evaluated the effect of the solvent in the energy profiles using the continuum IPCM method as described in the methodological section. Results of the IPCM calculations are given in Figure 1 inside parentheses. The energies are somewhat different from the isolated (gas phase) ones but no major changes are seen so that the basic picture of the reaction remains unchanged.

A molecular orbital analysis of both minima, ^{3}**K** and ^{3}**E**, reveals the presence of a crossing of diabatic states along the T_1 proton-transfer process. The lowest energy configurations for ^{3}**K** and ^{3}**E** minima correspond to n,π^* and π,π^* configurations, respectively. Our results also indicate that this crossing is taking place around the saddle-point region, as a mixture of both n,π^* and π,π^* characters have been found for the electronic configuration at the transition-state structure. Again this picture is not modified when the solvent effect is included. It should be noted that our theoretical results are somewhat different from the predictions made by Garcia-Garibay and co-workers[17] assuming that the keto structure of T_1 corresponds to a mixture of n,π^* and π,π^* excitations, the π,π^* character being the dominant when a more polar solvent was used. Our results indicate that, regardless of the environment, such a mixing only occurs in the transition state region.

Analysis of the geometries of the stationary points corresponding to the proton transfer in both the ground and first triplet electronic states (S_0 and T_1, respectively) reveals the presence of a symmetry molecular plane. Curiously enough, the transferring hydrogen does not belong to the symmetry plane. Conversely, this symmetry plane is not present in the enol form so that the transition state also shows the loss of this plane. Also, it is noteworthy the change in the distance of the C−C bond that involves the methyl group from which the hydrogen transfer takes place, which is followed by a change in the dihedral angle of the methyl hydrogens that gets close to 120°. On the ground state this change in distance goes from 1.51 Å in the keto form, passing the transition-state structure with 1.42 Å, to 1.37 Å in the enol form. But on the triplet state this change in distance is

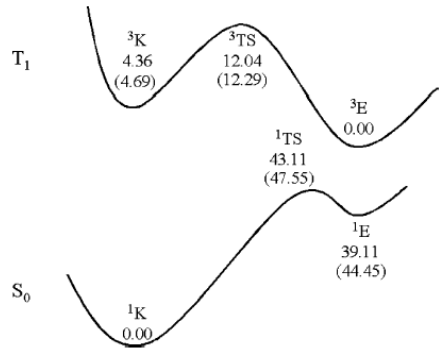

Figure 1. Energy profiles of the proton-transfer reaction coordinate for 1,4-dimethylanthrone in the ground and triplet states. Values in parentheses include the solvent effect.

reduced and goes from 1.51 Å in the keto form to 1.42 Å in the enol form, through a value of 1.49 Å in the transition state. This shortening of the carbon−carbon bond is a direct consequence of the hydrogen transfer. That is, the methyl group becomes a methylene group. This change in distance is less relevant in the triplet-state structures than in the ground-state ones so that this carbon−carbon bond of the enol form in the ground state has a stronger double bond character than in the triplet state. Concomitantly with that fact, the C−O distance of the initial keto structure increases when the oxygen atom receives the proton, the change being again less noticeable in T_1.

Related to the reaction coordinate, which essentially consists of the proton motion, the changes in distance between the carbonylic oxygen and the transferring hydrogen in the ground-state go from 2.47 Å in the keto form through a value of 1.12 Å at the transition-state structure to 0.98 Å in the final enol tautomer. In the triplet state this distance changes from 2.44 Å in the keto form to 1.24 Å in the transition state and, finally, 0.97 Å in the enol tautomer.

It is interesting to note that the initial electronic excitation in 1,4-MAT does not facilitate the proton-transfer reaction. In fact, the n → π^* excitation withdraws electronic density from the proton-acceptor oxygen atom (where the n orbital is mainly located) so that, tautomerization is disfavored. In fact, the Mulliken population analysis quantifies this change with values of −0.51 and −0.34 au for the proton-acceptor oxygen in S_0 and T_1, respectively. Conversely, the charges on the donor-carbon and transferring hydrogen do not change noticeably upon electronic excitation. The reason the proton transfer is easier in T_1 is the presence of a crossing with the π,π^* state, as this excitation does not affect oxygen but withdraws electronic density from the transferring hydrogen, making it more likely to transfer to the proton-acceptor oxygen atom.

Dynamic Results. We are now ready to analyze the proton-transfer reaction in the lowest triplet state T_1. As this state can only be obtained upon ISC from the singlet excited state initially obtained upon irradiation, a priori it is not possible to know the exact point of the triplet state potential energy surface that will be accessed. Also in this situation of nonequilibrium, temperature cannot be defined so that a calculation of the rate constant can only be done at the microcanonical level. That is, we have to calculate the rate constant at a given energy $k(E)$.

The initial photoexcitation leads the system to the first excited singlet state (S_1). We have calculated the energy corresponding to the vertical excitation from the minimum in the ground state to S_1. This Franck−Condon structure is 14.13 kcal/mol above

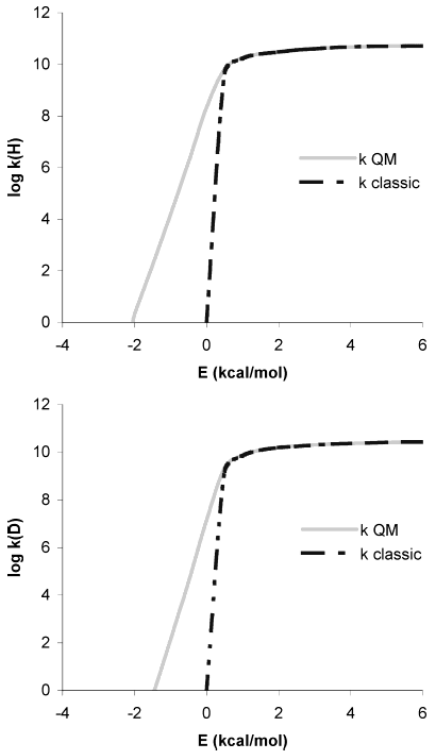

Figure 2. Graphical presentation of the logarithm of microcanonical rate constant (solid) and classical rate constant (dashed) for 1,4-dimethylanthrone (top) and 1,4-dimethylanthrone-d_8 (bottom) as a function of the energy.

the T_1 keto minimum and also well above the energy of the transition state structure for the tautomerization in T_1 (6.45 kcal/mol). So it is quite clear that upon intersystem crossing the structure may still possess enough energy to overcome the transition-state barrier and the excited-state proton transfer will occur. But we should also consider the situation when energy is not enough to overcome the adiabatic barrier and proton transfer takes place through quantum tunneling. To analyze all the possibilities, the classical RRKM theory, adapted to take into account tunneling, has been used as described in the methodological section to evaluate the rate constant at a wide range of available energies.

The obtained rate constants are depicted in Figure 2. Both the perprotio (1,4-MAT, Figure 2, top) and the deuterated (1,4-DMAT, Figure 2, bottom) species are considered as in the experimental data. We have only considered the gas phase energy profile. The energy in the plots is given relative to the transition-state structure for each isotopomer. It includes also the zero point energy so that a positive energy corresponds to an over-the-barrier process, whereas at negative energies the only operative mechanism for the reaction is through quantum tunneling. This explains the main difference between classic and quantum RRKM results shown in Figure 2 as the former suddenly fall to zero at negative energies whereas the quantum rates show a more progressive decay, tunneling becoming less probable as the energy goes further below the threshold. As the energy goes above the adiabatic barrier, both curves quickly merge so that tunneling is not playing any role when the energy is just one kcal/mol above the barrier. Of course this result

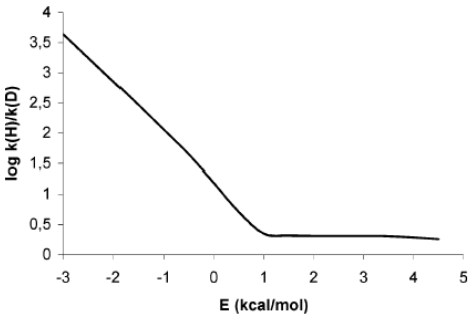

Figure 3. Kinetic isotope effect (KIE) in logarithmic scale as a function of the energy.

appears, in part, as a result of the statistical nature of the RRKM theory that does not take into acccount the actual mechanism of energy transfer between the different degrees of freedom. A more elaborated treatment taking in consideration the dynamics of the energy transfer between the different degrees of freedom would probably show that tunneling is still noticeable at energies slightly above the adiabatic barrier.

It is also to be noted that tunneling is not important when the energy is more than 0.5 kcal/mol below the transition state. This means that the only relevant zone of the reaction path is reduced to the neighbouring of the transition state. Therefore the use of transition-state frequencies as constant values does not imply significant errors.

A simple visual comparison between the 1,4-MAT and 1,4-DMAT rate constants depicted in Figure 2 reveals a clear difference between both isotopomers: the rate constant for the deuterated species decreases more rapidly at negative energies. To obtain a more clear comparison, it is necessary to evaluate the kinetic isotope effect (KIE) by dividing the values of the two rate constants at any given energy. The obtained results are depicted in Figure 3. We have only considered the quantum rate constants as these are the values actually predicted by our calculations. The decrease of tunneling of the deuterated species was, of course, to be expected given the higher mass of the transferring atom. When tunneling is not important, at positive energies, the KIE remains almost invariant taking a limit value of around 2. This value comes from the modification of the normal vibrational modes upon isotopic substitution. At negative energies the KIE rapidly increases so that at 2 kcal/mol below the barrier the KIE is already higher than 10^3.

From the obtained rate constants and the resulting KIEs, it is now possible to compare with the previous experimental data of Garcia-Garibay and co-workers.[17] One of the most striking results was the huge KIE predicted for the reaction of 10^3 or higher. This value is obtained from estimated rate constants k_H and k_D of 10^7 and 10^3 s^{-1}, respectively. Analysis of the results depicted in Figures 2 and 3 reveals that a rate constant of 10^7 s^{-1} for 1,4-MAT is obtained at energies slightly below the adiabatic barrier (around −0.5 kcal/mol). At these energies, the rate for the deuterated species is approximately 10^5 so that the KIE is around 10^2. Of course, given the approximations of our calculations, an exact match between our results and the experimental ones is not expected but the comparison clearly points to the proton-transfer reaction taking place, as expected, through tunneling. However, our results also indicate that the system energy is not far away from the classical energy threshold. At lower energies the KIE would rapidly increase (note the use of a logarithmic scale for the KIE in Figure 3) but the rate constants would become too low to be experimentally measured. On the other hand, at higher available energies, as the adiabatic energy barrier is surpassed, the isotope effect rapidly reaches the limit value given by the frequency changes upon isotopic substitution (in this case around 2.0 as commented above).

Once proton transfer in T_1 is over, another intersystem crossing has to take place to decay to the ground state singlet enol structure. Once on the ground state, the enol structure will easily revert to keto tautomer by a back proton transfer because of the quite low barrier (≤4 kcal/mol) and high exothermicity of the process.

Conclusions

Electronic calculations on the tautomerization of 1,4-dimethylanthrone (1,4-MAT) and its isotopomer 1,4-dimethylanthrone-d_8 (1,4-DMAT) for both the singlet ground state (S_0) and the first triplet state (T_1) reveal that tautomerization is very unlikely in S_0 but energetically favored in T_1 where a barrier of only 7.68 kcal/mol has to be surpassed from the minimum energy structure. In any case, T_1 can only be accessed from S_0 after photoexcitation to a higher singlet excited state (probably S_1) followed by vibrational relaxation and intersystem crossing with T_1. A calculation of the energy of the first singlet excited state at the geometry of the minimum in S_0 (Franck−Condon transition) puts the molecule 6.45 kcal/mol above the transition state structure for the tautomerization in T_1. As it is not possible to know the exact point (below that energy) where the singlet−triplet crossing takes place, purely electronic calculations cannot tell us whether the reaction in T_1 will be possible as an over-the-barrier process or it will take place through quantum tunneling.

A dynamic calculation of the microcanonical rate constant, using a modified RRKM formalism that takes into account the tunneling of the transferring hydrogen, has revealed that the rate constant rapidly decreases as energy goes below the barrier. However, the experimental proposed values of the rate constants for 1,4-MAT and 1,4-DMAT and the predicted large kinetic isotope effect of 10^3 for this reaction can only be explained if the proton transfer takes place through tunneling at an energy only slightly below the adiabatic barrier. Then our dynamic calculations provide an explanation to the lack of phosphorence emission experimentally observed for 1,4-MAT and the large kinetic isotope effect measured for the deuterated 1,4-DMAT.

Acknowledgment. We are grateful for financial support from the Spanish "Ministerio de Ciencia y Tecnología" and the "Fondo Europeo de Desarrollo Regional" through project No. BQU2002-00301, and the use of the computational facilities of the CESCA.

References and Notes

(1) Michl, J.; Bonačić-Koutecký, V. *Electronic Aspects of Organic Photochemistry*; John Wiley and Sons: New York, 1990.

(2) Turro, N. J. *Modern Molecular Photochemistry*; Benjamin Cummings Publishing Co.: Menlo Park, CA, 1978.

(3) Porter, G.; Tchir, M. F. *J. Chem. Soc., Chem. Commun.* **1970**, 1372−1373.

(4) Haag, R.; Wirz, J.; Wagner, P. J. *Helv. Chim. Acta* **1977**, *60*, 2595−2607.

(5) Das, P. K.; Encinas, M. V.; Small, R. D., Jr.; Scaiano, J. C. *J. Am. Chem. Soc.* **1979**, *101*, 6965−6970.

(6) Scaiano, J. C. *Chem. Phys. Lett.* **1980**, *73*, 319−322.

(7) Ito, Y.; Inada, N.; Matsuura, T. *J. Chem. Soc., Perkin Trans. 2* **1983**, 1857−1861.

(8) Nakayama, T.; Hamanoute, K.; Hidaka, T.; Okamoto, M.; Terenashi, H. *J. Photochem.* **1984**, *24*, 71−78.

(9) Findlay, D. M.; Tchir, M. F. *J. Chem. Soc., Faraday Trans. 1* **1976**, *72*, 1096−1100.

(10) Kumar, C. V.; Chattopadhyay, S. K.; Das, P. K. *J. Am. Chem. Soc.* **1983**, *105*, 5143−5144.
(11) Redmond, R. W.; Scaiano, J. C. *J. Phys. Chem.* **1989**, *93*, 5347−5349.
(12) Akiyama, K.; Ikegami, Y.; Tero-Kubota, S. *J. Am. Chem. Soc.* **1987**, *109*, 2538−2539.
(13) Garcia-Garibay, M. A.; Gamarnik, A.; Pang, L.; Jenks, W. S. *J. Am. Chem. Soc.* **1994**, *116*, 12095−12096.
(14) Garcia-Garibay, M. A.; Gamarnik, A.; Bise, R.; Pang, L.; Jenks, W. S. *J. Am. Chem. Soc.* **1995**, *117*, 10264−10275.
(15) Johnson, B. A.; Gamarnik, A.; Garcia-Garibay, M. A. *J. Phys. Chem.* **1996**, *100*, 4697−4700.
(16) Garcia-Garibay, M. A.; Jenks, W. S.; Pang, L. *J. Photochem. Photobiol. A* **1996**, *96*, 51−55.
(17) Gamarnik, A.; Johnson, B. A.; Garcia-Garibay, M. A. *J. Phys. Chem. A* **1998**, *102*, 5491−5498.
(18) Francl, M. M.; Pietro, W. J.; Hehre, W. J.; Binkley, J. S.; Gordon, M. S.; DeFrees, D. J.; Pople, J. A. *J. Chem. Phys.* **1982**, *77*, 3654.
(19) (a) Lee, C.; Yang, W.; Parr, R. G. *Phys. Rev. B* **1988**, *37*, 785. (b) Becke, A. D. *J. Chem. Phys.* **1993**, *98*, 5648.
(20) Casida, M. E.; Jamorski, C.; Casida, K. C.; Salahub, D. R. *J. Chem. Phys.* **1998**, *108*, 4439.
(21) Stratmann, R. E.; Scuseria, G. E.; Frisch, M. J. *J. Chem. Phys.* **1998**, *37*, 785.
(22) Peng, C.; Ayala, P. Y.; Schlegel, H. B.; Frisch, M. J. *J. Comput. Chem.* **1996**, *17*, 49.
(23) Foresman, J. B.; Keith, T. A.; Wiberg, K. B.; Snoonian, J.; Frisch, M. J. *J. Phys. Chem.* **1996**, *100*, 16098.
(24) Weast, R. C., Ed.; *Handbook of Chemistry and Physics*; The Chemical Rubber Co.: Cleveland, OH, 1970.
(25) Frisch, M. J.; Trucks, G. W.; Schlegel, H. B.; Scuseria, G. E.; Robb, M. A.; Cheeseman, J. R.; Strain, M. C.; Burant, J. C.; Stratmann, R. E.; Dapprich, S.; Kudin, K. N.; Millam, J. M.; Daniels, A. D.; Petersson, G. A.; Montgomery, J. A.; Zakrzewski, V. G.; Raghavachari, K.; Ayala, P. Y.; Cui, Q.; Morokuma, K.; Foresman, J. B.; Cioslowski, J.; Ortiz, J. V.; Barone, V.; Stefanov, B. B.; Liu, G.; Liashenko, A.; Piskorz, P.; Chen, W.; Wong, M. W.; Andres, J. L.; Replogle, E. S.; Gomperts, R.; Martin, R. L.; Fox, D. J.; Keith, T.; Al-Laham, M. A.; Nanayakkara, A.; Challacombe, M.; Peng, C. Y.; Stewart, J. P.; Gonzalez, C.; Head-Gordon, M.; Gill, P. M. W.; Johnson, B. G.; Pople, J. A. *Gaussian98*; Gaussian Inc.: Pittsburgh, PA, 1998.
(26) Miller, W. H. *J. Am. Chem. Soc.* **1979**, *101*, 6810−6814.
(27) Steinfeld, J. I.; Francisco, J. S.; Hase, W. L. *Chemical Kinetics and Dynamics*; Prentice Hall: Englewood Cliffs, NJ, 1989.
(28) Bell, R. P. *The Tunnel Effect in Chemistry*; Chapman and Hall: New York, 1980.
(29) Zhang, S.; Truong, T. N. *J. Phys. Chem. A* **2001**, *105*, 2427−2434.

ANNEX I

ALTRES PUBLICACIONS

En aquest annex es presenten la resta d'articles, un ja publicat i l'altre enviat, però pendent encara de publicació, que també formen part d'aquesta tesi doctoral. Aquests són:

- ARTICLE 4: R. Casadesús, M. Moreno, A. González-Lafont, J.M. Lluch, M.P. Repasky, "Testing electronic structure methods for describing intermolecular H···H interactions in supramolecular chemistry", *Journal of Computational Chemistry*, **25**, (2004), 99-105. [pàgina 136]

- ARTICLE 5: R. Casadesús, M. Moreno, J.M. Lluch, "On the planarity of the tropolone molecule in the $\tilde{A}^1B_2$ excited state. A time dependent DFT geometry optimisation.", *Chemical Physics Letters*, (acceptat). [pàgina 143]

Testing Electronic Structure Methods for Describing Intermolecular H · · · H Interactions in Supramolecular Chemistry

RICARD CASADESÚS,[1] MIQUEL MORENO,[1] ÀNGELS GONZÁLEZ-LAFONT,[1] JOSÉ M. LLUCH,[1] MATTHEW P. REPASKY,[2]

[1]*Departament de Química, Universitat Autònoma de Barcelona, 08193 Bellaterra, Barcelona, Spain*

[2]*Schrodinger, LLC, 120 W. 45th St., New York, New York 10036*

Received 11 May 2003; Accepted 19 August 2003

Abstract: In this article a wide variety of computational approaches (molecular mechanics force fields, semiempirical formalisms, and hybrid methods, namely ONIOM calculations) have been used to calculate the energy and geometry of the supramolecular system 2-(2′-hydroxyphenyl)-4-methyloxazole (HPMO) encapsulated in β-cyclodextrin (β-CD). The main objective of the present study has been to examine the performance of these computational methods when describing the short range H · · · H intermolecular interactions between guest (HPMO) and host (β-CD) molecules. The analyzed molecular mechanics methods do not provide unphysical short H · · · H contacts, but it is obvious that their applicability to the study of supramolecular systems is rather limited. For the semiempirical methods, MNDO is found to generate more reliable geometries than AM1, PM3 and the two recently developed schemes PDDG/MNDO and PDDG/PM3. MNDO results only give one slightly short H · · · H distance, whereas the NDDO formalisms with modifications of the Core Repulsion Function (CRF) via Gaussians exhibit a large number of short to very short and unphysical H · · · H intermolecular distances. In contrast, the PM5 method, which is the successor to PM3, gives very promising results. Our ONIOM calculations indicate that the unphysical optimized geometries from PM3 are retained when this semiempirical method is used as the low level layer in a QM:QM formulation. On the other hand, *ab initio* methods involving good enough basis sets, at least for the high level layer in a hybrid ONIOM calculation, behave well, but they may be too expensive in practice for most supramolecular chemistry applications. Finally, the performance of the evaluated computational methods has also been tested by evaluating the energetic difference between the two most stable conformations of the host(β-CD)-guest(HPMO) system.

 J Comput Chem 25: 99–105, 2004

Key words: H · · · H interactions; supramolecular chemistry; semiempirical methods; ONIOM; molecular mechanics

Introduction

Today, one of the most important research fields in chemistry is the study of large systems. In this sense, one of the most active research areas is the field of supramolecular chemistry,[1] which involves the use of noncovalent interactions to assemble molecules into stable, well-defined structures and which plays an important role in biological processes. Thus, it is crucial to examine the interactions between molecules and their environment. Well-known systems include host–guest and protein–substrate complexes, molecular clusters, or simply molecules within their medium.

Currently, there is great interest in the theoretical study of supramolecular systems. For this purpose, molecular mechanics (MM) or semiempirical methods are the most widely used as *ab initio* and Density Functional Theory (DFT) methods are prohibitively expensive in treating such large systems. Unfortunately, in general, MM and semiempirical methods do not accurately describe the geometries or energetics of intermolecular interactions. With no representation of electron density, many chemically important quantum based effects are missed. Additionally, intermolecular interactions for a number of MM force fields are known to be poorly reproduced.[2] Semiempirical methods employ approximations to accelerate solution of the Roothan-Hall equations; thus,

Correspondence to: J. M. Lluch; e-mail: lluch@klingon.uab.es

Contract/grant sponsor: the Spanish "Ministerio de Ciencia y Tecnología" and the "Fondo Europeo de Desarrollo Regional"; contract/grant number: BQU2002-00301

they are quantum mechanical in nature and are an improvement over MM methods in accounting for quantum phenomena. However, empirical solutions are substituted for the large number of multielectron integrals, and these are parameterized to reproduce experimental observables for a large number of molecules. These approximations sharply limit the precision of semiempirical methods, particularly in treating systems that were not present in the initial parameterization procedure. Among the most widely used semiempirical methods are MNDO[3] (Modified Neglect of Diatomic Overlap), AM1[4] (Austin Model 1), and PM3[5] (Parametric Method 3). These methods are parametrizations of the Neglect of Diatomic Difference Overlap (NDDO) model[6] and differ primarily in the treatment of the core–core repulsion function. A concern in applying these semiempirical methods to supramolecular problems lies in the fact that they were parameterized to reproduce molecular rather than intermolecular properties. Over the last few years there have been some efforts[7–11] to improve treatment of the core parameters in semiempirical methods that play a large role in the nonreproducibility of experimental data. One particular problem of semiempirical methods is that they present an unphysical stabilization effect for short-range H · · · H interactions. The first analysis of H · · · H interactions in AM1 and PM3 was reported by Buss et al.[12] More recently, Cavitiela et al.[13] found that the H · · · H interactions were at the origin of erroneous selectivities in asymmetric synthesis. Sekušak et al.[14] noted that PM3 overestimates the strength of H · · · H interactions. Csonka et al.[15] found unphysical minima with intermolecular H · · · H distances between 1.8 and 2.0 Å in AM1 and PM3 calculations. Csonka et al.[16] also advised that the oscillating nature of the Gaussian Correction Functions (GCF) used in the evaluation of CRF in PM3 introduces energetic errors into calculated heats of formation. A further issue has been revealed in the comparison of decomposition energies for intermolecular interactions between *ab initio* methods and PM3 and AM1. Electrostatic stabilization was found to provide the majority of intermolecular attraction in *ab initio* methods, while this term is repulsive for PM3 and AM1.[17] To improve the energetic accuracy and consistency of NDDO based methods, Repasky et al.[9] have recently proposed new schemes employing Pairwise Distance Directed Gaussians (PDDG) to introduce functional group information into the CRF. Another recently introduced method is PM5,[28] which is the successor to PM3. As PDDG/MNDO, PDDG/PM3, and PM5 have only recently been introduced their performance in treating H · · · H interactions is unknown.

In the continual drive to treat ever-larger systems with ever-greater precision, theoretical chemistry has turned its interest to the so-called hybrid methods that use multiple approaches of varying accuracy and cost to simultaneously treat different parts of a system. The use of hybrid methods is very important for the study of large molecules or supramolecular systems. Within these schemes the computational cost diminishes considerably and the entire system can be considered without needing to generate simplistic model systems. Among these hybrid approaches, the ONIOM method developed by Morokuma et al.[18] is especially appealing as it can combine any quantum and MM method within one other.

With an aim toward increasing our knowledge of supramolecular interactions, in this article we focus on the short range H · · · H interactions between host and guest molecules. This study is related to a previous work[19] in which we found too short intermolecular H · · · H interactions between 2-(2′-hydroxyphenyl)-4-methyloxazole (HPMO, Scheme 1) and the β-cyclodextrin (β-CD) in which HPMO was encapsulated. Cyclodextrins are cyclic oligosaccharides usually consisting of a different number of glucose units. In the case of β-CD there are seven glucopyranose units. These compounds form a hydrophobic cavity, and are able to embed guests of the appropriate size. We theoretically studied this host–guest system using ONIOM(RHF/6-31G(d):PM3). Surprisingly, rather short intermolecular R—C—H · · · H—C—R′ distances (less than 2.00 Å) between the host (β-CD) and guest (HPMO) were found.

A very limited body of work regarding the treatment of intermolecular H · · · H interactions using semiempirical methods was found in the literature. For this reason we have examined the performance of different computational methods when describing H · · · H interactions in a host–guest supramolecular system. We will use the structures of HPMO encapsulated in β-CD as a model system to test a large number of theoretical methods ranging from pure MM to "full" *ab initio* calculations.

Computational Details

A wide variety of computational methods were used to calculate the energy and geometry of the supramolecular system. For testing the capabilities of molecular mechanics methods, the MM2,[20] OPLS-AA,[21] and MMFF[22] force fields were applied. The Molecular Mechanics 2 (MM2) method of Allinger was used for geometry optimization with subsequent energy evaluations made via the Universal Force Field[23] (UFF). In MM treatments, atoms are assumed to be spherical. However, in some cases this approximation is inadequate such as when dealing with hydrogen atoms. Hydrogen possesses only a single electron, which is always involved in bonding to a neighboring atom. For this reason the electron distribution about the hydrogen nucleus is not spherical, which could affect MM description of the hydrogen bonds. Then, although the main component of the hydrogen bond energy normally comes from electrostatic attraction between the positively charged hydrogen and the negatively charged heteroatom, special caution must be taken when applying MM methods to the calculation of hydrogen bonds.[24]

We have considered the most well-known semiempirical methods based on the NDDO formalism: MNDO, AM1, PM3, as well as three recent schemes, PDDG/MNDO, PDDG/PM3, and PM5. The PDDG and PM5 methods are very recent, and as such, their performance in treating intermolecular interactions is unproven. To our knowledge, there has been no published work regarding the development, approximations, or parameterization of PM5. Our study is one of the first to show how PDDG and PM5 methods perform in describing some of the typical intermolecular interactions present in host–guest systems.

Ab initio methods are anticipated to perform better than semiempirical and MM methods, depending on the complexity of the basis set and introduction of electron correlation. Because of the size of the entire host–guest system, we have used the Restricted Hartree–Fock (RHF) formalism with the STO-3G minimum basis set.[25] As explained in the preceding section, study of

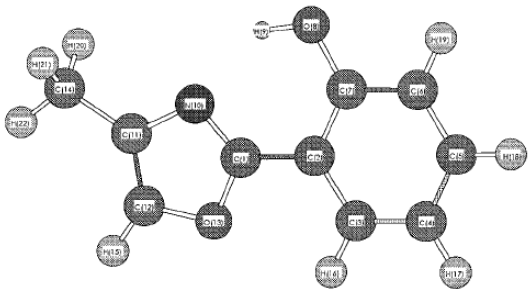

Scheme 1.

HPMO encapsulated in β-CD has also been done using hybrid methods, namely ONIOM. With this method it is possible to define up to three layers of atoms that are to be dealt with at different levels of theory. We have restricted the number of layers to only two (high and low levels). The HPMO molecule is treated in the high level layer and the β-CD in the low-level layer. Two possibilities of calculation in ONIOM were considered: mixing Quantum Mechanics (QM) with MM methods, i.e., QM:MM (IMOMM), and QM:QM (IMOMO). In the first case, RHF calculations were carried out using the split-valence 6-31G(d) basis set for the high-level layer and UFF for the low-level layer. Two cases arose in IMOMO treatment, using RHF and B3LYP with the 6-31G(d) basis set for the high-level layer and either PM3 or the STO-3G minimum basis set for the low-level layer.

MM2 calculations have been performed with the ChemOffice5.0 package. MMFF and OPLS-AA calculations were run using MacroModel.[26] MNDO, AM1, PM3, and PDDG calculations were performed using an adapted version of the MOPAC6.0 program.[27] The program was modified to include the new PDDG methods. PM5 results were generated via the CAChe 5.0 program.[28] The remaining methods, i.e., UFF, ONIOM, and RHF, have been performed with the Gaussian 98 series of programs.[29] Minimum energy structures were located through the minimization procedure of Schlegel[30] by using redundant internal coordinates in the case of calculations performed with Gaussian 98 program. For MOPAC calculations the Broyden–Fletcher–Goldfarb–Shanno[31] (BFGS) optimization procedure was used. MM2 optimizations were carried out by means of the Eigenvector Following[32] (EF) algorithm, while MMFF and OPLS-AA calculations employed the Polak–Ribiere conjugant gradient optimizer.[33]

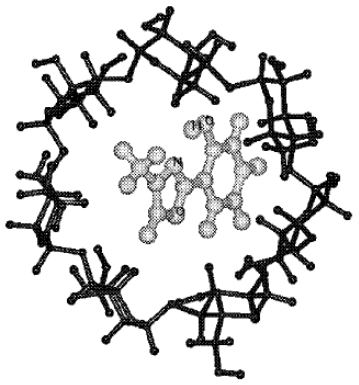

1

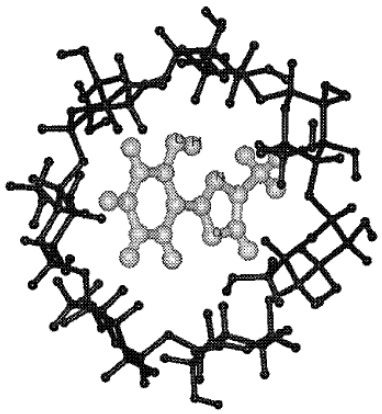

2

Figure 1. The two most stable conformations of the enol structure of HPMO encapsulated in β-CD.

Results

Equilibrium geometries of the enol structure of HPMO encapsulated in β-CD were recently analyzed.[19] By means of a quite exhaustive conformational search using the hybrid ONIOM method at the RHF/6-31G(d):PM3 level, we found two geometries of the host–guest system that were identified as the most stable conformations. Figure 1 depicts these two structures (labeled **1** and **2**), which are both lower in energy than the infinitely separated host and guest molecules. In both geometries the oxazole ring of the guest is sequestered by the CD cavity, whereas the phenol moiety is almost outside the host cavity. These results agree with experimental evidence based on ^{1}H-NMR spectra.[34] The two structures differ in the orientation of the host with respect to the guest. Considering, as usual,[35] the cavity of CD to have the shape of a truncated cone, **1** has the phenol ring near the larger diameter gate, whereas in **2** it is found near the smaller diameter gate.

Geometry optimization of both complexes has been carried out within the different levels of calculation referred to in the computational section. In all the cases minimum energy conformations

that can be ascribed either to **1** or **2** were obtained. Unsurprisingly, with such a disparate group of methods large differences in resultant geometrical parameters were obtained. Given the huge number of atoms in the supramolecular system under study, it is not practical nor actually of any interest to report here a full geometrical analysis. As explained in the introduction, our main purpose is to consider the quite elusive short-range H···H interactions that appear in a host–guest system that is linked only by (tenuous) intermolecular forces.

As we are interested in the ability of computational methods in reproducing short range H···H interactions, it is first necessary to define what constitutes an unphysically short contact. A threshold of 2.40 Å has been chosen as this corresponds to twice the van der Waals radius of hydrogen.[36] In fact, the presence of H···H distances slightly below this mark is not really significant, as the van der Waals radii are defined as the shortest distance a given atom can approach before the closed shell electronic repulsion comes to play. As the electronic distribution around a given atom depends on the entire molecular environment, the van der Waals radii are also a function of the electronic distribution. Thus, depending on whether hydrogen atoms are bonded to more or less electronegative atoms, the van der Waals radius will be respectively smaller or larger. Given that all the short H···H distances that were found correspond to hydrogen atoms bound to carbon atoms, the standard 1.20 Å value appears to be a very reasonable choice, although it should be noted that contacts lower than about 2.00 Å are not necessarily unphysical.

Results of this analysis are shown in Tables 1 and 2. The first column gives the different theoretical methods as they were presented in the computational section. They are ordered in what should be taken as increasing computational requirements so that purely MM methods are presented first followed by semiempirical methods, the hybrid ONIOM methods, and *ab initio* results are presented. The second column indicates H···H distances that fall below the chosen 2.40 Å threshold. Atom numbers are merely used to tag each particular interaction. Numbers below 22 correspond to atoms in HPMO, and larger figures indicate atoms in CD. The corresponding numeration for the HPMO is shown in Scheme 1. As for CD, it is sufficient to note that the involved hydrogen atoms are always bound to carbon atoms.

The first rows present the short H···H distances for three MM calculations. Five H···H distances shorter than 2.40 Å were observed for complex **1** and four for complex **2** with MM2. With OPLS-AA three short contacts were found for both **1** and **2**, while MMFF gave the smallest number of short contacts at one for both **1** and **2**. Most of the observed distances for the MM methods are close to the 2.40 Å limit. As such they are not necessarily indicative of an unphysical interaction.

As for the semiempirical methods, they have fewer empirical parameters trying to improve performance over MM methods. Conversely, they are much more computationally demanding as self-consistent energy calculations are now involved. However, they still suffer the flaw of needing parameters that were originally fitted for isolated molecules, and so it is again doubtful whether such methods can correctly describe supramolecular systems. Even *regular* hydrogen bonds are poorly described by semiempirical methods.[9] For instance, the MNDO and AM1 lowest energy hydrogen bond dimers are bifurcated structures while PM3 only reproduces the expected C_s dimer geometry due to an artifact in the PM3 CRF.[15] In general, semiempirical methods underestimate the strength of hydrogen bonds giving too long distances and too small energies for H-bonded systems. Although the H···H interactions in the current system are not hydrogen bonds, they apparently follow the same pattern of too short distances and too large

Table 1. Intermolecular H···H Distance (Å) Smaller than 2.40 Å Found in Complex **1** According to Different Computational Methods.

Computational method	d (H···H)
MM2/UFF	d (H14...H122) = 2.16
	d (H18...H142) = 2.15
	d (H18...H152) = 2.35
	d (H19...H114) = 2.32
	d (H20...H164) = 2.17
MMFF	d (H16...H78) = 2.38
OPLS-AA	d (H16...H78) = 2.27
	d (H16...H99) = 2.33
	d (H19...H162) = 2.26
MNDO	d (H15...H38) = 2.27
PDDG/MNDO	d (H15...H59) = 1.90
	d (H16...H78) = 1.84
	d (H17...H83) = 2.02
	d (H20...H164) = 1.89
AM1	d (H15...H59) = 2.00
	d (H16...H78) = 1.88
	d (H16...H83) = 2.34
	d (H17...H83) = 2.28
	d (H20...H143) = 2.16
	d (H20...H164) = 2.09
	d (H22...H38) = 2.28
PM3	d (H15...H59) = 1.74
	d (H16...H78) = 1.70
	d (H17...H83) = 1.84
	d (H20...H164) = 1.70
PDDG/PM3	d (H9...H141) = 2.36
	d (H15...H59) = 1.71
	d (H15...H64) = 2.31
	d (H16...H78) = 1.65
	d (H17...H83) = 2.12
	d (H20...H164) = 1.68
	d (H22...H38) = 2.31
PM5	None
ONIOM (RHF/6-31G(d):UFF)	d (H15...H59) = 2.31
	d (H16...H78) = 2.35
	d (H16...H83) = 2.36
	d (H20...H164) = 2.28
ONIOM (RHF/6-31G(d):PM3)	d (H15...H59) = 1.74
	d (H16...H78) = 1.70
	d (H17...H83) = 1.82
	d (H20...H164) = 1.70
	d (H21...H143) = 2.39
RHF/STO-3G	None
ONIOM (RHF/6-31G(d):STO-3G)	None
ONIOM (B3LYP/6-31G(d):PM3)	d (H15...H122) = 1.72
	d (H16...H99) = 1.73
	d (H21...H164) = 1.72

As for the hydrogen numbering, see text and Scheme 1.

Table 2. Intermolecular H · · · H Distances (Å) Smaller than 2.40 Å Found in Complex **2** According to Different Computational Methods.

Computational method	d (H . . . H)
MM2/UFF	d (H14 . . . H124) = 2.12
	d (H15 . . . H119) = 1.95
	d (H18 . . . H154) = 2.06
	d (H20 . . . H142) = 2.31
MMFF	d (H9 . . . H143) = 2.36
OPLS-AA	d (H9 . . . H143) = 2.27
	d (H15 . . . H59) = 2.36
	d (H16 . . . H60) = 2.33
MNDO	None
PM3	d (H9 . . . H143) = 2.39
	d (H17 . . . H64) = 1.75
	d (H16 . . . H80) = 2.36
	d (H20 . . . H120) = 1.71
	d (H21 . . . H141) = 2.38
PDDG/PM3	d (H9 . . . H143) = 1.84
	d (H15 . . . H99) = 2.37
	d (H17 . . . H64) = 1.70
	d (H20 . . . H120) = 1.65
	d (H21 . . . H141) = 2.28
PM5	d (H16 . . . H59) = 2.36
ONIOM (RHF/6-31G(d):UFF)	d (H15 . . . H78) = 2.37
	d (H20 . . . H120) = 2.33
ONIOM (RHF/6-31G(d):PM3)	d (H9 . . . H143) = 1.84
	d (H17 . . . H64) = 1.74
	d (H20 . . . H120) = 1.72
RHF(STO-3G)	d (H16 . . . H64) = 2.35
ONIOM (RHF/6-31G(d):STO-3G)	None
ONIOM (B3LYP/6-31G(d):PM3)	d (H9 . . . H143) = 1.90
	d (H17 . . . H64) = 1.74
	d (H20 . . . H120) = 1.71

As for the hydrogen numbering, see text and Figure 2.

stabilization energies observed in H-bonded systems. MNDO shows only a single short H · · · H distance for complex **1** and none for complex **2**, with the lone short contact being only shortly below the threshold. However, AM1 and PM3 methods exhibit a large number of short to very short H · · · H distances. In fact, both AM1 and, particularly, PM3, find some values that are below 1.90 Å. At these distances the interaction should be considered as a close contact that makes little physical sense.

The more recent semiempirical methods also produced mixed results. From a geometrical point of view, the problem with short H · · · H distances remains with the PDDG/PM3 method. In fact, four short H · · · H distances for complex **1** are found by PDDG/MNDO compared to only one with MNDO, whereas the PDDG version of PM3 leads to even shorter distances than PM3. This is not surprising, as the PDDG methods are local reparameterizations of the standard NDDO methods in which significant deviation from the original parameters was forbidden. As such, the PDDG methods introduced their improvements, namely greater consistency and accuracy in calculating the energies of molecules, while retaining some of the known problems with the NDDO methods, in this case their weak H · · · H repulsions.

Conversely, results are more promising for the very recent PM5 parametrization, as only one small distance (2.36 Å) appears in the two calculated geometries, with a value not far from the imposed limit. The performance of the PDDG methods in the current geometry optimization, particularly degradation in the results of PDDG/MNDO relative to MNDO, further illustrates the fact that NDDO approaches with modifications of the CRF via Gaussians are at a disadvantage when evaluating intermolecular potential energies.

To examine the strength of intermolecular repulsion between two hydrogen atoms, a repulsive energy profile as a function of intermolecular separation has been generated for the methane dimer comparing results from MNDO, AM1, PM3, PDDG/MNDO, and PDDG/PM3 with results from RHF/6-31G(d) and RHF/STO-3G calculations. This profile is shown in Figure 2. The methane molecules are arranged in a staggered orientation, and the distance between the two hydrogen atoms lying on the vector between carbon atoms was varied. The STO-3G and 6-31G(d) calculations show similar smooth repulsion profiles. MNDO is most similar to the *ab initio* profiles being slightly too repulsive. The effect of adding the PDDG Gaussians and reparameterization may be seen as the PDDG/MNDO method has a broad, spurious minimum at 1.8 Å and reduced repulsion relative to MNDO. AM1 shows weaker repulsion than PDDG/MNDO along a smoothly increasing profile. PM3 and PDDG/PM3 have similar repulsion profiles with PM3 having a minimum at 1.7 Å and PDDG/PM3 shifting this minimum to 1.6 Å. The methane dimers by PM3 and PDDG/PM3 are attractive to contacts as short as 1.5 and 1.4 Å, respectively. As AM1, PM3, and PDDG/PM3 show little to no repulsion at distances greater than 2 Å and particularly with PM3 and PDDG/PM3 being attractive to very short distances, it is

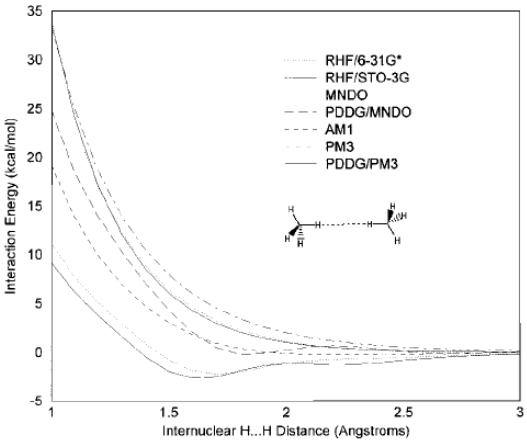

Figure 2. Energy profiles as a function of the H · · · H intermolecular distance between two methane molecules arranged in a staggered orientation. Ordering of the profiles at 1.5 Å from top to bottom: MNDO, RHF/6-31G(d), RHF/STO-3G, PDDG/MNDO, AM1, PM3, and PDDG/PM3.

unsurprising that they exhibit the largest number of short H · · · H contacts.

In going to more computer-demanding procedures, the next step are the hybrid approaches. The ONIOM method was previously used to analyze this system. As explained in the computational details section, ONIOM can take up to three different layers, though the current calculations utilize only two. The high level layer includes the host (HPMO) and it is dealt with either by the Hartree–Fock *ab initio* procedure or B3LYP Density Functional Theory with the 6-31G(d) basis set. The lower layer includes the large guest (CD), and is dealt with either by the UFF molecular mechanics procedure or by PM3. In the former, the calculation is formally of the QM:MM type (IMOMM), whereas the other two are models of QM:QM (IMOMO) calculations. It should be stressed that within the ONIOM scheme calculations of the full host + guest system are only performed using the low level method. Thus, it is not surprising that in Tables 1 and 2 very small H · · · H distances are found for the IMOMO calculations, comparable to those obtained with pure PM3. Curiously enough, the simpler IMOMM scheme appears to perform better than the IMOMO method as fewer and not-as-small short H · · · H distances are found, in good agreement with results corresponding to the pure UFF method described above.

Finally, the behavior of purely *ab initio* methods has been analyzed. Given the large size of the molecular system we were restricted to performing calculations including the entire host + guest complex at the Hartree–Fock level with the minimum basis set, STO-3G. It is well known that very accurate geometries are unlikely to be found using such a small basis set; however, analysis of a large series of different molecular systems has revealed that STO-3G geometries are usually similar to geometries from higher level basis sets. In general, STO-3G geometries are quite close, on average, to experimental values.[37] Geometrical analysis of the STO-3G results further suggests that the very small H · · · H distances found by AM1, PM3, MDDG, and PDDG are unphysical, as no short distances are found for optimized structure **1** and only one distance (2.35 Å), not far from the threshold, is found in complex **2**. To verify these results we have also carried out an ONIOM(RHF/6-31G(d):STO-3G) calculation. As seen in Tables 1 and 2, no H · · · H distances below 2.40 Å have been found at this level.

Of equal importance to the optimized geometries obtained by the range of computational methods is the computed energy difference between complexes **1** and **2**. Relative energy differences are presented in Table 3. A rather large range in energy differences was found. However, all the methods except ONIOM(RHF/6-31G(d):UFF) and MMFF find complex **1** to be more stable than complex **2**. Furthermore, all the methods that (probably correctly) predict complex **1** as being more stable have energy differences that are separated by no more than 10 kcal/mol. The largest discrepancy among the different levels is found between the ONIOM(RHF/6-31G(d):UFF) method that predicts **2** to be more stable by 2.09 kcal/mol and the RHF/STO-3G calculation that puts **1** 11.69 kcal/mol lower in energy than **2**. Whereas the simple *ab initio* STO-3G calculation is probably good enough to obtain equilibrium geometries, its energies may be subject to larger errors. Thus, the large energy difference predicted by STO-3G might not be the most accurate value. Instead, the ONIOM(RHF/6-31G(d):STO-3G) calculation in which the much more reliable 6-31G(d) basis set is used to describe the host part, provides a more reasonable energy difference (2.14 kcal/mol). In a previous article we used the ONIOM method to analyze the ground and excited states of intramolecular proton transfer in HPMO encapsulated in β-CD and found quite good agreement between our theoretical results and the experimental data if an equilibrium between **1** and **2** were present. This implies that the energy gap between the two complexes must be quite small, probably no larger than 5 kcal/mol. The PM5 value lies within this limit, and is quite close to the ONIOM(RHF/6-31G(d):STO-3G) result. This suggests that this relatively cheap procedure is promising for use in the field of supramolecular chemistry. Of course, this conclusion depends on further analysis of the performance of PM5 in treating other complicated situations. As a very recently launched method and as far as we know, detailed examination of its behavior remains to be reported.

Table 3. Relative Potential Energy (kcal/mol) of Complex **2** Taking Complex **1** as Origin of Energies.

Computational method	E
UFF	1.45
MMFF	−0.98
OPLS-AA	1.14
MNDO	7.05
PM3	7.15
PDDG/PM3	8.42
PM5	3.32
ONIOM (RHF/6-31G(d):UFF)	−2.09
ONIOM (RHF/6-31G(d):PM3)	4.43
RHF(STO-3G)	11.69
ONIOM (RHF/6-31G(d):STO-3G)	2.14
ONIOM (B3LYP/6-31G(d):PM3)	2.84

To conclude, it is clear that reliable electronic methods are needed to study supramolecular systems with a high degree of accuracy. This is balanced by the need for a reasonable computational effort. However, most of the current semiempirical methods have not been designed explicitly for describing intermolecular interactions. As a consequence shown in this article, they can present unphysical results both when used to treat the entire supramolecular system and when restricted to the low-level layer in a hybrid ONIOM calculation. On the other hand, *ab initio* methods involving good enough basis sets, at least for the high-level layer in a hybrid ONIOM calculation, behave well but they can become too expensive in practice for most of the sizeable systems currently of interest in supramolecular chemistry. At this point, the very recently developed PM5 semiempirical method seems to be promising, although additional theoretical work involving a number of other supramolecular systems would be required to generalize the trends obtained in the present article.

Acknowledgments

We are grateful for the use of the computational facilities of the CESCA.

References

1. Atwood, J. L.; Lehn, J.-M., Eds. Comprehensive Supramolecular Chemistry; Pergamon: New York, 1996, p. 3.
2. Halgren, T. A. J Comp Chem 1999, 20, 730.
3. Dewar, M. J. S.; Thiel, W. J Am Chem Soc 1977, 99, 4899.
4. Dewar, M. J. S.; Zoebisch, E. G.; Healy, E. F.; Stewart, J. P. P. J Am Chem Soc 1985, 107, 3902.
5. Stewart, J. J. P. J Comp Chem 1989, 209, 221.
6. Pople, J. A.; Beveridge, D. L. Approximate Molecular Orbital Theory; McGraw-Hill: New York, 1970.
7. Bernal–Uruchurtu, M. I.; Ruiz–López, M. F. Chem Phys Lett 2000, 330, 118.
8. Bernal–Uruchurtu, M. I.; Martins–Costa, M. T. C.; Millot, C.; Ruiz–López, M. F. J Comp Chem 2000, 21, 572.
9. Repasky, M. P.; Chandrasekhar, J.; Jorgensen, W. L. J Comp Chem 2002, 23, 1601.
10. González–Lafont, A.; Truong, T. N.; Truhlar, D. G. J Phys Chem 1991, 95, 4618.
11. Csonka, G. I. J Comp Chem 1993, 14, 895.
12. Buss, V.; Messinger, J.; Heuser, N. QCPE Bull 1991, 11, 5.
13. Cavitiela, C.; Dillet, V.; Garcia, J. I.; Mayoral, J. A.; Ruiz–López, M. F.; Salvatella, L. J Mol Struct (Theochem) 1995, 331, 37.
14. Sekušak, S.; Cory, M. G.; Bartlett, R. J.; Sabljić A. J Phys Chem A 1999, 103, 11394.
15. Csonka, G. I.; Ángyán, J. G. J Mol Struct (Theochem) 1997, 393, 31.
16. Csonka, G. I.; Éliás, K.; Csizmadia, I. G. J Comp Chem 1997, 18, 330.
17. Cummins, P. L.; Titmuss, S. J.; Jayatilaka, D.; Bliznyuk, A. A.; Rendell, A. P.; Gready, G. E. Chem Phys Lett 2002, 352, 245.
18. Dapprich, S.; Komáromi, I.; Byun, K. S.; Morokuma, K.; Frisch, M. J. J Mol Struct (Theochem) 1999, 461–462, 1.
19. Casadesús, R.; Moreno, M.; Lluch, J. M. Chem Phys Lett 2002, 356, 423.
20. Allinger, N. L. J Am Chem Soc 1977, 99, 8127.
21. Jorgensen, W. L.; Maxwell, D. S.; Tirado–Rives, J. J Am Chem Soc 1996, 118, 11225.
22. Halgren, T. A. J Comput Chem 1996, 17, 490.
23. Rappé, A. K.; Casewitt, C. J.; Colwell, K. S.; Goddard, W. A.; Skiff, W. M. J Am Chem Soc 1992, 114, 10024.
24. Jensen, F. Introduction to Computational Chemistry; John Wiley & Sons: Chichester, 1992; p. 23.
25. Hehre, W. J.; Stewart, R. F.; Pople, J. A. J Chem Phys 1969, 51, 2657.
26. Mohamadi, F.; Richards, N. G. J.; Guida, W. C.; Liskamp, R.; Lipton, M.; Caufield, C.; Chang, G.; Hendrickson, T.; Still, W. C. J Comp Chem 1990, 11, 440.
27. Stewart, J. J. P. J Comput Aided Mol Des 1990, 4, 1.
28. Stewart, J. J. P. Mopac 2002; Fujitsu Limited: Tokyo, 1999.
29. Frisch, M. J.; Trucks, G. W.; Schlegel, H. B.; Scuseria, G. E.; Robb, M. A.; Cheeseman, J. R.; Strain, M. C.; Burant, J. C.; Stratmann, R. E.; Dapprich, S.; Kudin, K. N.; Millam, J. M.; Daniels, A. D.; Petersson, G. A.; Montgomery, J. A.; Zakrzewski, V. G.; Raghavachari K.; Ayala, P.Y.; Cui, Q.; Morokuma, K.; Foresman, J. B.; Cioslowski, J.; Ortiz, J. V.; Barone, V.; Stefanov, B. B.; Liu, G.; Liashenko, A.; Piskorz, P.; Chen, W.; Wong, M. W.; Andres, J. L.; Replogle, E. S.; Gomperts, R.; Martin, R. L.; Fox, D. J.; Keith, T.; Al-Laham, M. A.; Nanayakkara, A.; Challacombe, M.; Peng, C. Y.; Stewart, J. P.; Gonzalez, C.; Head–Gordon, M.; Gill, P. M. W.; Johnson, B. G.; Pople, J. A. Gaussian98; Gaussian Inc.: Pittsburg, PA, 1998.
30. Peng, C.; Ayala, P. Y.; Schlegel, H. B.; Frisch, M. J. J Comp Chem 1996, 17, 49.
31. Shanno, D. F. J OptimisatTheory Appl 1985, 46, 87.
32. Baker, J. J Comp Chem 1986, 7, 385; 1987, 8, 563.
33. Polak, E.; Ribiere, G. Rev Fr Informat Recher Operat 1969, 16, 35.
34. García–Ochoa, I.; Díez López, M.-A.; Viñas, M. H.; Santos, L.; Martínez Ataz, E.; Amat–Guerri, F.; Douhal, A. Chem Eur J 1999, 5, 897.
35. Szejtli, J. Cyclodextrins and Their Inclusion Complexes; Académiai Kiadó: Budapest, 1982.
36. Bondi, A. J Phys Chem 1964, 68, 441.
37. Hehre, W. J.; Radom, L.; Schleyer, P. v. R.; Pople, J. A. Ab Initio Molecular Orbital Theory; John Wiley & Sons: New York, 1986.

ON THE PLANARITY OF THE TROPOLONE MOLECULE IN THE $\tilde{A}^1B_2$ EXCITED STATE. A TIME DEPENDENT DFT GEOMETRY OPTIMISATION.

Ricard Casadesús, Miquel Moreno* and José M. Lluch

Departament de Química, Universitat Autònoma de Barcelona, 08193 Bellaterra, Barcelona, Spain

Abstract

Density functional theory along with the time-dependent formalism (TD-DFT) are used to directly localise the stationary points in the $\tilde{A}^1B_2$ first singlet excited state of tropolone. The optimisation reveals that the equilibrium geometry of tropolone in the excited state is planar, a result that seems in contradiction with recent analysis of the electronic spectrum of tropolone using the high-resolution degenerate four-wave mixing (DFWM) technique that finds a large inertial defect. A theoretical evaluation of the vibrational modes reveals the presence of a very small out-of-plane frequency that could also account for the observed large inertial defect. Our full TD-DFT optimisation has also allowed a direct localisation of the transition state for the excited state intramolecular proton-transfer (ESIPT) reaction in the $\tilde{A}^1B_2$ state. According to our results the energy barrier of this process, including the zero point energy, is 7.12 kcal/mol.

Corresponding author:
Miquel Moreno
Departament de Química
Universitat Autònoma de Barcelona
08193 Bellaterra (Barcelona), Spain
FAX: +34935812920
e-mail: mmf@klingon.uab.es

INTRODUCTION

The intramolecular proton-transfer reaction in tropolone (2-hydroxy-2,4,6-cycloheptatriene-1-one) is one of the most extensively studied chemical processes both from the experimental[1-15] and the theoretical[16-22] points of view. From these studies it is now well known that the proton transfer in the ground electronic state $\widetilde{X}\,^1A_1$ occurs through a tunnelling mechanism giving a zero-point tunnelling splitting of 0.98 cm^{-1}.[12] In the first excited singlet state $\tilde{A}^1B_2$ that comes from a $\pi\rightarrow\pi^*$ electron transition, the tunnelling is considerably enhanced up to 19.85 cm^{-1}.[15] This enhancement of tunnelling is customarily attributed to a diminution of the energy barrier for the proton transfer upon electronic excitation, a fact that is confirmed by virtually all the theoretical studies carried out up to now for the excited state.[17-19,21]

In a very recent publication[15] the tunnelling-split origin region of the $\tilde{A}^1B_2$ - $\widetilde{X}\,^1A_1$ electronic absorption transition is analysed through the use of the high-resolution degenerate four-wave mixing (DFWM) technique. An adequate selection of transverse characteristics for the incident and generated electromagnetic fields participating in a resonant DFWM interaction provides a means for discriminating rovibronic transitions according to their changes in rotational angular momentum ΔJ. The rotational constants deduced from these experiments yielded unexpectedly large inertial defects, thereby suggesting that the tropolone molecule has lost its planarity upon electronic excitation. Previous theoretical calculations using the configuration interaction all singles excitation method (CIS) had come to a virtually planar equilibrium geometry.[17-19] However, Wójcik and co-workers [21] found a slightly non-planar minimum when diffuse functions were included in the split-valence basis set (6-31++G(d,p)). This lead to Bracamonte *et al*.[15] to perform again CIS calculations now with the substantial 6-311++G(d,p) basis set that has a triple-ζ quality. They come to a minimum-energy configuration of the electronically excited state clearly non-planar with a root-mean-square (rms) displacement of atomic co-ordinates from planarity of 0.305 Å.

However, the CIS method leads to very unrealistic energy barriers for the proton- transfer reaction. The use of more complete basis sets does not improve this fact. On the contrary, the barrier height of 12.0 kcal/mol obtained with the 6-31G(d,p) basis set[21] increases to 13.0 kcal/mol when adding diffuse functions (6-31++G(d,p)) and to 13.6 kcal/mol in the final calculation by Bracamonte *et al.* at the 6-311++G(d,p) level.[15] The inability of the CIS method to correctly describe the energies of proton-

transfer reactions is very well documented[23-25] and comes from the neglect of the dynamical correlation at the CIS level (which, according to the theorem of Brillouin is the electronic excited-state equivalent of the Hartree-Fock method for the ground state).[26] Introduction of the correlation can be done in the CIS scheme by using the method of perturbations of Møller-Plesset up to the second order (CIS-MP2) or including the double excitations in the configuration interactions (CISD method). However, only single-point calculations can be done at these levels as no analytic gradients are available. For the tropolone molecule, the energy corrected through either one of these methods using the CIS geometries as reference led to the erroneous prediction of negative proton-transfer barrier heights.[15] A different strategy could be envisaged using the now quite popular complete-active self-consistent field space method (CASSCF) to optimise the geometry and the CASPT2 method (that includes the correlation perturbatively up to the second order) to correct the energy. Again, the CASSCF method lacks dynamical correlation and the CASPT2 level is quite expensive and, up to now, only single-point calculations are feasible at the correlated level. For the 5-hydroxytropolone and 5-methyltropolone molecules it has been found that the CASPT2 calculations upon CASSCF optimised geometries leads also to unrealistic negative barriers.[24,27]

In the recent years, the Density Functional Theory (DFT) has become a widespread methodology that competes with conventional *ab initio* methods as it may give quite reliable results with less computational effort than the traditional methods. However DFT calculations are restricted to the ground electronic state (unless the symmetry of the excited state is different from the one of the ground state). Quite recently a scheme has been proposed to deal with excited states at the DFT level that is based on the time-dependent formalism.[28,29] The performance of this method, called TD-DFT, on different chemical processes is presently a hot topic in the world of quantum chemistry.[30-32] However, until very recently the TD-DFT method suffered the same drawback of the correlated CIS-MP2 and CASPT2 levels, that is, the analytic gradients were not available so that it was not possible to optimise geometries. Quite recently the problem of obtaining the analytic derivatives of TD-DFT energies has been solved [35] and TD-DFT geometry optimisations are now finally feasible.

In this work we have performed a TD-DFT study of the intramolecular proton-transfer reaction of tropolone in the first singlet excited electronic state. We have optimised both the minimum energy structure and the transition state so that energies

and geometries are obtained at the same level of calculation. We hope that these results will constitute a new step in the stair that leads to the understanding of the mechanism of excited state intramolecular proton-transfer reactions (ESIPT) in symmetric systems of which tropolone molecule is a paradigm. Given that the electronic spectra of tropolone are obtained with great accuracy so that the vibrational structure is partially known (and it will be for sure improved in the next future), we have also calculated the vibrational frequencies for the excited state.

CALCULATIONAL DETAILS

TD-DFT calculations have been carried out using the B3LYP method[36,37] which includes the LYP expresion and the VWN5 local correlation functional.[38] The basis set used has been the triple-ζ quality 6-311++G(d,p),[39] the same used in the recent work by Bracamonte *et al.*[15] Optimisations have been carried out using the recent 5.6 version of the TURBOMOLE program [35,40] that incorporates analytic gradients at the TD-DFT level. Optimisation of geometries is done with the Ahlrichs method.[41] For the transition state, a full geometry optimisation is performed but restricted to the C_{2v} symmetry. In order to ascertain the nature of the obtained stationary points, the second derivative energy matrix (Hessian) is obtained through numerical differentiation. No negative eigenvalues of the Hessian indicate a minimum whereas one negative eigenvalue characterises a transition state. The diagonalisation of the Hessian allows also the theoretical attainment of the vibrational frequencies of the excited state through the harmonic approximation.

RESULTS AND DISCUSSION

The optimised geometries of the stationary points located for the $\tilde{A}^1B_2$ excited state of tropolone are given in Figure 1. The more relevant interatomic distance are also given in this Figure. For clarity purposes the C-H distances, which are always 1.08 Å, are not posted. Though these geometries were directly obtained upon the Ahlrichs optimisation algorithm as implemented in the TURBOMOLE program, a second derivative calculation was also performed to insure the nature of the stationary points. As expected, we found that the structure of Figure 1a has no negative eigenvalues so that it is a true minimum and corresponds to the equilibrium geometry of the tropolone molecule in this excited state. Conversely, the geometry of Figure 1b has one imaginary frequency, so that it is a saddle point structure. Analysis of the motion along the

imaginary frequency mode confirms what is obviously seen in the geometry: the saddle point connects two equivalent minima with the hydroxylic hydrogen bonded to either one or the other oxygen. It is then the transition state for the $\tilde{A}^1B_2$ ESIPT in tropolone.

FIGURE 1 AROUND HERE

As this is one of the first optimisations of an excited electronic state carried out using the TD-DFT method, it is quite interesting to compare with previous results. Unfortunately, in the recent work of Bracamonte *et al*.[15] the geometries of the minimum and saddle point structures are not explicitly given, so that we will have to compare with the CIS/6-31++G(d,p) results of Wójcik *et al.*[21] Curiously enough, as far as we know, there is also no report of $\tilde{A}^1B_2$ tropolone geometry optimisation at the CASSCF level. Quite recently [24] we compared geometries for the substituted 5-methyltropolone with different theoretical methods and found no significant differences between CIS and CASSCF optimised equilibrium geometries (energies were not so close). Comparison of the bond distances given in Figure 1 with CIS results reveals some non negligible differences. Curiously enough, these differences are much more relevant in the minimum than in the transition state, so that whereas in the transition state the maximum difference between both sets of geometries is 0.03 Å for the O-H distances, in the minimum some distances differ by as much as 0.07 Å. It is also noteworthy that the larger differences are located in the fragment where the intramolecular proton transfer occurs. In particular these are the C=O distance (1.22 vs. 1.29 Å) and the C-C distance between the two carbon atoms bonded to oxygen (1.51 vs. 1.44 Å). To be also noted that differences are not systematically shifted either side, so that sometimes TD-DFT distances are higher than CIS ones but sometimes they are smaller.

The more controversial point related to the geometry of tropolone in the $\tilde{A}^1B_2$ state is the loss of planarity upon electronic excitation as suggested by recent experimental data and somewhat confirmed by the large basis set CIS calculations carried out previously.[15] As cited in the introduction, older CIS calculations that did not incorporate diffuse functions found a completely planar geometry but the recent CIS/6-311++G(d,p) calculation came to a clearly non-planar geometry with an rms displacement of atomic co-ordinates from planarity of 0.305 Å.[15] The discrepancy between the different results was attributed to the lack of diffuse functions in the previous calculations. However, our TD-DFT results with the same 6-311++G(d,p) basis set gives again a virtually planar geometry with a negligible rms displacement of

atomic co-ordinates from planarity of 7.55×10^{-4} Å. Of course this result seems in contradiction with the recent finding of a large inertial defect for tropolone molecule in the $\tilde{A}^1B_2$ state, that apparently points also to a non- planar geometry of tropolone in the excited state. As this is the more controversial point to be discussed in this letter and is related to the vibrational analysis to be carried out later on, we will defer the discussion until then. As for the planarity of the transition state, there is no controversy as all the calculations, including ours, predict a fully planar geometry.

Another interesting data to discuss here are the energies for the proton-transfer reaction in the excited state. The range of energy barriers obtained in the previous theoretical works goes from negative values [15] to near +20 kcal/mol [18]. Our TD-DFT calculation gives a pure electronic energy barrier of 9.61 kcal/mol, a value which is noticeably lowered to 7.12 kcal/mol when the zero point energy is accounted for. This value is clearly lower than the best estimated result using purely the CIS method (13.6 kcal/mol) but higher than the value recently reported at the TD-DFT level with CIS geometries (5.1 kcal/mol).[15] Experimentally there is no direct measure of this barrier but the large tunnelling splitting observed in the electronic spectra suggests a quite low energy barrier. As the tunnelling splitting strictly depends not only on the energy barrier but also on the length of the tunnelling path there is no way to know a priori what is the best estimate of the energy barrier. This would require a rigorous dynamical calculation of the tunnelling splitting in the global potential energy surface of the $\tilde{A}^1B_2$ electronic state of tropolone.

Let us finally analyse the vibrational harmonic frequencies for the $\tilde{A}^1B_2$ minimum calculated at the TD-DFT level. Table 1 gives the full list of vibrations ordered in decreasing frequency. As the equilibrium geometry in the excited state is planar, vibrations are classified according to their symmetry as in-plane A' or out-of-plane A".

TABLE 1 AROUND HERE

Again it is not possible a direct comparison with experimental data as detailed studies of the electronic spectra have been able to identify only quite a few number of vibrations.[6,7] These are also given in Table 1. Comparison of these cases reveals that, in general, our calculated values are quite in agreement with data obtained from analysis of the electronic spectra. In one case (the 34^{th} frequency) there is a great discrepancy between the two sets of experimental data. Our result lies between both data though much closer to the value reported by Sekiya *et al*.[7] We also give in Table 1 the

theoretical frequencies obtained at the CIS level with the 6-31++G(d,p) basis set.[21] There are not much relevant differences. We note that TD-DFT frequencies are usually higher than CIS ones obtained with a slightly smaller basis set. In Figure 2 the motion along the normal modes for which there is experimental data is given. An analogous Figure has been provided for the CIS results (see Figure 2 in Ref. 21). Though qualitatively there are no serious differences between both set of results, it is noteworthy that the arrow lengths depicting the amount of motion of each atom are quite different.

FIGURE 2 AROUND HERE

Special attention has to be devoted to the lowest frequency usually identified as ν_{26}. This out-of-plane motion is the best studied experimentally as the electronic spectra presents a nice vibrational progression, so that transitions from the ground vibrational level of ν_{39} n"=0 in S_0 to the vibrational levels n'={0,2,4,6,8,10} in the $\tilde{A}^1B_2$ electronic state have been identified.[6,7] Both experimental studies agree in that case to assign to this frequency a value of 38-39 cm^{-1}. Our theoretical calculation predicts a noticeably higher frequency of 60 cm^{-1}. Curiously enough, the CIS calculation gives a remarkably closer value (37 cm^{-1}). [21] However, given the well known deficiencies of CIS to reproduce excited state energies, this agreement has to be looked merely as a cancellation of errors. To further analyse this point, it has to be reminded that theoretical frequencies are obtained through diagonalisation of the second derivative energy matrix, so that the calculated frequencies are purely harmonic. The actual frequencies, as measured in the spectra will not coincide with harmonic values unless anharmonicity is very small. Analysis of the values for the n"$\rightarrow$n' frequencies measured in the electronic spectra reveals that they are not equally spaced as they should in a harmonic oscillator, so that anharmonicity is not disregardful. What is more, trying to fit the experimental data to an anharmonic potential including just the first anharmonic correction term (the one that depends on the square of the quantum number) gives also quite disparate results, so that anharmonicity must be very important for this deformation mode, a result which was to be expected for a motion with such a low frequency. Thus, the harmonic approximation is not to be applied for this mode. Instead, a study of the energy profile along the ν_{39} normal mode should be carried out and the vibrational levels obtained directly over this energy profile using some nuclear dynamics method. This calculation is out of the scope of the present letter.

We can now return to the question of the planarity of the tropolone molecule in the equilibrium geometry of the excited state. The large number of transitions corresponding to the ν_{39} series, seen in the electronic spectra, is one of the facts suggested to be in support of a non-planar geometry as the substantial Franck-Condon activity of this mode would be caused by the shift of the equilibrium geometry of the excited state in the direction of ν_{39} (so that breaking the planar geometry). However, as just discussed, this mode has a high degree of anharmonicity and a very low frequency, so that the nuclear wave functions are probably widespread along the configurational space giving rise to the large Franck-Condon activity observed in the electronic spectra. The other factor in favour of a non-planar geometry is the large inertial defect ΔI_0 measured by means of the DFWM technique.[15] However, as already pointed out by the same authors of the ΔI_0 measure, this large inertial defect can also be accounted for if the planar molecule exhibits a single (isolated) low-frequency out-of-plane vibration. Of course this is the case in tropolone with the ν_{39} mode. For a planar molecule the semiempirical approximation suggested by Oka can be applied:[42]

$$\Delta I_0 = -\frac{33.715}{\bar{\upsilon}} + 0.00803\sqrt{I_c} \qquad (1)$$

where I_c (in amuÅ^2) denotes the moment of inertia orthogonal to the molecular plane and $\bar{\upsilon}$ is the low frequency in cm^{-1}. Assuming a frequency of 39 cm^{-1} the inertial defect is calculated to be -0.686 amuÅ^2 , lower, in absolute value, than the value extracted from DFWM spectral simulations (-0.802 amuÅ^2) but close enough so that it is not possible to disregard this as the origin of the measured inertial defect. Also in favour of this interpretation is the fact that ν_{39} takes a much higher value of 168 cm^{-1} in the ground electronic state,[14] so that Equation (1) predicts a very small inertial defect in the ground state.

Just to close this discussion, we would like to point out that a non-planar equilibrium geometry would be in contradiction with the high tunnelling splittings measured for the $\tilde{A}^1B_2$ excited state. As the transition state for the ESIPT is planar, the whole tunnelling path would not only imply in-plane motions (the actual hydrogen transfer and reorganisation of the seven member ring) but also out-of-plane motions, as the path should approach the transition state to overcome a high energy barrier. This large tunnelling path would quench down the tunnelling splitting. Of course this reasoning is merely qualitative. A rigorous quantitative analysis would require a

dynamical calculation on the whole potential energy surface of the $\tilde{A}^1B_2$ electronic state of tropolone. Work devoted to this aim is currently in progress in our laboratory.

CONCLUSIONS

TD-DFT geometry optimisations carried out for the $\tilde{A}^1B_2$ excited state of tropolone have disclosed that the equilibrium geometry of the excited state molecule is planar (C_s symmetry). A numerical evaluation of the second derivative energy matrix has allowed the attainment of the vibrational frequencies disclosing the presence of a very small out-of-plane frequency that would account for the large inertial defect extracted from degenerate four-wave mixing (DFWM) spectral simulations of tropolone. The transition state for the ESIPT has also been directly localised. As expected it is totally symmetric, its geometry belonging to the C_{2v} symmetry group. The barrier height for the proton transfer from our calculations is predicted to be 7.12 kcal/mol (including the zero point energy correction), a value lower than the previous CIS calculations but slightly higher than the single-point TD-DFT calculations performed on the stationary points located at the CIS level.

ACKNOWLEDGMENTS

We are grateful for financial support from the Spanish “Ministerio de Ciencia y Tecnología” and the “Fondo Europeo de Desarrollo Regional” through Project No. BQU2002-00301.

REFERENCES

[1] A.C.P. Alves, J.M. Hollas, Mol. Phys. 23 (1972) 927; 25 (1973) 1305.

[2] R.L. Redington, T.E. Redington, J. Mol. Spectrosc. 78 (1979) 229.

[3] R. Rosseti, L.E. Brus, J. Chem. Phys. 73 (1980) 1546.

[4] Y. Tomioka, M. Ito, N. Mikami, J. Phys. Chem. 87 (1983) 4401.

[5] A.C.P. Alves, J.M. Hollas, H. Musa, T. Ridley, J. Mol. Spectrosc. 99 (1985) 109.

[6] R.L. Redington, Y. Chen, G.J. Scherer, R.W. Field, J. Chem. Phys. 88 (1988) 627.

[7] H. Sekiya, Y. Nagashima, Y. Nishimura, Bull. Chem. Soc. Jpn. 62 (1989) 3229; Chem. Phys. Lett. 160 (1981)581; J. Chem. Phys. 92 (1990) 5761.

[8] H. Sekiya, K. Sasaki, Y. Nishimura, Z.-H. Li, A. Mori , H. Takeshita, Chem. Phys. Lett. 173 (1990) 285.

[9] R.L. Redington, T.E. Redington, M.A. Hunter, R.W. Field, J. Chem. Phys. 92 (1990) 6456.
[10] R.L. Redington, J. Chem. Phys. 92 (1990) 6447.
[11] H. Sekiya, T. Nakajima, H. Ujita, T. Tsuji, S. Ito, Y. Nishimura, Chem. Phys. Lett. 215 (1993) 449.
[12] K. Tanaka, H. Honjo, T. Tanaka, H. Kohguchi, Y. Ohshima, Y. Endo, J. Chem. Phys. 110 (1999) 1969.
[13] R.L. Redington, T.E. Redington, J.M. Montgomery, J. Chem. Phys. 113 (2000) 2304.
[14] R.L. Redington, R.L. Sams, J. Phys. Chem. A 106 (2002) 7494.
[15] A.E. Bracamonte, P.H. Vaccaro, J. Chem. Phys. 120 (2004) 4638.
[16] R.L. Redington, C.W. Bock, J. Phys. Chem. 95 (1991) 10284
[17] M.V. Vener, S. Scheiner, N.D. Sokolov, J. Chem. Phys. 101 (1994) 9755.
[18] J.J. Paz, M. Moreno, J.M. Lluch, J. Chem. Phys. 103 (1995) 353.
[19] Z. Smedarchina, W. Siebrand, M.Z. Zgierski, J. Chem. Phys. 104 (1996) 1203.
[20] O. Mo, M. Yáñez, J. Phys. Chem. A 102 (1998) 8174.
[21] M.J. Wójcik, H. Nakamura, S. Iwata, W. Tatara, J. Chem. Phys. 112 (2000) 6322.
[22] R.L. Redington, J. Chem. Phys. 113 (2000) 2319
[23] J.F. Stanton, J. Gauss, N. Ishikawa, M. Head.Gordon, J. Chem. Phys.103 (1995) 4160.
[24] O. Vendrell, M. Moreno, J.M. Lluch, J. Chem. Phys. 117 (2002) 7525.
[25] C. Neiss, P. Saalfrank, M. Parac, S. Grimme, J. Phys. Chem. A 107 (2003) 140.
[26] J.B. Foresman, M. Head-Gordon, J.A. Pople, M.J. Frisch, J. Phys. Chem. 96 (1992) 135.
[27] J.J. Paz, M. Moreno, J.M. Lluch, J. Chem. Phys. 107 (1997) 6275.
[28] M.E. Casida, C. Jamorski, K.C. Casida, D.R. Salahub, J. Chem. Phys. 108 (1998) 4439.
[29] R.E. Stratmann, G.E. Scuseria, M.J. Frisch, J. Chem. Phys. 109 (1998) 8218.
[30] M. Parac, S. Grimme, J. Phys. Chem. A 106 (2002) 6844.
[31] A. Dreuw, J.L Weisman, M. Head-Gordon, J. Chem. Phys. 119 (2003) 2943.
[32] M. Wanko, M. Garavelli, F. Bernardi, T.A. Niehaus, T. Frauenheim, M. Elstner, J. Chem. Phys. 120 (2004) 1674.
[33] Y. Tawada, T. Tsuneda, S. Yanagisawa, T. Yanai, K. Hirao, J. Chem. Phys. 120 (2004) 8425.

[34] S. Fantacci, A. Migani, M. Olivucci, J. Phys. Chem. A 108 (2004) 1208.
[35] F. Furche, R. Ahlrichs, J. Chem. Phys. 117 (2002) 7433.
[36] C. Lee, W. Yang, R.G. Parr, Phys. Rev. B 37 (1988) 785.
[37] A.D. Becke, J. Chem. Phys. 98 (1993) 5648.
[38] S. H. Vosko, L. Wilk, M. Nusair, Can. J. Phys. 58 (1980) 1200.
[39] R. Krishnan, J.S. Binkley, R. Seeger, J.A. Pople, J. Chem. Phys. 72 (1980) 650.
[40] R. Ahlrichs, M. Bär, M. Häser, H. Horn, C. Kölmel, Chem. Phys. Lett. 162 (1989) 165.
[41] M. Von Arnim, R. Ahlrichs, J. Chem. Phys. 111 (1999) 9183.
[42] T. Oka, J. Mol. Struct. 352/353 (1995) 225.

TABLE 1. Harmonic frequencies[a] for the equilibrium structure of tropolone in the $\tilde{A}^1B_2$ excited state obtained with the TD-DFT method.

Mode	Symmetry	TD-DFT[b]	CIS[c]	Experimental
1	A’	3612	3591	
2	A’	3200	3041	
3	A’	3182	3035	
4	A’	3166	3021	
5	A’	3159	3015	
6	A’	3147	3003	
7	A’	1631	1615	
8	A’	1558	1548	
9	A’	1511	1517	
10	A’	1458	1478	
11	A’	1433	1431	
12	A’	1405	1395	
13	A’	1331	1353	
14	A’	1277	1281	
15	A’	1254	1231	
16	A’	1248	1183	
17	A’	1193	1145	
18	A’	1066	1059	
19	A’	1040	1007	
20	A”	983	945	
21	A”	950	926	
22	A’	927	899	
23	A’	883	842	
24	A”	824	827	
25	A”	778	760	
26	A’	738	703	
27	A’	690	616	
28	A”	689	675	
29	A”	650	631	
30	A”	583	575	
31	A’	523	516	
32	A”	499	477	
33	A’	440	417	415[d], 414[e]
34	A’	362	350	378[d], 296[e]
35	A’	356	317	
36	A”	346	347	
37	A”	288	259	
38	A”	173	132	164[d], 171[e]
39	A”	60	37	38[d], 39[e]

[a] In cm^{-1}.
[b] This work.
[c] From ref. 21.
[d] Experimental results from Reference 6.
[e] Experimental results from Reference 7.

FIGURE CAPTIONS

Figure 1. Geometries of the stationary points obtained in the $\tilde{A}^1B_2$ excited state through direct optimisation at the TD-DFT level. (a) Minimum. (b) Transition state for the intramolecular proton-transfer reaction. Interatomic distances are given in Å.

Figure 2. Normal modes of tropolone in the $\tilde{A}^1B_2$ excited state equilibrium geometry. The numeration refers to that in Table 1. Arrows indicate the relative direction and magnitude of the motion of each atom.

FIGURE 1

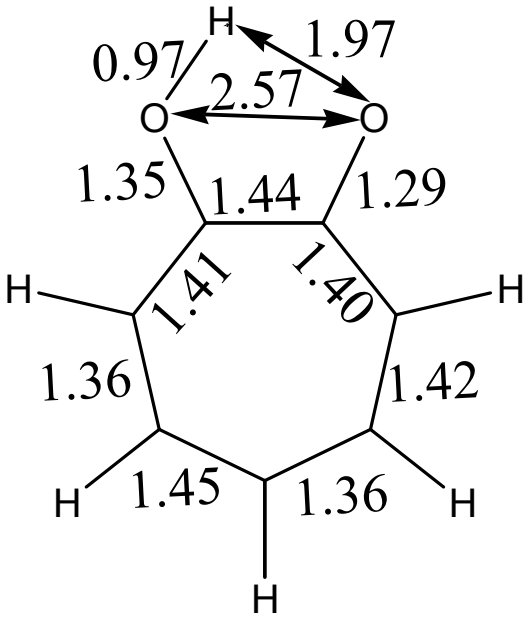
H
0.97
1.97
2.57
O
O
1.35
1.44
1.29
H
H
1.41
1.40
1.36
1.42
H
1.45
1.36
H
H

(a)

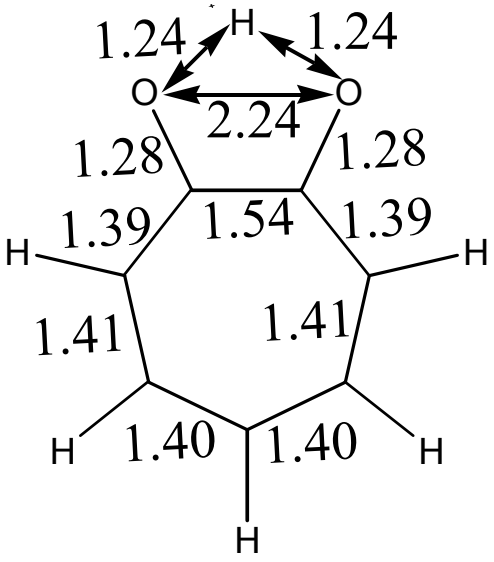
1.24
H
1.24
O
O
2.24
1.28
1.28
1.39
1.54
1.39
H
H
1.41
1.41
H
1.40
1.40
H
H

(b)

FIGURE 2

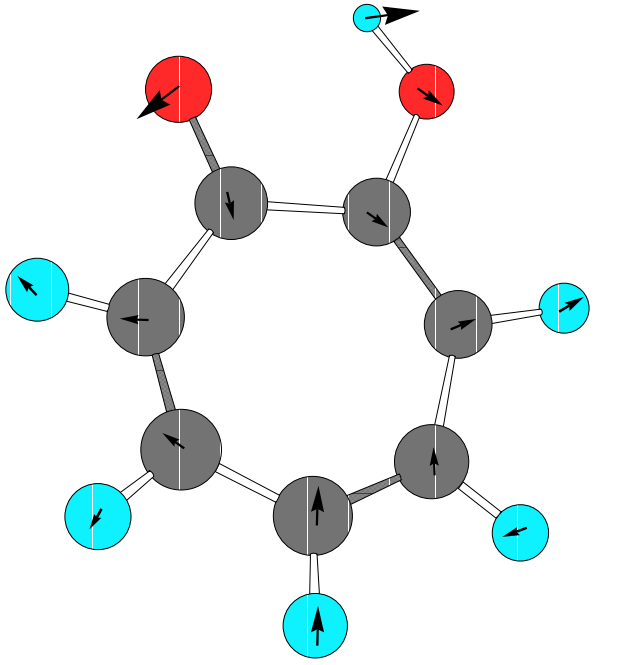

ν_{33}

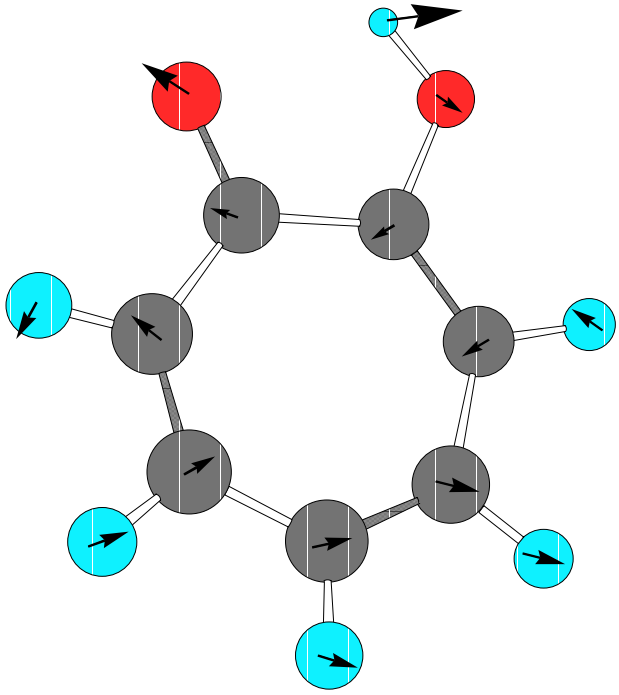

ν_{34}

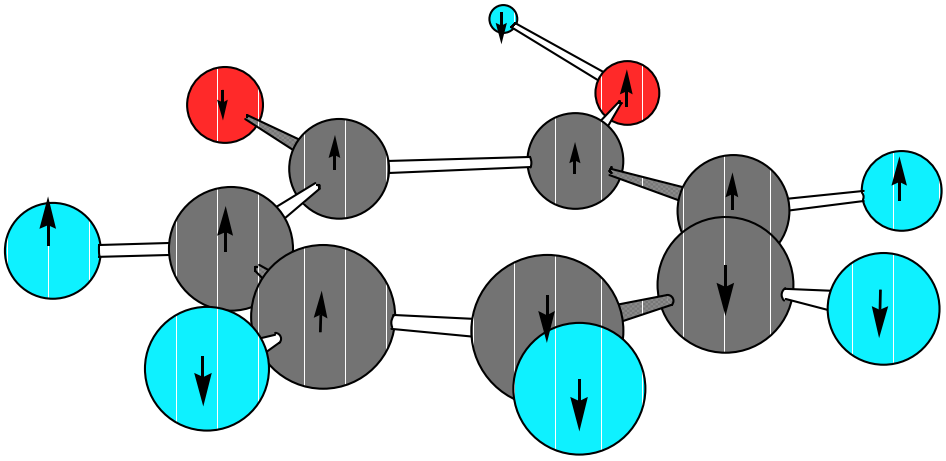

ν_{38}

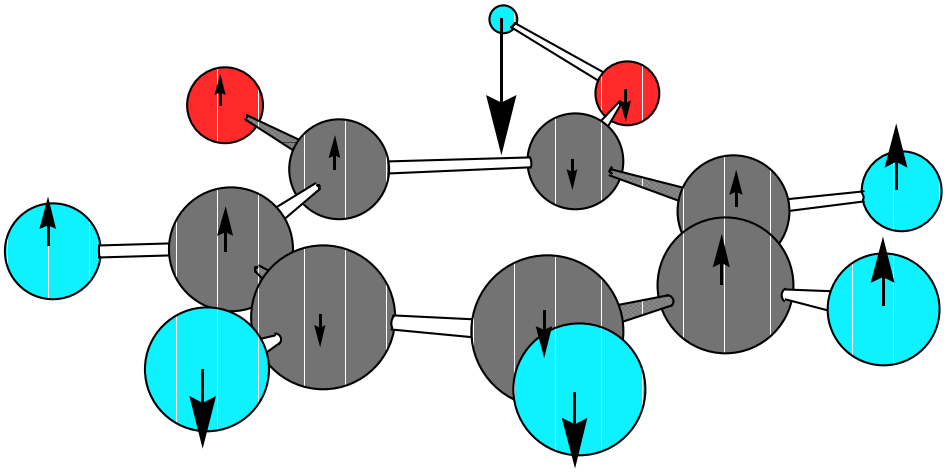

ν_{39}

A N N E X II

FONAMENTS METODOLÒGICS

Un pas previ a, pràcticament, qualsevol estudi teòric de les propietats o reactivitat d'un sistema químic consisteix en el càlcul de la funció d'ona electrònica, que contindrà tota la informació electrònica del sistema que representa. Per tal d'arribar a determinar la funció d'ona electrònica exacta d'un sistema químic aïllat són necessàries successives aproximacions.

AII.1.CÀLCUL DE L'ENERGIA I FUNCIÓ D'ONA ELECTRÒNIQUES

Els postulats de la Mecànica Quàntica estableixen que qualsevol sistema pot ser descrit per una funció d'ona Ψ. A tota magnitud física li correspon un operador lineal i hermític. L'operador que dóna l'energia del sistema s'anomena hamiltonià ($\hat{H}$). Si es té un sistema no relativista independent del temps (estats estacionaris) amb *N* nuclis amb coordenades **R** i *n* electrons amb coordenades **r**, el càlcul de l'energia del sistema passa per la resolució de l'equació d'Schrödinger independent del temps[73] que adopta la forma:

$$\hat{H}\,\Psi(\mathbf{r},\mathbf{R}) = \mathrm{E}\,\Psi(\mathbf{r},\mathbf{R}) \qquad \text{(AII-1)}$$

essent $\hat{H}$, el hamiltonià del sistema, la suma dels operadors "energia cinètica" $\hat{T}$ i "energia potencial" $\hat{V}$, $\Psi(\mathbf{r},\mathbf{R})$ la funció d'ona total i E l'energia total del sistema. Aleshores,

$$\hat{H}=\hat{T}_N+\hat{T}_e+\hat{V}(\mathbf{r},\mathbf{R})=\hat{T}_N+\hat{T}_e+\hat{V}_{NN}(\mathbf{R})+\hat{V}_{ee}(\mathbf{r})+\hat{V}_{eN}(\mathbf{r},\mathbf{R}) \qquad \text{(AII-2)}$$

[73] E. Schrödinger, *Ann. Physik*, **79**, (1926), 489; **80**, (1926), 437; **81**, (1926), 109.

en què hi apareix el terme cinètic dels nuclis $\hat{T}_N$, el terme cinètic dels electrons $\hat{T}_e$, el terme potencial d'electrons i nuclis $\hat{V}$ (**r**,**R**) que es desglosa en el terme de potencial de repulsió nuclear $\hat{V}_{NN}$(**R**), el terme de potencial de repulsió electrònica $\hat{V}_{ee}$(**R**) i el terme de potencial d'interacció nucli-electró $\hat{V}_{eN}$(**r**,**R**).

Ara bé, agrupant els termes electrònics, es defineix $\hat{H}_e$, el hamiltonià electrònic del sistema:

$$\hat{H}_e = \hat{T}_e + \hat{V}_{ee}(\mathbf{r}) + \hat{V}_{eN}(\mathbf{r},\mathbf{R}) \qquad \text{(AII-3)}$$

L'equació AII-1 no pot resoldre's exactament perquè les coordenades nuclears i electròniques estan acoblades. Per això, una aproximació habitual, donat que els nuclis són molt més pesats que els electrons, és considerar aquells fixos respecte aquests. Així, per a cada configuració nuclear, la reorganització electrònica es suposa suficientment ràpida com per considerar que els electrons estan sempre en "equilibri" (**Aproximació de Born-Oppenheimer**[74]). Aquesta aproximació permet separar el moviment electrònic del nuclear i dividir el hamiltonià en una part electrònica i una part nuclear. Això equival, de fet, a suposar que els electrons es mouen sota un potencial creat per uns nuclis "congelats" de forma que els lents desplaçaments d'aquests -molt més massius- no alteren significativament la funció d'ona electrònica. Així doncs, ara l'equació d'Schrödinger es desdobla en:

$$\hat{H}_e \Psi_i^e(\mathbf{r};\mathbf{R}) = E_i^e \Psi_i^e(\mathbf{r};\mathbf{R}) \qquad \text{(AII-4)}$$

$$\left(\hat{T}_N + U_i(\mathbf{R})\right)\Gamma_N(\mathbf{R}) = \mathrm{E_i}\,\Gamma_N(\mathbf{R}) \qquad \text{(AII-5)}$$

on $$U_i(\mathbf{R}) = E_i^e + V_{NN}(\mathbf{R}) \qquad \text{(AII-6)}$$

i

$$\Psi(\mathbf{r},\mathbf{R}) = \Psi_\mathrm{i}^\mathrm{e}(\mathbf{r};\mathbf{R})\cdot\Gamma_N(\mathbf{R}) \qquad \text{(AII-7)}$$

En aquest context, a U_i(**R**) se l'anomena "hipersuperfície d'energia potencial" i aquest potencial nuclear efectiu porta al coneixement dels nivells vibracionals i rotacionals

[74] M. Born, J.R. Oppenheimer, *Ann. Physik*, **84**, (1927), 457.

d'un determinat estat electrònic *i*. D'aquesta manera, si es vol conèixer la forma de la hipersuperfície d'energia potencial, caldrà resoldre per a cada punt de la superfície l'equació d'Schrödinger electrònica. Malauradament, per a sistemes de més d'un electró ja no és possible trobar una solució analítica. Cal recórrer, doncs, a mètodes que ajudin a superar aquest greu inconvenient.

AII.2.MÈTODES *AB INITIO*

En aquesta família de mètodes es treballa amb una Ψ aproximada inicial (funció de prova) que permeti resoldre l'equació d'Schrödinger. Els mètodes de càlcul *ab initio* convencionals basen el càlcul de l'energia d'un sistema químic en la seva funció d'ona polielectrònica.

L'inconvenient d'aquests mètodes és que, malgrat permetre fer prediccions a nivell quantitatiu, requereixen un elevat cost computacional.

AII.2.1.MÈTODES VARIACIONALS

Es considera una funció de prova ψ. Aquesta funció, en general, no serà funció pròpia del hamiltonià electrònic exacte del sistema. Llavors, l'energia electrònica es troba segons:

$$E_e = \frac{<\psi_i^e \mid \hat{H}_e \mid \psi_i^e>}{<\psi_i^e \mid \psi_i^e>} \qquad \text{(AII-8)}$$

El teorema d'Eckart[75] mostra que l'energia electrònica calculada amb aquesta funció de prova aproximada és sempre superior a l'exacta. En conseqüència, la millor funció d'ona serà aquella que doni el valor més baix de l'energia en aplicar-li l'equació AII-8. Per tant, el camí per obtenir Ψ_i^e passarà per minimitzar variacionalment E_e respecte als paràmetres de què depengui la funció de prova utilitzada. Segons quin tipus de funció de prova acceptable s'utilitzi, s'obtindran diferents mètodes:

[75] C.E. Eckart, *Phys. Rev.*, **36**, (1930), 878.

A. MÈTODE DE HARTREE-FOCK

En aquest mètode, ψ és descrita per un únic *determinant de Slater* (producte antisimetritzat de funcions monoelectròniques anomenades spin-orbitals). Minimitzant E_e respecte els spin-orbitals (χ) i imposant la condició d'ortonormalitat amb el mètode dels multiplicadors indeterminats de Lagrange s'obtenen les equacions de Hartree-Fock[76,77]. Per a un sistema de *n* electrons existeixen *n* equacions monoelectròniques del tipus:

$$\hat{f}(1)\chi_i(1) = \varepsilon_i \chi_i(1) \qquad \text{(AII-9)}$$

on $\hat{f}(1)$ és l'operador de Fock. Aquest operador és monoelectrònic i inclou de forma promitjada el potencial que experimenta un electró a causa de la presència de la resta d'electrons i nuclis. L'expressió de l'operador de Fock depèn, en conseqüència, de la forma de la funció d'ona del sistema.

Cada spin-orbital χ_i pot expressar-se com un producte d'una funció espacial (orbital molecular) ψ_i i una funció d'spin α o β segons si el valor propi de l'operador $\hat{S}_z$ és ½ o -½ respectivament:

$$\chi_i = \psi_i . \alpha \quad \text{o} \quad \overline{\chi}_i = \psi_i . \beta \qquad \text{(AII-10)}$$

A partir d'aquestes expressions s'obtenen les equacions de Fock amb orbitals enlloc de spin-orbitals.

Un dels punts claus del mètode és que l'operador de Fock depèn dels orbitals ψ_i. Per tant, les equacions s'han de resoldre de forma iterativa a partir d'uns orbitals de partida que es van optimitzant durant el procés.

Per calcular l'energia potencial d'una molècula amb una geometria concreta *R* s'haurà de resoldre l'equació de Schrödinger electrònica (AII-4), però la presència de termes bielectrònics no separables en el hamiltonià no permet fer-ho de manera exacta. Les estratègies adoptades per a la resolució d'aquest problema es poden agrupar en dos conjunts: (a) les que intenten aconseguir el hamiltonià del sistema en estudi introduint pertorbacions en el $\hat{H}$ d'un sistema més senzill però conegut i (b) les que parteixen del

[76] D.R. Hartree, *Proc. Cambridge Phil. Soc.*, **24**, (1928), 89.
[77] V. Fock, *Z. Phys*., **61**, (1939), 126.

$\hat{H}$ exacte però treballen amb funcions d'ona aproximades que cal optimitzar. La primera estratègia dóna lloc als *mètodes pertorbatius* i la segona és la base dels *mètodes variacionals*, dels quals el més emprat és el del **camp autoconsistent SCF** (*Self-Consistent Field*).

La clau del mètode SCF és considerar que cada electró es mou dins el camp de potencial creat pels nuclis i la resta d'electrons del sistema, de manera que les repulsions electró-electró es tracten de manera promitjada (estrictament caldria considerar les interaccions instantànies entre els electrons ja que la posició d'un electró en un instant determinat depèn de la posició de la resta dels electrons en aquell moment). Com que la distribució d'electrons depèn del camp creat pel conjunt de nuclis i electrons, i aquest camp depèn alhora de la distribució dels electrons, la resolució del problema és iterativa: es parteix d'una distribució electrònica inicial i es calcula el camp associat a aquesta, després es contemplen els efectes que aquest camp provoca a la distribució inicial i d'aquí s'obté una segona distribució que servirà per calcular el camp de nou i així successivament fins a obtenir una distribució electrònica autoconsistent amb el seu camp associat.

A.1. Mètode *Restricted Hartree-Fock*

En el mètode *Restricted Hartree-Fock* (RHF) s'imposa una restricció a la forma dels spin-orbitals. La restricció consisteix en què dos electrons que ocupen el mateix orbital molecular siguin descrits per la mateixa funció d'ona espacial i únicament difereixin en la funció de spin:

$$\chi_{2i-1} = \psi_i(r)\cdot\alpha(\omega)$$
$$\chi_{2i} = \psi_i(r)\cdot\beta(\omega) \qquad \text{(AII-11)}$$

on $\psi_i(r)$ és la part espacial del spin-orbital i $\alpha(\omega)$ i $\beta(\omega)$ són les funcions de spin. Les equacions de Hartree-Fock que s'obtenen en aquest cas a partir del mètode variacional i imposant la condició d'ortonormalitat són:

$$\hat{f}(r_1)\psi_i(r_1) = \varepsilon_i\psi_i(r_1) \qquad \text{(AII-12)}$$

on ε_i és l'energia d'un electró a l'orbital ψ_i i $\hat{f}$ és l'operador monoelectrònic de Fock, la forma del qual depèn de ψ_i i, per tant, cal resoldre de forma iterativa aquestes equacions, partint d'una funció orbital inicial ψ^o_i.

El desenvolupament estricte del problema topa amb certes complexitats matemàtiques com ara la resolució d'un sistema d'equacions íntegro-diferencials (irresoluble numèricament per a molècules).

Tanmateix, per resoldre aquestes equacions es necessita definir unes noves funcions que, habitualment, consisteixen en expressar els orbitals moleculars ψ_i com una combinació lineal d'orbitals atòmics ϕ_j anomenades **funcions de base**. Aquesta aproximació s'anomena **OM-CLOA** (Orbitals Moleculars-Combinació Linial d'Orbitals Atòmics) i fou introduïda per Roothaan[78] i Hall[79]. Aleshores, es converteix el problema del sistema d'equacions íntegro-diferencials en un problema matricial, de resolució matemàticament més simple.

$$\psi_i = \sum_{\mu} C_{\mu i} \cdot \phi_{\mu} \qquad \text{(AII-13)}$$

on ψ_i i ϕ_μ són els orbitals moleculars i atòmics, respectivament. El conjunt de coeficients $C_{\mu i}$ són els paràmetres a optimitzar que determinen els millors orbitals moleculars obtenint-se de la resolució iterativa de les anomenades equacions de Roothaan-Hall:

$$\sum_{\mu} \left(F_{\mu\nu} - \varepsilon_i S_{\mu\nu} \right) \cdot C_{\mu i} = 0 \qquad \text{(AII-14)}$$

que en forma matricial esdevenen:

$$\mathbf{F\,C = S\,C\,E} \qquad \text{(AII-15)}$$

on **F** és la representació matricial de l'operador de Fock i **S** és la matriu de solapament, ambdues avaluades sobre la base de funcions atòmiques. **E** és una matriu diagonal que té per elements els valors de ε_i, i **C** és la matriu de coeficients (les columnes de la qual corresponen als coeficients dels orbitals moleculars). El mètode de Hartree-Fock-Roothaan-Hall és iteratiu, i comparteix amb d'altres tècniques similars el problema de la convergència.

[78] C.C.J. Roothaan, *Rev. Mod. Phys.*, **23**, (1951), 69.
[79] G.G. Hall, *Proc. Roy. Soc.*, **A 205,** (1951), 541.

Els mètodes de càlcul *ab initio* convencionals basen el càlcul de l'energia d'un sistema químic en la seva funció d'ona polielectrònica. Gairebé tots es poden considerar diferents vies d'introducció del terme de correlació electrònica a l'energia trobada mitjançant la teoria de Hartree-Fock[76,77]. Segons aquesta teoria, l'energia val:

$$E_e = \sum_{i=1}^{N} H_{ii} + \frac{1}{2}\sum_{i=1}^{N}\sum_{j=1}^{N}(J_{ij} - K_{ij}) \qquad \text{(AII-16)}$$

on N és el nombre total d'electrons en el sistema, H_{ii} representa l'energia d'un electró en un orbital molecular, J_{ij} és la integral de Coulomb, que representa la interacció repulsiva entre les distribucions de càrrega de dos electrons, i K_{ij}, la integral d'intercanvi, és la correcció de l'energia de repulsió entre dos electrons d'spins paral·lels.

A.2. Mètode *Unrestricted Hartree-Fock*

Per la seva part, el mètode UHF (*Unrestricted Hartree-Fock*) no manté la restricció d'spin, podent considerar càlculs d'estats triplets. Així s'arriba a dues sèries d'equacions:

$$\mathbf{F}^{\alpha}\,\mathbf{C}^{\alpha} = \mathbf{S}\,\mathbf{C}^{\alpha}\,\mathbf{E}^{\alpha} \quad \text{i} \quad \mathbf{F}^{\beta}\,\mathbf{C}^{\beta} = \mathbf{S}\,\mathbf{C}^{\beta}\,\mathbf{E}^{\beta} \qquad \text{(AII-17)}$$

amb dues matrius de Fock que s'han de resoldre conjuntament, ja que ambdues depenen dels coeficients $\mathbf{C}^{\alpha}$ i $\mathbf{C}^{\beta}$.

A.3. Conjunts de Funcions de Base

Els orbitals atòmics actuen com a conjunt de funcions de base, però quina forma matemàtica tenen aquests? Convé un tipus de funció que pugui descriure les característiques dels orbitals però que no dificulti l'avaluació d'integrals bielectròniques.

Si el nombre de funcions de base per descriure el sistema fos infinit (conjunt complet), es tindria la millor aproximació possible del mètode OM-CLOA. A partir d'aquí, s'obtindria l'energia límit Hartree-Fock.

Evidentment, no és possible treballar amb bases infinites. Aleshores, a la pràctica hom es veu obligat a utilitzar bases truncades. Com que l'obtenció de millors o pitjors resultats dependrà força de la qualitat de la base emprada, l'elecció del conjunt de funcions de base és un dels aspectes crucials del treball del químic teòric.

Normalment, s'utilitzen dos tipus de funcions matemàtiques per descriure els orbitals atòmics:

a) Slater (STO, *Slater Type Orbital*): dependència radial proporcional a $e^{-\xi r}$

b) Gaussiana (GTO, *Gaussian Type Orbital*): dependència radial proporcional a $e^{-\alpha r^2}$

Les funcions tipus Slater descriuen millor la densitat electrònica, però les funcions gaussianes simplifiquen el càlcul d'integrals multicèntriques i per aquesta raó són les més utilitzades. La utilització de GTO implica que per a una correcta descripció de la densitat electrònica al voltant d'un àtom s´han d'utilitzar moltes funcions de base o representar cada funció com una combinació lineal de gaussianes amb coeficients fixats.

El nombre de gaussianes emprades per descriure cada orbital atòmic serà el que caracteritzarà els diferents tipus de base:

base mínima: cada orbital ve representat per una única funció o combinació linial de funcions.

base extesa: cada orbital ve representat per més d'una funció o combinació linial de funcions. Es distingeixen les bases *doble*-ζ, *triple*-ζ, etc ... segons si l'orbital és representat per dues, tres, ... funcions o combinacions linials de funcions.

base *split valence*: és un cas intermedi entre les dues anteriors. Els orbitals interns són descrits amb una sola funció o combinació linial de funcions (base mínima), mentre que els orbitals de la capa de valència són descrits amb més d'una funció o combinació linial de funcions (base extesa).

Les bases emprades més sovint són les bases *split valence* N-21G, N-31G, doble-ζ a la capa de valència, en les que cada orbital de valència és desdoblat en dos grups de gaussianes de diferents exponents, aconseguint d'aquesta manera una major flexibilitat.

Cal destacar que sovint s'han d'afegir als conjunts de base altres funcions de polarització i/o funcions difoses per tal de descriure millor els orbitals dels àtoms, que poden tenir importància a la descripció de les propietats moleculars. Una altra consideració a fer és que la despesa computacional augmenta molt amb el nombre de funcions de base del sistema.

B. INSUFICIÈNCIES DEL MÈTODE HARTREE-FOCK

En el mètode Hartree-Fock es suposa que un electró es mou en un camp de potencial mitjà creat pels nuclis i la resta d'electrons. És a dir, no es consideren les interaccions instantànies electró-electró (correlació dinàmica). A més, per la seva naturalesa monodeterminantal no es considera la influència d'estats excitats propers en energia a l'estat fonamental (correlació no dinàmica). Per això, es diu que en el mètode Hartree-Fock els electrons no estan correlacionats. Com a conseqüència, no serà raonable aspirar a obtenir resultats quantitatius amb aquest mètode.

Si el nombre de funcions del conjunt de base fos infinit -com ja s'ha dit *a priori*- s'obtindria l'anomenat límit de Hartree-Fock (E_{HF}) que seria la millor energia que es podria obtenir dins les aproximacions d'un càlcul SCF. Però, no obstant això, no s'assoliria l'energia experimental quan aquest conjunt esdevingués complet perquè la funció d'ona electrònica Hartree-Fock, descrita per un producte antisimetritzat de spin-orbitals, només té en compte les interaccions entre electrons de forma promitjada. Caldria considerar d'alguna forma les interaccions instantànies entre els electrons, ja que la posició d'un electró en un instant donat depèn de la posició de la resta dels electrons en aquell moment. Com que els moviments dels electrons estan correlacionats per això es parla de correlació electrònica.

La correcció que caldria fer a l'energia Hartree-Fock (E_{HF}) per tal de suplir les deficiències del mètode SCF i obtenir així l'energia real (E_e), s'anomena energia de

correlació (E_{cor}). Es defineix **energia de correlació** com la diferència entre l'energia no relativista exacta i l'energia límit Hartree-Fock:

$$E_e = E_{HF} + E_{cor} \qquad \text{(AII-18)}$$

Part d'aquesta correlació ja queda inclosa dins la funció d'ona pel sol fet d'expressar-se en forma de determinant de Slater (correlació que s'anomena "bescanvi electrònic") però aquesta només fa referència a les interaccions entre electrons de spins paral·lels.

Amb l'intent d'introduir més correlació electrònica s'han desenvolupat diverses estratègies: els mètodes postHartree-Fock[80] i els mètodes basats en la Teoria del Funcional de la Densitat (DFT) que introdueixen la correlació en el hamiltonià i no pas en la funció d'ona, que es presentaran més endavant.

C. MÈTODES POSTHARTREE-FOCK

Com acabem de dir, els mètodes postHartree-Fock intenten introduir la correlació electrònica, la qual no es té en compte en el mètode SCF. Aquests es poden agrupar en: mètode d'interacció de configuracions (l'únic dels tres que és variacional), mètodes pertorbatius i els mètodes *Coupled Cluster*.

C.1. Mètode d'Interacció de Configuracions

El desenvolupament de la fotoquímica i de les tècniques experimentals associades a mesures cinètico-dinàmiques de mecanismes en estats excitats (femtoquímica) estan dirigint molts càlculs vers aquests estats. Aquesta és una tasca interessant però, alhora, difícil car els estats excitats requereixen un cost tècnico-computacional molt gran.

El mètode d'Interacció de Configuracions[81] és un mètode postHartree-Fock que incorpora la correlació electrònica. La funció d'ona s'expressa com una combinació lineal de determinants de Slater construïts a partir de les funcions monoelectròniques que s'obtenen en resoldre les equacions de Hartree-Fock:

$$\left|\Psi\right\rangle = c_0\psi_0 + \sum_a c_a^r \left|\psi_a^r\right\rangle + \sum_{ab} c_{ab}^{rs} \left|\psi_{ab}^{rs}\right\rangle + \ldots \qquad \text{(AII-19)}$$

[80] J. Andrés, J. Bertran (editors), Química Teórica y Computacional, Universitat Jaume I, Castelló, 2000.
[81] E.A. Hylleraas, *Z. Physik*, **48**, (1928), 469.

on ψ_0 és el determinant de referència (normalment el determinant Hartree-Fock), ψ_a^r és el determinant de la configuració monoexcitada on l'spin-orbital *a* s´ha substituït per l'spin-orbital *r* , ψ_{ab}^{rs} és el determinant d'una configuració diexcitada i així successivament...
Els coeficients c_a^r, c_{ab}^{rs}, ... es determinen variacionalment, així com l'energia. A més, poden optimitzar-se també els coeficients dels orbitals moleculars (mètodes multiconfiguracionals) (veure subapartat C.2).

Si es tingués una combinació lineal d'infinits determinants de Slater amb una base infinita, Ψ seria la funció d'ona exacta. Com que s'utilitzen bases truncades, es té un nombre finit de combinacions possibles de spin-orbitals. Considerar-les totes (espai "*Full-CI*"), però, és prohibitiu -excepte en sistemes petits tractats amb bases petites- per l'enorme cost computacional que se'n deriva. Per això, es fan diverses aproximacions per reduir l'espai CI (*Configuration Interaction*), truncant l'expansió, normalment, a les biexcitacions.

En la present tesi, s'ha utilitzat el mètode CIS (*Configuration Interaction Singles*), que pot entendre's com una interacció de configuracions completa a l'espai de les substitucions simples, és a dir, la funció d'ona de l'estat excitat s'expressa com a combinació linial de tots els determinants amb excitacions simples.

La determinació variacional dels coeficients CIS permet a la funció d'ona global relaxar-se. Per a sistemes de capa tancada –com són els casos aquí estudiats- la ψ_{CIS} pot descriure estats singlets i triplets sense contaminació de spin gràcies a la seva capacitat de combinar diferents determinants. A més, el mètode CIS porta a una funció d'ona ben definida, sobre la qual es poden aplicar tècniques de gradients analítics i així permetre l'optimització de geometries directes en estats excitats. El mètode CIS és *size-consistent* (consistent amb la grandària) i, segons el Teorema de Brillouin[82], els seus càlculs aplicats a l'estat fonamental corresponen al nivell Hartree-Fock.

[82] L. Brillouin, *C. R. Acad. Sci.,* **46**, (1934), 618; *J. Phys.*, **7**, (1926), 353.

C.2. Mètode CASSCF

El mètode CASSCF (*Complete Active Space Self-Consistent Field*) pertany als mètodes MCSCF (*Multi-Configuration Self-Consistent Field*). Aquests mètodes vindrien a ser com el mètode d'Interacció de Configuracions (CI) però optimitzant, a més, els orbitals moleculars usats per construir els determinants de Slater. Són també mètodes iteratius com el SCF.

L'objectiu dels mètodes CASSCF és cobrir tots els canvis que ocorren en l'energia de correlació (estàtica) per a un procés donat. El principal problema d'aquests mètodes és seleccionar les configuracions necessàries que s'han d'incloure per tenir el sistema ben definit.

Pel que fa al CASSCF, s'han de seleccionar les configuracions repartint els orbitals moleculars en l'espai actiu. Els orbitals moleculars actius solen ser els ocupats energèticament més alts i alguns dels virtuals energèticament més baixos d'un càlcul RHF, que cal fer prèviament. Entre els orbitals moleculars actius es realitza un càlcul CI i totes les configuracions apropiades per simetria s'inclouen en l'optimització CASSCF.

La decisió més important que hom ha de prendre és quins orbitals moleculars s'han d'incloure en l'espai actiu, tenint en compte el cost computacional. La notació que s'usa normalment és CASSCF(*n*, *m*), on *n* és el número d'electrons distribuïts de totes les maneres possibles en *m* orbitals.

La funció d'ona CASSCF es forma mitjançant una combinació lineal de totes les configuracions possibles que es poden construir entre els orbitals i els electrons actius consistents amb la simetria espacial i d'spin requerida.

AII.2.2.MÈTODES PERTORBACIONALS

Aquests tipus de mètodes es basen en introduir una pertobació externa al sistema per dur a terme el càlcul d'aquest. Aquesta pertorbació farà que s'afegeixin termes (lineals i quadràtics) extra al hamiltonià que descriu el sistema. Així tindrem:

$$\hat{H} = \hat{H}_0 + \lambda\hat{P}_1 + \lambda^2\hat{P}_2 \qquad \text{(AII-20)}$$

on $\hat{H}_0$ és l'operador hamiltonià electrònic estàndard, $\hat{P}_1$ i $\hat{P}_2$ són els operadors que descriuen la pertorbació i λ és un factor multiplicatiu que determina el grau d'aplicació de la pertorbació.

Hi ha diferents mètodes pertorbatius, però els més comuns són el Møller-Plesset i, més recentment, el *Coupled Cluster*.

AII.2.2.1. MÈTODE *COUPLED CLUSTER*

El mètode *Coupled Cluster* (CC) té la seva base en els mètodes pertorbatius i pretén incloure totes les correccions d'un tipus donat per a un ordre infinit. Aquestes correccions poden ser *Singles*, *Doubles*, ... en referència al nombre d'excitacions de la funció d'ona. En el cas del CCSD (*Coupled Cluster Singles and Doubles*), la correcció es trunca al segon ordre.

La funció d'ona CC es descriu així:

$$\Psi_{CC} = e^{\hat{T}}\Phi_0 \qquad \text{(AII-21)}$$

on $e^{\hat{T}} = 1 + \hat{T} + \frac{1}{2}\hat{T}^2 + \frac{1}{6}\hat{T}^3 + ... = \sum_{k=0}^{\infty}\frac{1}{k!}\hat{T}^k$,

on l'operador de *cluster* ($\hat{T}$) s'expandeix en funció dels operadors d'excitació ($\hat{T}_i$) com $\hat{T} = \hat{T}_1 + \hat{T}_2 + \hat{T}_3 + ... + \hat{T}_N$.

Aquest operador $\hat{T}_i$ actuant sobre una funció d'ona Hartree-Fock genera *i* determinants d'Slater:

$$\hat{T}_1\Phi_0 = \sum_{i}^{oc}\sum_{a}^{vir} t_i^a \Phi_i^a$$

$$\hat{T}_2\Phi_0 = \sum_{i<j}^{oc}\sum_{a<b}^{vir} t_{ij}^{ab}\Phi_{ij}^{ab} \qquad \text{(AII-22)}$$

on *t* són els coeficients d'expansió o amplituts del *cluster*.

D'aquesta manera, en la construcció de l'operador exponencial, es genera un primer terme de referència Hartree-Fock, seguit del segon terme que correpon a totes les monoexcitacions, el tercer correspon a tots els estats doblement excitats, ...

Partint, doncs, de l'equació de Schrödinger amb la funció d'ona CC

$$\hat{H}e^{\hat{T}}\Phi_0 = E_{CC}e^{\hat{T}}\Phi_0 \qquad \text{(AII-23)}$$

obtenim $E_{CC} = \langle \Phi_0 | \hat{H}e^{\hat{T}} | \Phi_0 \rangle$ (AII-24)

En el cas CCSD, es truncarà als estats doblement excitats i, per tant, tindrem que $\hat{T} = \hat{T}_1 + \hat{T}_2$ i $e^{\hat{T}_1+\hat{T}_2} = 1 + \hat{T}_1 + \left(\hat{T}_2 + \frac{1}{2}\hat{T}_1^2\right) + \ldots$

Tenint en compte això, segons el desenvolupament exposat abans, s'obtindran les amplituts i l'energia de correlació.

AII.3.MÈTODES SEMIEMPÍRICS

Aquest grup de mètodes simplifica el càlcul de l'energia Hartree-Fock mitjançant l'aproximació del recobriment diferencial zero (ZDO, *Zero Diferential Overlap*). Usa només bases mínimes pels electrons de valència, no contemplant així les funcions de polarització i difoses i la correlació electrònica només s'inclou en els paràmetres. L'ús de paràmetres ajustats empíricament redueix la construcció de la matriu de Fock de $O(M^4)$ a $O(M^2)$.

AII.3.1.MÈTODE MNDO

El mètode MNDO[83] (*Modified Neglect of Diatomic Overlap*) és un mètode semiempíric parametritzat per diversos àtoms (H, C, N, O, ...) a partir del model NDDO[84] (*Neglect of Diatomic Differential Overlap Approximation*).

El MNDO és previ al PM3 i AM1, però tots ells es basen en el NDDO encara que es diferencien en la forma de tractar el potencial *core-core* i en l'assignació dels paràmetres. Malgrat això, el MNDO encara s'utilitza en alguns tipus de càlculs perquè sembla donar millors resultats que aquests.

[83] M.J.S. Dewar, W. Thiel, *J. Am. Chem. Soc.*, **99**, (1977), 4899.
[84] J.A. Pople, D.L. Beveridge, Approximate Molecular Orbital Theory, McGraw-Hill, New York, 1970.

No obstant això, el MNDO presenta moltes limitacions, com per exemple: la descripció que fa de les interaccions febles, no predir bé els enllaços d'hidrogen, predir energies massa grans per a la formació i trencaments d'alguns tipus de reaccions, ...

Concretament, el potencial de repulsió *core-core* que usa el MNDO, considerant A i B dos àtoms qualssevol, és:

$$V_{nn}(A,B) = Z'_A Z'_B \langle s_A s_B | s_A s_B \rangle \left(1 + e^{-\alpha_A R_{AB}} + e^{-\alpha_B R_{AB}}\right) \qquad \text{(AII-25)}$$

on α són paràmetres d'ajust.

Però per a les interaccions que impliquen enllaços O-H i N-H, el potencial és:

$$V_{nn}(A,H) = Z'_A Z'_H \langle s_A s_H | s_A s_H \rangle \left(1 + \frac{e^{-\alpha_A R_{AH}}}{R_{AH}} + e^{-\alpha_H R_{AH}}\right) \qquad \text{(AII-26)}$$

AII.3.2.MÈTODE AM1

Dins el grup dels mètodes semiempírics, s'hi troba també l'AM1 (*Austin Model 1*) creat pel Prof. M.J.S. Dewar[85] (Universitat d'Austin, Texas) que sorgeix com a conseqüència dels errors sistemàtics que es troben en el mètode MNDO. Així, l'AM1 és una modificació del MNDO. L'AM1 ha estat parametritzat per diversos elements entre els quals s'hi troben els que s'estudien en aquesta tesi (H, C, O i N). No obstant això, i a part de ser semiempíric, presenta –com tot mètode- limitacions. Dues d'elles són la tendència a exagerar els enllaços d'hidrogen i la mala predicció de les interaccions de Van der Waals.

AII.3.3.MÈTODE PM3

El Prof. J.J.P. Stewart[86] creà el PM3 (*Parametric Method 3*) fent un procés d'optimització automàtic a partir d'implementar fórmules de l'AM1 i així poder optimitzar tots els paràmetres simultàniament. En aquesta reparametrització, l'expressió de repulsió *core-core* és la mateixa que en AM1 excepte que només s'assignen dues funcions gaussianes per àtom. El PM3 ha estat parametritzat per diferents elements d'entre els quals s'hi troben també els que s'estudien aquí (H, C, O i N). Les limitacions més importants del PM3 –tenint en compte que és un mètode semiempíric- són: predir,

[85] M.J.S. Dewar, E.G. Zoebisch, E.F. Healy, J.J.P. Stewart, *J. Am. Chem. Soc.*, **107**, (1985), 3902.
[86] J.J.P. Stewart, *J. Comput. Chem.*, **209**, (1989), 221.

sistemàticament, els enllaços d'hidrogen més curts que l'experimental, no predir bé les interaccions de van der Waals i predir unes barreres de rotació massa baixes per enllaços amb cert caràcter de doble enllaç sobretot pel cas de l'enllaç C-N.

AII.3.4.MÈTODES PDDG

El PDDG[87] (*Pairwise Distance Directed Gaussian*) és un nou mètode elaborat pel grup del Prof. W. Jorgensen que es basa en la modificació de les funcions de repulsió de *core* (CRF) en els mètodes semiempírics PM3 i MNDO del programa MOPAC 6.0. D'aquesta reparametrització, sorgeixen els mètodes PDDG/MNDO i PDDG/PM3. Aquests mètodes neixen del fet d'intentar eliminar errors sistemàtics del PM3 i MNDO i minimitzar els errors globals en el càlcul dels calors de formació en aquests dos mètodes.

AII.3.5.MÈTODE PM5

El mètode PM5[29] (*Parametric Method 5*) és un mètode molt recent i, per ara, hi ha molt pocs treballs publicats. Amb això, es vol dir que la seva aplicació no ha estat posada a prova encara en molts aspectes. A més, no hi ha cap publicació, fins avui, sobre el seu desenvolupament i parametrització, la qual cosa fa que hi hagi una certa obscuritat sobre aquest mètode i el seu funcionament. Pel que sembla, el PM5 és una reparametrització del l'anterior mètode de Stewart (PM3) amb millores. El PM5 es troba incorporat dins el programa MOPAC2002.

AII.4.MÈTODES EMPÍRICS: MECÀNICA MOLECULAR

La Mecànica Molecular tracta els nuclis dels àtoms com a masses puntuals clàssiques de Newton que es mouen per una funció d'energia potencial (camp de forces conservatiu) definida pels núvols electrònics del voltant. No es determina la posició dels electrons, ni tan sols es tenen en compte explícitament; les posicions dels nuclis defineixen directament les forces que actuen entre ells.

[87] M.P. Repasky, J. Chandrasekhar, W.L. Jorgensen, *J. Comput. Chem.*, **23**, (2002), 1601.

Els models de Mecànica Molecular descriuen els àtoms com esferes subjectes a una atracció i repulsió mútua. Tanmateix, la Mecànica Molecular té limitacions: les dades energètiques que s'obtenen no tenen cap sentit físic per sí soles. A més, només es poden considerar diferències energètiques en determinades situacions, ja que l'energia obtinguda depèn del nombre d'àtoms i de la seva connectivitat. A més, no es tenen en compte els efectes electrònics.

AII.4.1.MÈTODE MM2

El MM2 (*Molecular Mechanics 2*) és un mètode creat per N.L. Allinger[88] que es basa en la mecànica molecular. Per al càlcul de l'energia utilitza la següent expressió:

$$E = \sum E_s(l) + \sum E_b(\theta) + \sum E_t(\omega) + \sum E_{vdW}(r) + \sum E_{sb} \qquad \text{(AII-27)}$$

Aquests termes són, respectivament: l'energia associada a la vibració dels enllaços (*stretching*), l'energia de deformació dels angles (*bending*), l'energia adscrita a les rotacions internes (*torsional*), l'energia de les interaccions de van der Waals i el terme d'acoblament energètic *stretching-bending*.

AII.4.2.MÈTODE UFF

Un altre tipus de parametrització dels camps de força en mecànica molecular és el UFF (*Universal Force Field*). L'UFF usa un nombre reduït de conjunts de paràmetres que troba a partir de les constants atòmiques (radi atòmic, potencial d'ionització, electronegativitat, polaritzabilitat, ...). En principi, l'UFF pot calcular molècules que continguin qualsevol àtom de, pràcticament tota, la taula periòdica. Encara que aquest mètode és menys acurat en el càlcul d'energies que el MM2, les geometries les calcula qualitativament correctament.

[88] N.L. Allinger, *J. Am. Chem. Soc.*, **99**, (1977), 8127.

AII.5.MÈTODES DEL FUNCIONAL DE LA DENSITAT[89]

Els mètodes Hartree-Fock presentats abans tenen l'inconvenient de que, malgrat permetre fer prediccions a nivell quantitatiu, requereixen un elevat cost computacional. En canvi, els mètodes basats en la Teoria del Funcional de la Densitat introdueixen la correlació electrònica en l'expressió de l'energia amb un cost computacional molt inferior als mètodes *ab initio* convencionals, i donant resultats comparables amb alguns mètodes postHartree-Fock, els quals són més cars computacionalment.

La Teoria del Funcional de la Densitat parteix dels teoremes formulats per Hohenberg i Kohn el 1964[90].

Aquests sostenen que, coneguda la densitat electrònica $\rho(\mathbf{r})$ d'un sistema de N electrons, es té prou informació com per determinar completament les propietats electròniques del seu estat fonamental (no degenerat). Llavors, l'energia en funció de la densitat electrònica del sistema vindria donada per l'expressió:

$$E[\rho] = T[\rho] + E_{ee}[\rho] + V_{ext}[\rho] \qquad \text{(AII-28)}$$

on T és l'energia cinètica dels electrons, E_{ee} és el potencial de repulsió electró-electró i V_{ext} és el potencial extern aplicat sobre els electrons, en absència d'altres pertorbacions, el potencial d'interacció nucli-electró. És a dir,

$$V_{ext}[\rho] = \int \rho(\mathbf{r})\nu(\mathbf{r})d\mathbf{r} \qquad \text{(AII-29)}$$

essent $\nu(\mathbf{r})$ el potencial local nucli-electró.

Ara bé, $E_{ee}[\rho] = J[\rho] + K[\rho]$, on J i K són, respectivament, els potencials d'interacció coulòmbica i d'intercanvi electrònic.

L'ús dels mètodes DFT en química computacional va veure's augmentat gràcies a la introducció d'orbitals en el formalisme per Kohn i Sham[91].

[89] F. Jensen, Introduction to Computational Chemistry, John Wiley & Sons, Chichester, 1999.
[90] P. Hohenberg, W. Kohn, *Phys. Rev.*, **136**, (1964), B864.
[91] W. Kohn, L.J. Sham, *Phys. Rev.*, **140**, (1965), A1133.

La idea en que es basa el formalisme de Kohn-Sham és dividir el funcional d'energia cinètica ($T[\rho]$) en dues parts, una de les quals pot ser calculada exactament (T_S), més un terme de correlació (T_C).

De la solució exacta de l'equació de Schrödinger electrònica s'obtindria el funcional d'energia cinètica exacta ($T[\rho]$). Com que això no és possible, en comptes d'això, es resol iterativament el sistema de N equacions monoelectròniques anomenades equacions de Kohn-Sham, a partir de les quals s'obtindrà $T_S[\rho]$.

$$\hat{h}_{ks}\varphi_i = \left[-\frac{1}{2}\nabla^2 + \nu_{eff}(\mathbf{r})\right]\varphi_i = \varepsilon_i\varphi_i \qquad \text{(AII-30)}$$

on $\hat{h}_{KS}$ és el hamiltonià de Kohn-Sham que conté ν_{eff}, l'anomenat potencial efectiu de Kohn-Sham, que es defineix com:

$$\nu_{eff}(\mathbf{r}) = \nu(\mathbf{r}) + \int \frac{\rho(\mathbf{r}')}{|\mathbf{r}-\mathbf{r}'|} d\mathbf{r}' + \nu_{xc}(\mathbf{r}) \qquad \text{(AII-31)}$$

essent ν_{xc}:

$$\nu_{xc}(\mathbf{r}) = \frac{\partial E_{XC}[\rho]}{\partial \rho(\mathbf{r})} \qquad \text{(AII-32)}$$

La clau de la teoria de Kohn-Sham és el càlcul de l'energia cinètica assumint la no interacció dels electrons; és a dir, $T_S = \sum_{i=1}^{N} \langle \varphi_i | -\frac{1}{2}\nabla^2 | \varphi_i \rangle$. No obstant això, realment els electrons sí interaccionen i, per tant, T_S no proporciona l'energia cinètica total, encara que la diferència entre aquesta i l'exacta sembla ser petita.

Aquesta energia cinètica que no contempla T_S (T_C) s'inclou en un terme de correlació-intercanvi ($E_{XC}[\rho]$). Així l'expressió de l'energia DFT pot escriure's com:

$$E_{DFT}[\rho] = T_S[\rho] + V_{ext}[\rho] + J'[\rho] + E_{XC}[\rho] \qquad \text{(AII-33)}$$

Així, com que $E[\rho]$ i $E_{DFT}[\rho]$ són iguals, restant l'equació AII-28 de la AII-33 s'obtindrà E_{XC}:

$$E_{XC}[\rho] = (T[\rho] - T_S[\rho]) + (E_{ee}[\rho] - J'[\rho]) \qquad \text{(AII-34)}$$

d'on agrupem l'energia cinètica de correlació i les energies potencials d'intercanvi i correlació electròniques:

$T_C[\rho] = T[\rho] - T_S[\rho]$ i $\tilde{E}_{XC}[\rho] = E_{ee}[\rho] - J'[\rho] = (J[\rho] - J'[\rho]) + K[\rho]$

on *J'[ρ]* és el potencial clàssic de repulsió electrònica,

$$J'[\rho] = \frac{1}{2}\int\int \frac{\rho(\mathbf{r}_1)\rho(\mathbf{r}_2)}{\mathbf{r}_{12}} d\mathbf{r}_1 d\mathbf{r}_2 \qquad \text{(AII-35)}$$

essent $\boldsymbol{r_{12}} = |\boldsymbol{r_1} - \boldsymbol{r_2}|$.

Finalment, doncs, quedaria: $E_{XC}[\rho] = T_C[\rho] + \tilde{E}_{XC}[\rho]$ (AII-36)

Però el problema de tot el desenvolupament del mètode DFT és que no coneixem exactament el valor de $E_{XC}[\rho]$.

Existeixen dos tipus d'aproximacions per calcular-lo: les aproximacions de la densitat local (LDA) i les aproximacions generalitzades de gradient (GGA). Ambdues categories suposen que s'està en presència d'un gas uniforme d'electrons, de manera que els termes d'intercanvi i de correlació es poden tractar independentment. En concret, segons aquestes aproximacions, podríem escriure l'energia d'intercanvi (E_X) i correlació (E_C) com:

$$E_{XC}[\rho] = E_X[\rho] + E_C[\rho] \qquad \text{(AII-37)}$$

i així obtenir l'energia total a partir de:

$$E_{DFT}[\rho] = T_S[\rho] + V_{ext}[\rho] + J'[\rho] + E_X[\rho] + E_C[\rho] \qquad \text{(AII-38)}$$

AII.5.1.MÈTODES AMB LDA

L'aproximació de densitat local[92] LDA (*Local Density Approximation*) consisteix en considerar que E_{XC} és només funció de la densitat electrònica. Llavors,

[92] O. Gunnarsson, I. Lundquist, *Phys. Rev.,* **B10**, (1974), 1319.

l'energia d'intercanvi es pot calcular en termes de la densitat d'un gas uniforme d'electrons:

$$E_X(\rho) = -\frac{3}{4}\left(\frac{3}{\pi}\right)^{\frac{1}{3}} \int \rho^{\frac{4}{3}}(\mathbf{r})d\mathbf{r} \qquad \text{(AII-39)}$$

Quant a l'energia de correlació E_C, es determina a partir d'una de les diverses parametritzacions que es poden trobar a la literatura. La més usada és la VWN[93], basada en simulacions de Monte Carlo.

L'inconvenient que s'observa en els càlculs DFT amb LDA és que en nombrosos sistemes l'energia E_{XC} està sobreestimada, el que es tradueix en una exageració de l'energia d'enllaç.

AII.5.2.MÈTODES AMB GGA

Les aproximacions que utilitzen algun tipus de correcció de gradient tenen en compte les fluctuacions locals que conté la densitat electrònica, és a dir, que el gas d'electrons no és uniforme.

Així, en aquests mètodes, el terme E_{XC} depèn tant de la densitat com del seu gradient. Generalment, s'afegeix un terme de correcció de gradient al funcional d'intercanvi de l'aproximació local (AII-39), com és el cas del funcional de Becke de 1988[94].

Per això, ha aparegut una sèrie de mètodes de càlcul que també afegeixen una correcció de gradient al funcional de correlació de l'aproximació local. D'aquí provenen els potencials de Perdew de 1986[95] i 1991[96], i el LYP de Lee, Yang i Parr de 1988[97].

[93] S.H. Vosko, L. Wilk, M. Nusair, *Can. J. Phys.*, **58**, (1980), 1200.
[94] A.D. Becke, *Phys. Rev.,* **A38**, (1988), 3098.
[95] J.P. Perdew, *Phys. Rev.,* **B33**, (1986), 8822.
[96] P. Ziesche, H. Eschring (editors), Electronic Structure of Solids, Akademie, Berlín, 1991.
[97] C. Lee, W. Yang, R.G. Parr, *Phys. Rev.,* **B37***,* (1988), 785.

AII.5.3.MÈTODES AMB FUNCIONALS HÍBRIDS

Són una alternativa als mètodes amb GGA, i es basen en la introducció de l'energia d'intercanvi exacta trobada en l'aproximació Hartree-Fock (E_x^{HF}).

De fet, l'energia de Hartree-Fock, que en funció de la densitat es formula com:

$$E[\rho] = T[\rho] + J[\rho] + K[\rho] + V_{ext}[\rho] \qquad \text{(AII-40)}$$

es pot considerar com un cas especial de la DFT on $J'[\rho] = J[\rho]$, $E_X[\rho] = K[\rho]$, $E_C[\rho] = 0$ i $T[\rho] = T_S[\rho]$.

El mètode híbrid més simple és l'anomenat *half and half* [98], que aplica un funcional al qual E_x^{HF} i E_c^{LDA} hi contribueixen cadascun en un 50%.

D'altres mètodes més complexos es basen en dades empíriques per determinar la proporció amb què cal que contribueixi cada terme energètic. Per exemple, el mètode B3LYP i el seu anàleg sense restricció d'spin UB3LYP, desenvolupats a partir del que Becke proposà el 1993[99], combina l'energia d'intercanvi de Hartree-Fock (E_x^{HF}) amb el funcional d'intercanvi d'Slater[100] (E_x^{Slater}), la correcció de gradient del funcional d'intercanvi de Becke de 1993[99] (ΔE_x^{B93}), l'energia de correlació local de Vosko, Wilk i Nusair[93] (E_c^{VWN}) i la correcció de gradient del funcional de correlació no local de Lee, Yang i Parr[97] (ΔE_c^{LYP}):

$$E_{xc} = A \cdot E_x^{Slater} + (1-A) \cdot E_x^{HF} + B \cdot \Delta E_x^{B93} + E_c^{VWN} + C \cdot \Delta E_c^{LYP} \qquad \text{(AII-41)}$$

Els paràmetres A, B i C van ser establerts per Becke ajustant-los a valors experimentals d'energies d'atomització, potencials d'ionització, afinitats protòniques i energies atòmiques de diversos sistemes.

Ara per ara, el caràcter semiempíric dels funcionals híbrids constitueix l'únic problema a superar en aquests mètodes de càlcul DFT.

[98] A.D. Becke, *J. Chem. Phys.,* **98**,(1993), 1372.
[99] A.D. Becke, *J. Chem. Phys.,* **98**, (1993), 5648.
[100] J.C. Slater, Quantum Theory of Molecular and Solids, McGraw-Hill, New York, 1974.

AII.5.4.MÈTODE *TIME DEPENDENT DFT*

Els mètodes DFT són mètodes que no contemplen, per sí sols, l'estudi d'estats excitats i, per això, cal recórrer al formalisme denominat *Time Dependent* (TD). El mètode TD DFT[101,102] proporciona una extensió rigurosa del DFT de Hohenberg, Kohn i Sham, que és independent del temps, a una situació en la que un sistema, situat inicialment en el seu estat estacionari fonamental, es veu sotmès a una pertorbació depenent del temps mitjançant la modificació del potencial extern. Així, s'introdueix un potencial efectiu depenent del temps per a un sistema de partícules independents, els orbitals de les quals porten a la mateixa densitat que el sistema interaccionant.

Així, doncs, partint de l'equació de Kohn-Sham depenent del temps:

$$\left[-\frac{1}{2}\nabla^2 + v_{eff}(\mathbf{r},t)\right]\psi(\mathbf{r},t) = i\frac{\partial}{\partial t}\psi(\mathbf{r},t) \qquad \text{(AII-42)}$$

Aquesta equació pot derivar-se per a un sistema de partícules independents, els orbitals de les quals donen la mateixa densitat de càrrega que el sistema interaccionant, assumint l'existència d'un potencial ν_{eff} que pren la forma:

$$v_{eff}(\mathbf{r},t) = v(t) + v_{SCF}(\mathbf{r},t) \qquad \text{(AII-43)}$$

on $\nu(t)$ és una pertorbació que s'aplica sobre el sistema i ν_{SCF} (**r**,t) és el potencial SCF definit com:

$$v_{SCF}(\mathbf{r},t) = \int \frac{\rho(\mathbf{r},t)}{|\mathbf{r}-\mathbf{r}'|} d\mathbf{r} + v_{xc}(\mathbf{r},t) \qquad \text{(AII-44)}$$

on el potencial de correlació-intercanvi ν_{xc} es dóna com la derivada funcional de l'acció d'intercanvi-correlació (A_{xc}):

$$v_{xc}[\rho](r,t) = \frac{\delta A_{xc}[\rho]}{\delta\rho(r,t)} \approx \frac{\delta E_{xc}[\rho_t]}{\delta\rho_t(r)} = v_{xc}[\rho_t](r) \qquad \text{(AII-45)}$$

[101] E. Runge, E.K.U. Gross, *Phys. Rev. Lett.*, **52**, (1984), 997.
[102] R.E. Stratmann, G.E. Scuseria, M.J. Frisch, *J. Chem. Phys.*, **109**, (1998), 8218.

Aquí, encara que el funcional A_{xc} sigui desconegut, és aproximadament E_{xc}, el funcional de correlació-intercanvi de la teoria de Kohn-Sham, el qual és una funció ρ_t de l'espai a un temps fix. Aquesta aproximació rep el nom d'aproximació adiabàtica.

Per a un sistema, inicialment a l'estat fonamental, l'efecte de la pertorbació introduïda en el hamiltonià de Kohn-Sham per un camp aplicat $\delta v(t)$ és:

$$\delta v_{eff}(\mathbf{r},t) = \delta v(t) + \delta v_{SCF}(\mathbf{r},t) \qquad \text{(AII-46)}$$

on $\delta v_{SCF}(\mathbf{r},t)$ és la resposta linial SCF del canvi en la densitat de càrrega donat per:

$$\delta\rho(r,\omega) = \sum_{ai} \delta P_{ai}(\omega)\psi_a(\mathbf{r})\psi_i^*(\mathbf{r}) + \sum_{ia} \delta P_{ia}(\omega)\psi_i(\mathbf{r})\psi_a^*(\mathbf{r}) \qquad \text{(AII-47)}$$

on $\delta P(\varpi)$ és la resposta linial de la matriu densitat Kohn-Sham, usant els subindex *i,j* per indicar els orbitals moleculars ocupats, *a,b* pels virtuals i *s,t,u,v* pels orbitals moleculars com no pertorbats.

Així, es pot escriure la resposta linial de la matriu densitat de Kohn-Sham per a un camp aplicat com:

$$\delta P_{st}(\omega) = \frac{\Delta n_{st}}{(\varepsilon_s - \varepsilon_t) - w} \delta v_{st}^{eff}(\omega) \qquad \text{(AII-48)}$$

on Δn_{st} és la diferència en els nombres d'ocupació i és *1* per *st = ai* i *–1* per *st = ia*. ε és l'energia dels orbitals moleculars i *w* són les energies d'excitació, les quals es determinen com valors propis de

$$\begin{bmatrix} \mathbf{A} & \mathbf{B} \\ \mathbf{B} & \mathbf{A} \end{bmatrix} \begin{bmatrix} \mathbf{X} \\ \mathbf{Y} \end{bmatrix} = w \begin{bmatrix} 1 & 0 \\ 0 & -1 \end{bmatrix} \begin{bmatrix} \mathbf{X} \\ \mathbf{Y} \end{bmatrix} \qquad \text{(AII-49)}$$

on $\mathbf{X}_{ai} = \delta P_{ai}(\omega)$, $\mathbf{Y}_{ai} = \delta P_{ia}(\omega)$, $\mathbf{A}_{ai,bj} = \delta_{ab}\delta_{ij}(\varepsilon_a - \varepsilon_i) + \mathbf{K}_{ai,bj}$ i $\mathbf{B}_{ai,bj} = \mathbf{K}_{ai,jb}$.

Finalment, mitjançant la regla de la cadena i a partir de les equacions AII-44, AII-45 i AII-47 es calcula la matriu d'acoblament **K** pel TD DFT:

$$\mathbf{K}_{st\sigma,uv\tau} = \frac{\partial v_{st}^{SCF}}{\partial P_{uv}} = \left(\psi_{s\sigma}^{*}(\mathbf{r})\psi_{t\sigma}(\mathbf{r})\middle|\psi_{u\tau}^{*}(\mathbf{r}')\psi_{u\tau}(\mathbf{r}')\right) - \left(\psi_{s\sigma}^{*}(\mathbf{r})\psi_{u\tau}(\mathbf{r})\middle|\psi_{u\tau}^{*}(\mathbf{r}')\psi_{t\sigma}(\mathbf{r}')\right).$$

(AII-50)

S'ha de fer notar que la matriu **A** només implica les monoexcitacions, mentre que la matriu **B** implica les mono i les biexcitacions. Per tant, el TD inclou efectes de correlació de l'ordre de les biexcitacions, les quals no es tenen en compte en el mètode CIS. Per això, es pot dir que el TD introdueix una major correlació que el CIS.

AII.6.MÈTODES HÍBRIDS

Descriure teòricament les reaccions químiques amb un model acurat requereix mètodes que normalment no són aplicables a molècules grans. No obstant això, hi ha alguns mètodes per vorejar aquest problema. Sovint, s'usen sistemes model petits per descriure el centre reactiu que normalment es situa a una regió particular de la molècula[103,104]. Una altra aproximació és utilitzar hamiltonians simplificats com als mètodes empírics i semiempírics[105]. Encara que la validesa i l'aplicabilitat depèn enormement de la parametrització i no pot generalitzar-se, una solució òbvia d'aquest problema és la partició del sistema en dues o més parts o capes, on la part d'interès (capa interna) es tracti a un nivell computacional alt i la resta del sistema (capa externa) a un nivell computacional més baix. Aquesta idea no és nova, a la literatura s'hi troben moltes i diferents implementacions[106,107,108,109,110,111]. Aquests mètodes s'anomenen híbrids perquè inclouen diferents nivells de càlcul per a diferents parts d'un mateix sistema.

Els mètodes híbrids es distingeixen principalment en dos aspectes. El primer fa referència a les diferents maneres de tractar la regió frontera de les parts del sistema

[103] N. Koga, K. Morokuma, *Chem. Rev.*, **91**, (1991), 823.
[104] A.Veillard, *Chem. Rev.*, **91**, (1991), 743.
[105] J. Åqvist, A.Warshel, *Chem. Rev.*, **93**, (1993), 2523.
[106] J. Gao, Reviews in Computational Chemistry, vol.7, VCH, New York, 1995.
[107] D. Bakowies, W. Thiel, *J. Phys. Chem.*, **100**, (1996), 10580.
[108] D. Bakowies, W. Thiel, *J. Comput. Chem.*, **17**, (1996), 87.
[109] U.C. Singh, P.A. Kollman, *J. Comput. Chem.*, **7**, (1986), 718.
[110] M.J. Field, P.A. Bash, M. Karplus, *J. Comput. Chem.*, **11**, (1990), 700.
[111] U. Eichler, K.M. Kölmel, J. Sauer, *J. Comput. Chem.*, **18**, (1996), 463.

molecular. Entre dues capes hi ha una intercapa. Si no hi ha enllaços covalents entre les capes, aquesta regió fronterera no té perquè existir. I si n'hi ha s'ha d'escollir el lloc per delimitar la capa interna. Això fa que un enllaç covalent uneixi un àtom que és tractat a un nivell de càlcul amb un altre àtom tractat a un nivell de càlcul diferent i que per tant, aquest enllaç en delimitar les capes es "trenqui".

Hi ha diverses maneres de solventar el problema d'aquest trencament. Una possibilitat és construir un altre model químicament virtual, en el qual es substitueixin aquests àtoms units per un enllaç covalent fronterer per uns "àtoms d'unió" o *link atoms*, que solen ser hidròdens, per simular els enllaços covalents del sistema real.

Un segon aspecte a considerar és la interacció entre les parts interna i externa del sistema. També hi ha diverses formes de solventar això. Una d'elles es basa en l'aproximació:

$$E(X\text{-}Y) = E_1(X) + E_2(Y) + E_{intercapa}(X,Y) \qquad \text{(AII-51)}$$

on E(X-Y) l'energia total del sistema X-Y, essent X la regió interna i Y l'externa i 1 i 2 els diferents nivells de càlcul amb els que es tracta el sistema, i $E_{intercapa}(X,Y)$ és l'energia d'interacció entre les dues capes.

D'altra banda, si E(X-Y) es calcula així:

$$E(X\text{-}Y) = E_2(X\text{-}Y) - E_2(X) + E_1(X) \qquad \text{(AII-52)}$$

aleshores tindrem un model d'extrapolació[112] i, en aquest cas, no hi ha la necessitat d'un hamiltonià d'interacció especial, ja que la interacció entre les dues capes és tractada consistentment a nivell computacional baix. Òbviament, les dues aproximacions són equivalents si:

$$E_2(Y) + E_{intercapa}(X,Y) = E_2(X\text{-}Y) - E_2(X) \qquad \text{(AII-53)}$$

és a dir, si $E_{intercapa}(X,Y)$ correspon a l'energia d'interacció exacta al respectiu nivell de càlcul baix.

[112] S. Humbel, S. Sieber, K. Morokuma, *J. Chem. Phys.*, **105**, (1996), 1959.

AII.6.1.MÈTODE ONIOM

El programa GAUSSIAN inclou un mètode híbrid denominat ONIOM (*Our own N-layered Integrated molecular Orbital and molecular Mechanics*) que permet tractar un sistema amb diferents nivells de càlcul, que ha estat desenvolupat pel grup del Prof. Morokuma[113]. L'ús de dit programa ha estat fonamental per a la introducció dels efectes del medi i supramoleculars des del punt de vista d'aquest estudi; encara que donada la seva relativa novetat com a mètode quàntic electrònic, ha estat necessari un cert període d'ajust i assaig per optimitzar els mètodes a usar a cada zona depenent del nivell de càlcul, així com la frontera òptima per delimitar ambdues regions. Un avantatge del mètode ONIOM és la no necessitat intrínseca de limitar l'estudi a dues zones, podent-se així definir fins a tres zones de nivell de càlcul (es podria generalitzar fàcilment a més de tres) decreixent a mesura que hom s'allunya del centre reactiu. L'ONIOM inclou els mètodes IMOMM[114] (*Integrated Molecular Orbital and Molecular Mechanics*) i IMOMO[115] (*Integrated Molecular Orbital and Molecular Orbital*) i està basat en un sistema d'extrapolació. El sistema molecular pot dividir-se en tres capes diferents connectades arbitràriament i cada capa pot tractar-se a un nivell teòric distint.

L'ONIOM té, en potència, moltes aplicacions en càlculs de macrocicles[116], molècules orgàniques[117], compostos de coordinació, *clusters* i fenòmens de superfície[118], complexos organometàl·lics[119] i també per a l'elucidació estructural mitjançant la predicció d'espectres de RMN[120], així com l'obtenció de les freqüències en IR i Raman[121], ...

[113] S. Dapprich, I. Komáromi, K.S. Byun, K. Morokuma, M.J. Frisch, *J. Mol. Struct. (THEOCHEM)*, **461-462**, (1999), 1.
[114] F. Maseras, "Quantitative consideration of steric effects through hybrid Quantum Mechanics/Molecular Mechanics Methods" dins el llibre Computational Organometallic Chemistry, Cundary & Dekker, New York, 2001.
[115] K. Morokuma, T. Vreven, *J. Comput. Chem.*, **21**, (2000), 1419.
[116] H.E. Zimmerman, I.V. Alabugin, V.N. Smolenskaya, *Tetrahedron*, **56**, (2000), 6821.
[117] K. Morokuma, R.D.J. Froese, *Chem. Phys. Lett.*, **305**, (1999), 419.
[118] H.-R. Tang, K.-N. Fan, *Chem. Phys. Lett.*, **330**, (2000), 509.
[119] B. Goldfuss, F. Rominger, *Tetrahedron*, **56**, (2000), 881.
[120] P.B. Karadakov, K. Morokuma, *Chem. Phys. Lett.*, **317**, (2000), 589.
[121] M. Svensson, S. Humbel, R.D.J. Froese, T. Matsubara, S. Sieber, K. Morokuma, *J. Phys. Chem.*, **100**, (1996), 19357.

Considerem el cas de dues regions. Denotem doncs, quatre sistemes: Real a nivell baix, Model a nivell baix, Model a nivell alt i Real a nivell alt, on Model correspon a la zona interna (en el present cas és el *guest*).

Aleshores, l'energia extrapolada E_{ONIOM} es defineix com:

$$E_{ONIOM} = E_{baix}(Real) + E_{alt}(Model) – E_{baix}(Model) \qquad (AII\text{-}54)$$

on E_{ONIOM} és una aproximació a l'energia del sistema Real a nivell alt;

$$E_{alt}(Real) = E_{ONIOM} + D \qquad (AII\text{-}55)$$

$$D = E_{alt}(Real) - E_{alt}(Model) – [E_{baix}(Real) - E_{baix}(Model)] \qquad (AII\text{-}56)$$

Així, si l'error del procediment d'extrapolació (D) és constant per a dues estructures diferents, la seva energia relativa $\Delta E_{alt}(Real)$ pot ser avaluada correctament mitjançant ΔE_{ONIOM}. Davant de la impossibilitat de calcular $E_{alt}(Real)$, ja que si es pogués fer no tindria sentit usar l'ONIOM per a aquesta finalitat, calcular D només és possible per inducció, prenent com a variables geomètriques diverses estructures similars.

El sistema Model comprèn la capa interna i els *link atoms* (àtoms d'unió) i el sistema Real comprèn tant la capa interna com l'externa.

Es denoten les coordenades dels àtoms del sistema Model i del Real com R_1, les coordenades dels *link atoms* al sistema Model com R_2, les coordenades dels àtoms substituïts pels *link atoms* al sistema Real com R_3 i les coordenades dels àtoms de la capa externa no substituïts per *link atoms* com R_4. Així, la geometria del sistema Real és descrita per R_1, R_3 i R_4 i d'aquestes coordenades en dependrà l'energia $E_{ONIOM} = f(R_1, R_3, R_4)$.

De cara a generar el sistema Model, descrit per R_1 i els *link atoms* per R_2, es defineix R_2 en funció de R_1 i R_3 com $R_2 = f(R_1, R_3)$.

En els càlculs del sistema Model, els *link atoms* estan sempre aliniats al llarg dels vectors d'enllaç del sistema Real. Per a la posició exacta R_2 d'un simple àtom d'hidrogen al llarg de l'enllaç A-B (R_3-R_1), s'introdueix un paràmetre de distancia g. Així,

$$R_2 = R_1 + g\cdot(R_3 - R_1) \qquad \text{(AII-57)}$$

Per calcular el gradient de tot el sistema a partir de l'energia es té:

$$\nabla E_{ONIOM}(R_1, R_3, R_4) = \nabla E_{baix}(\text{Real})(R_1, R_3, R_4) + \nabla E_{alt}(\text{Model})(R_1, R_2)\cdot \mathbf{J}(R_2 \rightarrow R_1, R_3) + \\ - \nabla E_{baix}(\text{Model})(R_1, R_2)\cdot \mathbf{J}(R_2 \rightarrow R_1, R_3) \qquad \text{(AII-58)}$$

on **J** és la matriu jacobiana que projecta les forces de tots els *link atoms* (R_2) a R_1 i R_3. Ara només resta calcular la matriu de derivades segones de l'energia respecte les coordenades nuclears o matriu hessiana **H**.

Així s'obté:

$$\mathbf{H}_{ONIOM}(R_1, R_3, R_4) = \mathbf{H}_{baix}(\text{Real})(R_1, R_3, R_4) + \mathbf{J}^{\mathbf{t}}(R_2 \rightarrow R_1, R_3)\cdot \mathbf{H}_{alt}(\text{Model})(R_1, R_2)\cdot \mathbf{J}(R_2 \rightarrow R_1, R_3) + \\ - \mathbf{J}^{\mathbf{t}}(R_2 \rightarrow R_1, R_3)\cdot \mathbf{H}_{baix}(\text{Model})(R_1, R_2)\cdot \mathbf{J}(R_2 \rightarrow R_1, R_3) \qquad \text{(AII-59)}$$

Però les freqüències normals de vibració que s'obtenen d'aquesta matriu hessiana estan, normalment, sobreestimades; per això es realitza un escalat[122]. És clar que aquest escalat dependrà del conjunt de base i del mètode de càlcul. Aleshores, s'introduïran factors d'escala diferents a les matrius hessianes de nivells de càlcul distints com es pot veure a AII-60.

$$\mathbf{H}_{ONIOM}(R_1, R_3, R_4) = c^2_{baix}(\text{Real})\cdot \mathbf{H}_{baix}(\text{Real})(R_1, R_3, R_4) + \\ + c^2_{alt}(\text{Model})\cdot \mathbf{J}^{\mathbf{t}}(R_2 \rightarrow R_1, R_3)\cdot \mathbf{H}_{alt}(\text{Model})(R_1, R_2)\cdot \mathbf{J}(R_2 \rightarrow R_1, R_3) + \\ - c^2_{baix}(\text{Model})\cdot \mathbf{J}^{\mathbf{t}}(R_2 \rightarrow R_1, R_3)\cdot \mathbf{H}_{baix}(\text{Model})(R_1, R_2)\cdot \mathbf{J}(R_2 \rightarrow R_1, R_3) \qquad \text{(AII-60)}$$

El procés d'optimització en el mètode ONIOM no consisteix en una sèrie d'optimitzacions successives de diferents parts de la molècula, sinó que es tracta d'una successió d'iteracions a dos nivells: macroiteracions dins les quals s'inclou un procés microiteratiu tal i com il·lustra el diagrama de flux de la Fig.34.

[122] A.P. Scott, L. Radom, *J. Phys. Chem.*, **100**, (1996), 16502.

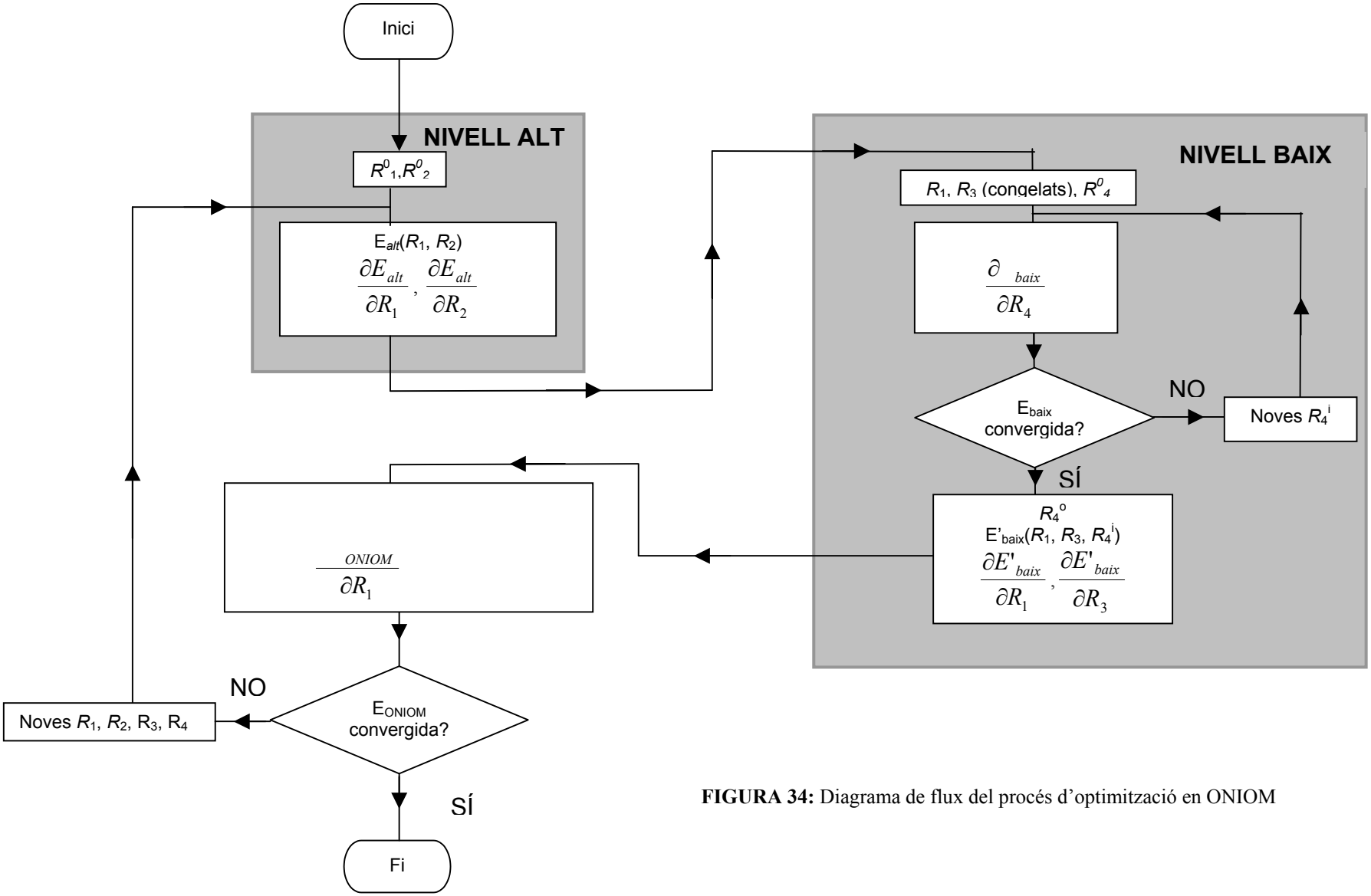

FIGURA 34: Diagrama de flux del procés d'optimització en ONIOM

Les macroiteracions són més cares, computacionalment parlant, ja que inclouen càlculs al nivell alt. Aleshores, el sistema ideat permet incorporar un procés de microiteracions que tenen un cost computacional molt més reduït. Les macroiteracions tenen lloc a un nivell de càlcul alt (pels casos estudiats, *ab initio* i DFT) i les microiteracions a un nivell baix (empíric o semiempíric). S'inicia el procés amb unes coordenades de partida que defineixen la geometria inicial R_1 i R_2. Seguidament, es calcula l'energia i el gradient inicials al nivell de càlcul alt i, a continuació, s'entra en el procés de microiteracions on, amb R_1 i R_3 fixats, s'optimitza R_4 al nivell de càlcul baix. Quan l'energia convergeix, es dóna per finalitzat el cicle de microiteracions, obtenint pel nivell de càlcul baix una energia i un gradient. Tal com s'ha exposat abans, l'energia i el gradient total es calculen sumant l'energia i gradient obtinguts pel nivell de càlcul baix del sistema Real amb l'energia i gradient inicialment calculats amb el nivell de càlcul alt del sistema Model, tot restant-li l'energia i el gradient pel nivell de càlcul baix del sistema Model. Una vegada obtinguts l'energia i el gradient totals, es passa a la següent macroiteració comprovant si aquests convergeixen a partir del criteri de convergència. Si és així, el càlcul ja ha finalitzat. Altrament, es defineixen unes noves coordenades R_1 i R_2 i es reinicia el procés.

En els casos que s'estudien, no caldrà definir R_2 ni R_3 ja que són coordenades que es refereixen als *link atoms* i aquests no es tenen en compte, car no hi ha enllaços covalents a l'intercapa; per tant el càlcul es simplifica donat que la matriu jacobiana que projecta les forces dels *link atoms* es converteix en la matriu unitat.

Tal com es defineix el mètode ONIOM, no es pot trobar una funció d'ona de tot el sistema complet. Encara que la densitat es pot definir clarament com la suma de densitats, igual que l'energia. Així,

$$\rho_{ONIOM} = \rho_{baix}(\text{Real}) + \rho_{alt}(\text{Model}) - \rho_{baix}(\text{Model}) \qquad \text{(AII-61)}$$

I a partir de la variació de l'energia amb el camp elèctric **F** es pot calcular el moment dipolar μ com:

$$\boldsymbol{\mu} = \frac{\partial E_{ONIOM}}{\partial \mathbf{F}} = \frac{\partial E_{baix}(\text{Real})}{\partial \mathbf{F}} + \frac{\partial E_{alt}(\text{Model})}{\partial \mathbf{F}} - \frac{\partial E_{baix}(\text{Model})}{\partial \mathbf{F}} \qquad \text{(AII-62)}$$

AII.7.CONSTRUCCIÓ D'UNA HIPERSUPERFÍCIE D'ENERGIA POTENCIAL

Fins ara, s'ha explicat com calcular l'energia electrònica d'un sistema químic donada la seva geometria. A continuació, es veurà com aquests càlculs energètics serveixen per construir una hipersuperfície d'energia potencial U(R).

Després de desacoblar el moviment nuclear del moviment electrònic mitjançant l'aproximació de Born-Oppenheimer, la resolució de l'equació de Schrödinger electrònica (AII-4) dóna l'energia U(R) que inclou tots els termes energètics, excepte el cinètic nuclear. Aquesta funció energètica rep el nom d'**hipersuperfície d'energia potencial** i el seu prefix fa referència a la impossibilitat de representar-la gràficament a l'espai tridimensional (quan la molècula té més de 2 àtoms) ja que la seva dimensionalitat és 3N-6 (essent N el nombre d'àtoms del sistema).

U(R) permet traduir qualsevol canvi estructural de la molècula a la variació d'energia potencial que aquest implica (es pot saber, per exemple, si augmentar un determinat angle estabilitza o desestabilitza el sistema), per això es converteix en una eina molt útil a l'hora d'estudiar la dinàmica d'una reacció.

Estrictament, s'hauria de treballar sempre a l'espai (3N-6)-dimensional representat per R. Això és possible quan es calcula U(R) però no pas a l'hora de representar-la gràficament. Per tal d'adaptar-ho a la visió tridimensional s'haurà d'escollir només una (cas monodimensional) o bé dues (cas bidimensional) coordenades que puguin reproduir les característiques més rellevants de la superfície real i així fer una reducció dimensional. La dificultat rau en l'elecció de la/les coordenades adients.

La superfície d'energia potencial que es representa, doncs, no serà (R, U(R)) sinó (x, U(x)) en el cas monodimensional i (x, y, U(x,y)) en el cas bidimensional.

Pel cas monodimensional, per exemple, només és necessari un conjunt de punts (x, U(x)) que descrigui l'evolució dels nuclis al llarg de la reacció química. Si es té la geometria de la molècula es pot calcular U(x), tal i com s'ha explicat a l'apartat anterior. Però, com se sap quina *x* correspon a cada geometria? El primer que s'ha de fer és calcular els punts

estacionaris que la superfície ha de descriure, de manera que es tinguin les estructures dels reactius, productes, intermedis i estats de transició. Després cal determinar aquestes geometries mitjancant mètodes d'optimització i finalment trobar les *x* dels punts intermedis a través de mètodes d'interpolació.

AII.7.1.OPTIMITZACIÓ DE GEOMETRIES

Les optimitzacions de geometria requereixen trobar els **punts estacionaris** de la superfície d'energia potencial.

Suposant que s'està situat a un punt de la superfície ($\vec{q}_i$) i es fa un petit desplaçament, l'energia del punt final ($\vec{q}_f$) pot expressar-se en funció de la del punt inicial mitjançant un desenvolupament en sèrie de Taylor. Si es fa l'expansió fins al terme quadràtic tenim:

$$U(\vec{q}_f) = U(\vec{q}_i) + \tilde{\vec{g}}\vec{S} + \frac{1}{2}\tilde{\vec{S}}\mathbf{H}(\vec{q}_i)\vec{S} \qquad \text{(AII-63)}$$

(el símbol ~ indica que s'ha transposat el vector)

on $\vec{S}$ és el vector desplaçament ($\vec{q}_f$ - $\vec{q}_i$), $\vec{g}$ és el vector gradient (derivades primeres de l'energia potencial *U*) i **H** la matriu hessiana o de derivades segones.

$$\mathbf{H}_{ij} = \left\{ \frac{\partial^2 U}{\partial s_i \partial s_j} \right\}_{i,j=1,..,3N} \qquad \text{(AII-64)}$$

Si el punt inicial és un punt estacionari, $\vec{g}(\vec{q}_i) = 0$ o el que és el mateix, $\frac{\partial U(i)}{\partial q_j} = 0$ per j=1,2,...,3N, en aquest cas

$$U(\vec{q}_f) = U(\vec{q}_i) + \frac{1}{2}\tilde{\vec{S}}\mathbf{H}(\vec{q}_i)\vec{S} \qquad \text{(AII-65)}$$

$$\Delta U(\vec{q}_i \rightarrow \vec{q}_f) = \frac{1}{2}\tilde{\vec{S}}\mathbf{H}(\vec{q}_i)\vec{S} \qquad \text{(AII-66)}$$

Truncant l'expansió en sèrie de l'energia al segon ordre, l'increment d'energia produït per un desplaçament ve donat només per **H**. En aquestes condicions, es podria diagonalitzar **H**

a través d'una matriu **P**, la qual cosa portaria a un sistema de coordenades *q'*. Vegi's el desenvolupament matemàtic a continuació:

$$\exists \mathbf{P} \text{ tal que } \quad \mathbf{P^{-1}} = \widetilde{\mathbf{P}}$$

$$\widetilde{\mathbf{P}}\mathbf{H}\mathbf{P} = \mathbf{\Lambda} \tag{AII-67}$$

essent Λ la matriu diagonal

$$\mathbf{\Lambda} = \begin{pmatrix} \lambda_1 & 0 & 0 & \cdots & 0 \\ 0 & \lambda_2 & 0 & \cdots & 0 \\ 0 & 0 & \ddots & 0 & \vdots \\ \vdots & \vdots & 0 & \ddots & \vdots \\ 0 & 0 & 0 & \cdots & \lambda_{3N} \end{pmatrix} \tag{AII-68}$$

I com que el producte de matrius és associatiu però no commutatiu, la diagonalització implicarà fer un canvi de base. Així,

$$\vec{V} = \widetilde{\mathbf{P}}\vec{S} \tag{AII-69}$$

essent $\vec{V} = \begin{pmatrix} v_1 \\ v_2 \\ \vdots \\ v_{3N} \end{pmatrix}$ el vector transformat de $\vec{S}$ en la nova base.

Aleshores, aplicant l'expressió AII-67 i l'AII-69 sobre l'AII-66 s'obté:

$$\Delta U = \frac{1}{2}\widetilde{\vec{V}}\widetilde{\mathbf{P}}\mathbf{H}\mathbf{P}\vec{V} = \frac{1}{2}\widetilde{\vec{V}}\mathbf{\Lambda}\vec{V} = \frac{1}{2}\sum_i \lambda_i \cdot v_i^2 \tag{AII-70}$$

I ja que els quadrats de $(v_1, v_2, \ldots)$ són positius, aleshores el signe de ΔU depèn de les λ_i que indiquen la corbatura. D'aquestes n'hi haurà sis que seran zero ja que al llarg de la rotació i la translació –en molècules poliatòmiques- la corbatura no canvia.

Els punts de més interès químic de la hipersuperfície de potencial són: mínims (reactius, productes i intermedis) i punts sella de primer ordre (estats de transició). Els primers es caracteritzen per tenir una **H** amb tots els valors propis positius i els segons per tenir-la amb un sol valor propi negatiu, a part dels sis zeros trivials.

Per localitzar efectivament els mínims energètics hi ha diferents mètodes segons es faci servir només l'energia, l'energia i el gradient o l'energia, el gradient i **H**. El mètode més rigorós, però que implica un alt cost computacional és el mètode iteratiu Newton-Raphson on:

$$\vec{q}_{n+1} = \vec{q}_n - \mathbf{H}_n^{-1}\vec{g}_n \qquad \text{(AII-71)}$$

Quan els punts inicials i les energies d'aquests punts estan suficientment a prop en iteracions successives, es considera que s'ha localitzat un punt estacionari sobre la superfície d'energia potencial. Això exigeix calcular l'energia i el gradient a cada punt. Estrictament, també s'hauria de conèixer la matriu de derivades segones **H**, però sovint es fa una aproximació per tal de no calcular-la. Això, tot i que redueix el temps de càlcul de cada pas, pot fer augmentar el nombre de passos necessaris per arribar al mínim. Serà, doncs, convenient fer una bona elecció del sistema de coordenades i de la geometria inicial si, com ha estat el cas, s'utilitza un mètode on **H** és aproximat.

El gradient $\vec{g}$ en una geometria optimitzada (és a dir, corresponent a un mínim local de la superfície d'energia potencial) ha de valer zero i, per tant, les coordenades corresponents a aquest punt estacionari vindran donades per l'equació (AII-71).

Aquest és el fonament del mètode de Newton-Raphson, pel qual és indispensable una geometria de partida ($\vec{q}_i$) i una **H** inicial, que generalment rep un valor aproximat, millorable a cada pas de l'optimització.

Uns altres algorismes són el de Berny Schlegel[123] (en coordenades internes redundants), el qual és una millora del seu algorisme de 1982[124], que està força extès, i el de Fletcher i Powell[125] que s'aplica a aquells mètodes de càlcul que els manca una expressió analítica pel gradient.

A diferència del que succeeix en el cas dels mínims, els estats de transició han d'ésser un mínim en totes direccions excepte en una, en la qual han de ser màxims. El vertader estat de transició per a un determinat procés elemental ha de complir una sèrie de requisits que vénen donats per les regles de McIver-Komornicki:

[123] H.B. Schlegel, *J. Comput. Chem.*, **17**, (1996), 49.
[124] H.B. Schlegel, *J. Comput. Chem.*, **3**, (1982), 214.
[125] R. Fletcher, M.J.D. Powell, *Comput. J.*, **6**, (1963), 163.

a) Ha de ser un punt estacionari (gradient nul).
b) La matriu hessiana ha de tenir un, i només un, valor propi negatiu.
c) Ha de ser un màxim energètic d'un camí monodimensional continu que uneixi els mínims de reactius i productes de la reacció que interessa.
d) Si més d'un punt compleix els requisits anteriors, l'estat de transició de la reacció serà el de menor energia de tots ells.

És necessari disposar d'una matriu hessiana molt acurada per tal d'arribar a l'estat de transició, fet pel qual esdevé quasi imprescindible avaluar-lo analíticament, com a mínim a l'inici de l'optimització.

D'estratègies per a localitzar un estat de transició n'hi ha més d'una. En aquest treball s'ha emprat, fonamentalment, l'algorisme de Berny Schlegel que s'engloba dins els mètodes anomenats de localització directa. Però, també s'ha usat en alguns moments el mètode de la coordenada de reacció.

El mètode de la coordenada de reacció, conegut també com el mètode de la coordenada distingida[126], té els seus orígens en el mètode de relaxació proposat per Empedocles[127]. Consisteix en seleccionar una o dues coordenades internes del sistema com a variables independents de la funció d'energia potencial. Llavors, per a cada conjunt de valors fixats d'aquestes variables es deixa que la resta adoptin aquells valors que facin mínima l'energia. D'aquesta manera es construeix una superfície reduïda.

El camí construït segons aquest mètode, sovint té el problema de la **histèresi química**[128], és a dir, camins de reacció diferents per a la reacció directa i la inversa, que poden no arribar a trobar-se. Això succeeix, sobretot, quan les variables triades no són bones representants de la vertadera coordenada de reacció.

Un cop construït el camí de reacció, per trobar l'estat de transició segons aquest mètode només és necessari trobar-ne el màxim. El mètode d'Empedocles, però, dóna únicament una orientació de la geometria del veritable estat de transició. Sovint és emprat per fer una

[126] Y.S. Kong, M.S. Jhon, *Theoret. Chim. Acta*, **70**, (1986), 123.
[127] P. Empedocles, *Theoret. Chim. Acta*, **13**, (1969), 139.
[128] M.J.S. Dewar, S. Kirschner, *J. Am. Chem. Soc.*, **93**, (1971), 4291.

exploració prèvia de la hipersuperfície de potencial, just abans d'emprar mètodes de localització directa.